

**DESIGN AND DEVELOPMENT OF
SPECTRAL SIGNATURE BASED CHIPLESS
RFID TAGS**

Thesis submitted by

DINESH R

in partial fulfillment of the requirements

for the award of the degree of

DOCTOR OF PHILOSOPHY

Under the guidance of

Prof. P. MOHANAN



Department of Electronics
Faculty of Technology
Cochin University of Science and Technology
Cochin - 682 022, Kerala, India

April 2015

DESIGN AND DEVELOPMENT OF SPECTRAL SIGNATURE BASED CHIPLESS RFID TAGS

Ph.D. Thesis under the Faculty of Technology

Author:

Dinesh R

Centre for Research in Electromagnetics and Antennas

Department of Electronics

Cochin University of Science and Technology

Cochin - 682 022, Kerala, India.

Email: dinsh84@gmail.com

Supervisor:

Dr. P.Mohanan

Professor

Centre for Research in Electromagnetics and Antennas

Department of Electronics

Cochin University of Science and Technology

Cochin - 682 022, Kerala, India.

Email:drmohan@gmail.com

Department of Electronics

Cochin University of Science and Technology

Cochin - 682 022, Kerala, India.

www.doe.cusat.edu

April 2015

*Dedicated to my parents, teachers and dear
ones.....*



DEPARTMENT OF ELECTRONICS
COCHIN UNIVERSITY OF SCIENCE AND TECHNOLOGY
COCHIN – 682 022

Prof. P. Mohanan

(Supervising Guide)

Professor

Department of Electronics

Cochin University of Science and Technology

Certificate

This is to certify that this thesis entitled “**Design and Development of Spectral Signature Based Chipless RFID Tags**” is a bonafide record of the research work carried out by DINESH R under my supervision in the Department of Electronics, Cochin University of Science and Technology. The results embodied in this thesis or parts of it have not presented for any other degree.

I further certify that the corrections and modifications suggested by the audience during the pre-synopsis seminar and recommended by the Doctoral committee of Mr. Dinesh R are incorporated in the thesis.

Cochin – 22

April 2015

Prof. P. Mohanan

Declaration

I hereby declare that the work presented in this thesis entitled “**Design and Development of Spectral Signature Based Chipless RFID Tags**” is based on the original research work carried out by me under the supervision and guidance of Prof. P. Mohanan, Professor, Department of Electronics, Cochin University of Science and Technology, Cochin-682 022 and has not been included in any other thesis submitted previously for the award of any degree.

Cochin - 22
April 2015

Dinesh R
Research scholar,
Department of Electronics,
CUSAT,
Cochin-22.

Acknowledgement

I take this opportunity to place on record my profound sense of indebtedness and deep appreciation to my supervising guide, Prof. P. Mohanan for his personal encouragement, patronly behaviour, stimulating discussions and able guidance right from the beginning to date as a consequence of which the present study reached fruition. My gratitude to him knows no bounds.

I am grateful to Prof. K. Vasudevan, Prof. C. K. Aanandan, Prof. K. T. Mathew, Prof. Tessanna Thomas, Prof. P. R. S. Pillai, Dr. James Kurian and Dr. M. H. Supriya, Faculties of the Department of Electronics for their constant encouragement and concern for my research. I also wish to thank for their valuable personal and professional suggestions throughout my research period.

I express my sincere gratitude to Prof. K. G. Nair, Director, Centre for Science in society, Cochin University of Science and Technology and former Head, Department of Electronics, Cochin University of Science and Technology for giving an opportunity to enter the field of research in electromagnetics and antennas by establishing Centre for Research in Electromagnetics and Antennas at Department of Electronics, Cochin University of Science and Technology.

I gratefully acknowledge the help and inspiration from Praveen sir, Sunil sir, Premlal sir, Sarita teacher, Reji teacher, Girija teacher, and Rekha teacher who has inspired me in both academic and personal development. I also gratefully acknowledge the help and inspiration from all the faculty members of the Department of Electronics, N. S. S. College, Rajakumari.

With pleasure, I acknowledge Dr. Sreemoolanathan VSSC, Trivandrum for his encouragement and valuable suggestions throughout the research carrier.

I am grateful to Abhilash, Manu, Jobin NIIST, Trivandrum for their technical support, encouragement and the friendly ambience provided to me during the research period.

I thank Vikram sarabhai Space centre (VSSC) and University Grant Commission (UGC) for financially supporting me during this endeavour.

I am thankful to all the office and library staff of the Department of Electronics for the help and co-operation. I express my gratitude to Mr. Ibrahim kutty, Mr. Anil P

Yohannan for providing a harmonious environment for work at the Department of Electronics.

My time at CUSAT was made enjoyable in large part by the many friends who have become a part of my life. It is my pleasure to acknowledge the advice and love received from my senior researchers in the Centre for research in Electromagnetics and Antennas(CREMA) Dr. Sujith R, Dr. Sarin P V, Dr. Nishamol M S, Dr. Shameena.V.A., Dr. Laila D., Dr. Deepu. V and Dr. Manoj Joseph. I express my special gratitude to Mr. Vivek R. Mr. Nijas C. M., Ms. Nimisha S., Mr. Deeapk U., Mr. Vinesh P. V., Mr. Abdul Rasheed, Mr. Sreenath S., Mr. Jayakrishnan, Mr. Tittu Samson, Mr. Ashkar ali, Mr. Paulbert Thomas, Mr.Lindo A.O., Mr. Tony D., Mr. Cyriac Odackal, Mr. Ullas G. Kalappura, Mr. Saneesh A.T., Mr. Ananthakrishnan, Mr. Sooraj Kamal, Ms. Sreekala. P. S, Mrs. Anju Lindo, Mr. Sreejith M. Nair, Mrs. Roshna T. K., Mrs. Sajitha V. R., Mrs. Anila P. V., Mr. Indu Kunjappan, Mr. Midhun M. S., Mr. Aji George, Ms. Theresa Bernard, Mr. Satheesh Chandran. Mr. Neeraj K. Pushkaran, Mr. Amarnath, Mr. Rakesh Balakrishnan, Mr. Prasanth P.P., Mr. Sujith Pai, Ms. Dibin Mary George, Mrs. Libimol P. V. and Mrs. Sarah Jacob for the utmost love and care in the entire academic life at CUSAT. I greatly acknowledge the helping hands provided by - Mr.Vinod V.K.T, Sumi chechi and Hariyettan in every patches of the research life.

I am especially grateful to my dear friends -Mr. Jaise, Mr. Rajshah, Mr. Vijesh. R., Mr. Anand. R, Mr. Jinesh, Mr. Deepak. C. Mukund and Jithin for their patience, encouragement and moral support at final stage of my PhD work.

Its my proud privilege to remember my parents, brother Gaganesh and all relatives for their selfless support, motivation, encouragement, patience and tolerance throughout.

With extreme pleasure, let me thank once again all my friends and well wishers for their endless support to all my endeavours.

Dinesh R

Abstract

The main objective of this thesis is to design and develop spectral signature based chipless RFID tags. Multiresonators are essential component of spectral signature based chipless tags. To enhance the data coding capacity in spectral signature based tags require large number of resonances in a limited bandwidth. The frequency of the resonators have to be close to each other. To achieve this condition, the quality factor of each resonance needs to be high. The thesis discusses about various types of multiresonators, their practical implementation and how they can be used in design. Encoding of data into spectral domain is another challenge in chipless tag design. Here, the technique used is the presence or absence encoding technique. The presence of a resonance is used to encode Logic 1 and absence of a specific resonance is used to encode Logic 0. Different types of multiresonators such as open stub multiresonators, coupled bunch hairpin resonators and shorted slot ground ring resonator are proposed in this thesis.

Contents

1	Introduction to Chipless RFID Tags	1
1.1	RFID Tags	1
1.2	RFID Applications	2
1.3	RFID Classifications	3
1.3.1	How RFID Tag is Powered	4
1.3.2	Chip RFID and Chipless RFID	6
1.3.3	Time Domain Reflectometry Based Chipless Tags	7
1.4	Motivation of Thesis	10
1.5	Thesis Organization	10
	REFERENCES	11
2	Literature Review of Chipless Tags	17
2.1	Spectral Signature Based Chipless Tags	18
2.2	Chipless Tag Reading Techniques	28
2.2.1	Reading Methods	28
2.2.2	Different Types of Chipless RFID Tag Readers	29
2.2.3	Chipless RFID Reader	31
2.3	Planar Resonators	32
2.3.1	Transmission Line Resonator	32
2.3.2	Stepped Impedance Resonator	38
2.3.3	Semi-lumped Resonators	43
	REFERENCES	47
3	Coupled Bunch Hairpin Resonator Based Chipless RFID Tags	53
3.1	Characteristics of Hairpin Resonator	54
3.2	Coupled Bunch Hairpin Resonator	61

3.3	Data Encoding Technique	64
3.4	Disc-Loaded Monopole Antennas	66
3.5	Operating Principle of Spectral Signature Based Chipless Tags	71
3.6	Results and Discussions	72
3.6.1	Field Trials	75
3.7	Conclusion	78
	REFERENCES	78
4	Open stub Multiresonator Based Chipless RFID Tag	83
4.1	Open Stub Resonator	84
4.2	Modified Microstrip Transmission Line	84
4.3	Open Stub resonators Incorporated the Modified Transmission Line	87
4.4	Spectral Signature Coding Technique	97
4.4.1	Generation of different Bit Combinations	97
4.5	Chipless RFID Tag Development	98
4.6	Conclusion	105
	REFERENCES	105
5	Loop Multiresonator Based Chipless RFID Tag	107
5.1	Different Loop Resonators	108
5.1.1	Loop Resonator Placed Near Transmission Line	108
5.1.2	Loop Resonator Placed on Slotted Ground	110
5.1.3	Loop resonators Placed on Bifurcated Transmission Line shorted with Ground through via	112
5.2	Results and Discussions	118
5.3	Conclusion	121
6	Conclusion	123

List of Figures

1.1	128-Bit Global SAW tag and reader system (Courtesy: Clinton S. Hartmann et. al.) [11]	8
1.2	(a) Transmission delay line based ID generation circuit (b) Schematic diagram of transmission delay line based ID generation circuit (c) Binary code generation by the superimposition of delayed signals and (d) Input and output waveforms of the ID (Courtesy: Aravind Chamarti) [13]	9
2.1	Capacitively-tuned planar dipoles for RFID Barcodes (Courtesy: I. Jalaly) [2]	19
2.2	Five bit peano- curve based tag (Courtesy: John Mc Vay) [3] .	19
2.3	Spiral resonator based 35-bit spectral signature chipless tag (Courtesy: S. Predrovic et. al.) [6]	20
2.4	Notched elliptical dipole tag using SEM method (Courtesy: Andrew T. Blischak et. al.) [38]	22
2.5	Normalized detected amplitude for five materials and for Teflon at several distances tag-reader (Courtesy: David Girbau et. al.) [40]	23
2.6	Dual polarization slotted tag (Courtesy: Md. Aminul Islam et. al.) [41]	23
2.7	Spectral signature tag based on dual band resonators (Courtesy: David Girbau et.al.) [42]	24
2.8	Concentric circular ring chipless tag (Courtesy: A. Vena et. al.) [44]	25
2.9	Chipless tag using two different coding approaches: (a) absence/presence of resonances and (b) frequency shift and absence/presence of resonances (Courtesy: A. Vena et. al.) [45] .	26
2.10	20-bit chipless tags (Courtesy: A.Vena et. al.) [46]	26

2.11 (a) Tag based on dual-L resonators (b) Tag based on shorted dipoles oriented at 45^0 (Courtesy: A. Vena et. al.) [47]	27
2.12 Substrate integrated tag (Courtesy: Hatem El Matbouly et. al.) [48]	28
2.13 Block diagram of time domain based reader for SAW tags (Courtesy: Nemaï Karmakar et. al.) [49]	30
2.14 Block diagram of spectral signature based chipless RFID reader (Courtesy: Nemaï Karmakar . et. al.) [49]	30
2.15 (a) Top view (b) Side view of shorted half wave microstrip resonator (Courtesy: David M. Pozar) ([51]	35
2.16 (a) Shorted circuit half wave length transmission line (b) Voltage distributions for $n = 1(l = \frac{\lambda}{2})$; $n = 2(l = \lambda)$ and $n = 3(l = 3\frac{\lambda}{2})$ (Courtesy: David M. Pozar) ([51]	35
2.17 (a)Top view (b) Side view of half wave microstrip resonator (Courtesy: David M. Pozar) ([51]	36
2.18 (a)Open circuited half wave length transmission line (b) Voltage distributions for $n = 1(l = \frac{\lambda}{2})$; $n = 2(l = \lambda)$ and $n = 3(l = 3\frac{\lambda}{2})$ (Courtesy: David M. Pozar) ([51]	36
2.19 (a)Top view (b) Side view of short circuited quarter wavelength microstrip resonator (Courtesy: David M. Pozar) ([51]	37
2.20 (a) Short circuited quarter wave length transmission line (b) Voltage distributions for $n = 1(l = 3\frac{\lambda}{4})$; $n = 2(l = 5\frac{\lambda}{4})$ and $n = 3(l = 7\frac{\lambda}{4})$ (Courtesy: David M. Pozar) ([51]	37
2.21 (a)Top view (b) Side view of open circuited quarter wave microstrip resonator (Courtesy: David M. Pozar) ([51]	38
2.22 (a)Open circuited quarter wave length transmission line (b) Voltage distributions for $n = 1(l = 3\frac{\lambda}{4})$; $n = 2(l = 5\frac{\lambda}{4})$ and $n = 3(l = 7\frac{\lambda}{4})$ (Courtesy: David M. Pozar) ([51]	38
2.23 Basic structure of SIR (a)Quarter wavelength SIR (b) Full wavelength SIR (C) Half wavelength SIR $K = \frac{Z_2}{Z_1} < 1$ (d) Half wavelength SIR $K = \frac{Z_2}{Z_1} > 1$ (Courtesy: Makimoto) ([50]	39
2.24 Relationship between electrical length θ_1 and normalized resonator length L_n taking R_z as parameter (Courtesy: M.Makimoto et al)	41

2.25	Ratios of the first higher order resonant frequency to the fundamental resonant frequency of SIRs (Courtesy: M. Makimoto et. al.) [50]	43
2.26	(a) Circular open ring (b) Square open ring (C) Circular split ring resonator (d) Rectangular split ring resonator	44
2.27	Equivalent circuit of SRR and CSRR	45
2.28	Different types SRR with equivalent circuits	46
3.1	Cross section of microstrip line($W = 3.4mm$, $h = 1.6mm$ and $\varepsilon_r = 3.7$)	54
3.2	Microstrip coupled line resonator($l = 34mm$, $t = 0.2mm$, $g = 0.35mm$, $W = 3.4mm$ and $\varepsilon_r = 3.7$)	55
3.3	Simulated insertion loss of the coupled line resonator($l = 34mm$, $t = 0.2mm$, $W = 3.4mm$, $h = 1.6mm$, $g = 0.35mm$ and $\varepsilon_r = 3.7$)	56
3.4	Coupled hairpin resonator ($a = b; t_1 = t_2$)	57
3.5	Simulated Insertion loss of the coupled hairpin resonator ($l = 34mm$, $t_1 = 0.2mm$, $t_2 = 0.2mm$, $W = 3.4mm$, $h = 1.6mm$, $g = 0.35mm$ and $\varepsilon_r = 3.7$)	58
3.6	Surface current distribution at resonance at 2.74 GHz	58
3.7	Effect of the variation in total length (L_1)of hairpin line resonator($L_1 = a + b + c$)	59
3.8	Geometry of asymmetric hairpin resonator ($a \neq b; t_1 \neq t_2$),($L_i = a + b + c = 34mm$)	60
3.9	Effect of length and width variation in the asymmetric hairpin resonator ($(a \neq b; t_1 \neq t_2)$,($L_i = a + b + c = 34mm$))	60
3.10	Coupled bunch hairpin resonator($L_1 = 34.15mm$, $L_2 = 34mm$, $L_3 = 32.35mm$, $L_4 = 32mm$, $L_5 = 30.5mm$, $L_6 = 30.2mm$, $L_7 = 28.55mm$, $L_8 = 28mm$, $h = 1.6mm$, $t_1 = 0.2mm$, $t_2 = 0.45mm$ and $g = 0.2mm$)	62
3.11	Simulated insertion loss of 8- bit coupled bunch hairpin multiresonator based band stop filter ($L_1 = 34.15mm$, $L_2 = 34mm$, $L_3 = 32.35mm$, $L_4 = 32mm$, $L_5 = 30.5mm$, $L_6 = 30.2mm$, $L_7 = 28.55mm$, $L_8 = 28mm$, $h = 1.6mm$, $t_1 = 0.2mm$, $t_2 = 0.45mm$ and $g = 0.2mm$)	63
3.12	Surface current distribution at each resonance	65

3.13	Data encoding technique	66
3.14	Generation of different spectral signature	67
3.15	Geometry of UWB antenna($L_g = 40mm$, $W_g = 20mm$, $W = 3mm$, $R = 15mm$, $\epsilon_r = 4.3$ and $h = 1.6mm$)	68
3.16	Measured returnloss of microstrip fed disc loaded monopole antenna	68
3.17	Surface current distribution of UWB monopole antenna at different frequencies	69
3.18	Measured radiation pattern of UWB monopole antenna	70
3.19	Measured gain of both horn antenna and microstrip fed disc loaded monopole antenna	71
3.20	Block diagram of Spectral signature based chipless RFID reader system (Courtesy: S.Predrovic et.al.) [3]	72
3.21	Photograph of the proposed multiresonator compared with INR 10 coin	73
3.22	Measured (a)Insertion loss (b) Group delay of bunch hairpin resonator	74
3.23	Bunch hairpin resonator fabricated on a substrate of ϵ_r 4.3 : Measured (a)Insertion loss (b) Group delay of the multiresonator	75
3.24	Bistatic measurement set up	76
3.25	Tag response 1111 1111	77
3.26	Different tag response of coupled bunch hairpin multiresonator based tag	77
4.1	Conventional microstrip transmission line ($w = 3.4mm$, $h = 1.6mm$ and $\epsilon_r = 3.7$)	85
4.2	Transmission characteristics of the microstrip line ($w = 3.4mm$, $h = 1.6mm$ and $\epsilon_r = 3.7$)	85
4.3	Modified transmission line ($L = 28mm$, $W = 13.8mm$, $h = 1.6mm$, $L_s = 20mm$, $W_s = 7mm$, $L_g = 28mm$, $W_g = 13.8mm$, $\epsilon_r = 3.7$ and $\tan\delta = 0.003$)	86
4.4	Insertion loss of the modified transmission line ($L = 28mm$, $W = 13.8mm$, $h = 1.6mm$, $L_s = 20mm$, $W_s = 7mm$, $L_g = 28mm$, $W_g = 13.8mm$, $\epsilon_r = 3.7$ and $\tan\delta = 0.003$)	86

4.5	Open stub resonator in the bifurcated transmission line ($L = 28mm$, $W = 13.8mm$, $h = 1.6mm$, $L_s = 20mm$, $W_s = 7mm$, $L_1 = 15mm$, $t_1 = 0.3mm$, $L_g = 28mm$, $W_g = 13.8mm$, $W_c = 3.4mm$, $\epsilon_r = 3.7$ and $\tan\delta = 0.003$)	87
4.6	Transmission and reflection characteristics of open stub resonator in the modified microstrip transmission line ($L = 28mm$, $W = 13.8mm$, $h = 1.6mm$, $L_s = 20mm$, $W_s = 7mm$, $L_1 = 15mm$, $t_1 = 0.3mm$, $L_g = 28mm$, $W_g = 13.8mm$, $W_c = 3.4mm$, $\epsilon_r = 3.7$ and $\tan\delta = 0.003$)	88
4.7	Surface current distribution of open stub resonator in the modified microstrip transmission line ($L = 28mm$, $W = 13.8mm$, $h = 1.6mm$, $L_s = 20mm$, $W_s = 7mm$, $L_1 = 15mm$, $t_1 = 0.3mm$, $L_g = 28mm$, $W_g = 13.8mm$, $W_c = 3.4mm$, $\epsilon_r = 3.7$ and $\tan\delta = 0.003$)	89
4.8	Effect of the length variation (L_1) on the insertion loss($L = 28mm$, $W = 13.8mm$, $h = 1.6mm$, $L_s = 20mm$, $W_s = 7mm$, $t_1 = 0.3mm$, $\epsilon_r = 3.7$, $L_g = 28mm$, $W_g = 13.8mm$, $W_c = 3.4mm$ and $\tan\delta = 0.003$)	90
4.9	Effect of thickness Variation(t_1) on insertion loss($L = 28mm$, $W = 13.8mm$, $h = 1.6mm$, $L_s = 20mm$, $W_s = 7mm$, $L_1 = 15mm$, $\epsilon_r = 3.7$, $L_g = 28mm$, $W_g = 13.8mm$, $W_c = 3.4mm$ and $\tan\delta = 0.003$)	91
4.10	Multiresonator circuit in the modified transmission line ($L = 28mm$, $W = 13.8mm$, $h = 1.6mm$, $L_s = 20mm$, $W_s = 7mm$, $L_1 = 18mm$, $L_2 = 17mm$, $L_3 = 16mm$, $L_4 = 15mm$, $L_5 = 14mm$, $L_6 = 13mm$, $L_7 = 12mm$, $L_8 = 11mm$, $s = 0.5mm$, $t = 0.3mm$, $\epsilon_r = 3.7$ and $\tan\delta = 0.003$)	92
4.11	Transmission and reflection characteristics of open stub multiresonators in the modified line ($L = 28mm$, $W = 13.8mm$, $h = 1.6mm$, $L_s = 20mm$, $W_s = 7mm$, $L_1 = 18mm$, $L_2 = 17mm$, $L_3 = 16mm$, $L_4 = 15mm$, $L_5 = 14mm$, $L_6 = 13mm$, $L_7 = 12mm$, $L_8 = 11mm$, $s = 0.5mm$, $t = 0.3mm$, $\epsilon_r = 3.7$, $L_g = 28mm$, $W_g = 10mm$, $W_c = 3.4mm$ and $\tan\delta = 0.003$)	93
4.12	Surface current distribution	94
4.13	(a)Data encoding technique (b) corresponding S21	97
4.14	Different bit combinations compared with 8 bit resonator	99

4.15	Generation of different bit combinations	100
4.16	Photograph of proposed multiresonator compared with INR 1 coin	100
4.17	Photograph of proposed chipless tag	101
4.18	Measured response of byte: 1111 1111 (a) Multiresonator (b) chipless tag	101
4.19	Measured response of byte: 1110 1111(a) Multiresonator (b) chipless tag	102
4.20	Measured response of byte: 1110 1110 (a) Multiresonator (b) chipless tag	103
4.21	Tag response as a function of distance from the reader	104
5.1	(a) Loop resonator coupled with transmission line ($W = 3.4mm$, $W_g = 25mm$, $L_g = 30mm$, $t = 0.3mm$, $R = 7.9mm$, $\epsilon_r = 3.7$ and $h = 1.6mm$) and (b) insertion loss	109
5.2	Surface current distribution of ring resonator at (a) resonant frequency 3.742 GHz and (b) non-resonant frequency 3GHz	109
5.3	Geometry of single loop resonator on slotted ground of transmission line ($W_c = 3.4mm$, $W_g = 25mm$, $L_g = 30mm$, $t = 0.3mm$, $s = 0.5mm$, $R = 7.9mm$, $\epsilon_r = 3.7$ and $h = 1.6mm$)	111
5.4	Insertion loss of loop resonator on truncated ground plane of transmission line ($W_c = 3.4mm$, $W_g = 25mm$, $L_g = 30mm$, $t = 0.3mm$, $s = 0.5mm$, $R = 7.9mm$, $\epsilon_r = 3.7$ and $h = 1.6mm$)	111
5.5	Surface current distribution of slotted ground ring resonator at (a) resonant frequency and (b) non-resonant frequency	112
5.6	(a) Geometry of loop resonator on bifurcated transmission line shorted with ground ($a = 20mm$, $W_c = 3.4mm$, $W_g = 25mm$, $L_g = 30mm$, $t = 0.3mm$, via $diameter = 0.2mm$ $s = 0.5mm$, $R = 7.9mm$, $\epsilon_r = 3.7$ and $h = 1.6mm$)(b) Transmission characteristics of loop resonator on bifurcated transmission line shorted with ground	113
5.7	Surface current distribution of loop resonator on bifurcated transmission line shorted with ground	113

5.8	Geometry of loop resonator on bifurcated transmission line shorted with ground ($W_c = 3.4mm$, $W_g = 25mm$, $L_g = 30mm$, $a = 20mm$, $R_1 = 7.9mm$, $R_2 = 7.1mm$, $R_3 = 6.3mm$, $R_4 = 5.5mm$, $R_5 = 4.7mm$, $R_6 = 3.9mm$, $R_7 = 3.1mm$, $viadiameter = 0.2mm$ and $s = 0.5mm$)	115
5.9	Transmission coefficient of loop resonator on bifurcated transmission line shorted with ground ($W_c = 3.4mm$, $W_g = 25mm$, $L_g = 30mm$, $a = 20mm$, $R_1 = 7.9mm$, $R_2 = 7.1mm$, $R_3 = 6.3mm$, $R_4 = 5.5mm$, $R_5 = 4.7mm$, $R_6 = 3.9mm$, $R_7 = 3.1mm$, $viadiameter = 0.2mm$ and $s = 0.5mm$)	116
5.10	Surface current distribution	117
5.11	Photograph of the shorted loop multiresonator compared with INR 5 coin	119
5.12	Photograph of shorted loop multiresonator based tag	119
5.13	Different measured tag responses	120

List of Tables

3.1	Effect of variation in arm length (a,b) and width (w)	60
3.2	Fractional bandwidth comparison	61
3.3	Geometric parameters of the coupled bunch hairpin multiresonator	63
3.4	Bandwidth, fractional bandwidth and Q at different resonances	64
3.5	Measured transmission characteristics of bunch hairpin resonator on a substrate with ϵ_r 3.7	74
3.6	Measured transmission characteristics of bunch hairpin resonator on a substrate with ϵ_r 4.3	75
4.1	Geometric parameters of the Open stub multiresonators inside the modified transmission line	91
4.2	Resonator length and corresponding frequency	92
4.3	Parametric studies of relative permittivity of resonator medium and corresponding resonance	95
4.4	Parametric studies of height variations of substrate	96
4.5	Measured response of eight bit multiresonator	103
4.6	Fractional bandwidth of Bunch coupled multiresonator and Open stub multiresonator in modified transmission line	104
5.1	Geometric parameters of the shorted ring multiresonator . . .	115
5.2	Shorted loop multiresonator's insertion loss and bandwidth at their resonant frequencies	116
5.3	Comparison of fractional bandwidth	120

Chapter 1

Introduction to Chipless RFID Tags

1.1 RFID Tags

Radio Frequency Identification (RFID) technology has become one of the most advanced and rapidly growing technologies that has the potential to make great economic progress for on many industries. RFID replaces barcode due to its large data carrying capacity, flexibility in its working, and versatility in application. More recent advancements in IC technology are making RFID practical for new applications, such as consumer item level tagging, supply chain management, inventory control, and logistics. The technology can be considered as the future of identification and it has the potential to replace all products that are identified by a number or barcode till date. The cost of the tag is a hindrance for mass deployment of RFID tags for item tagging. Application Specific Integrated Circuit(ASIC) is the main component of RFID tag and this is the reason for the increase in the cost of RFID tags.

Radio Frequency Identification (RFID) is a wireless data capturing technique using electromagnetic waves which are utilized for automatic tracking and identification. RFID is very similar to bar code technology, but it uses radio frequency waves to capture data from tags, rather than laser for the bar codes on a label. The data carrying devices are called RFID Tags or Transponders. Sometimes they are called inlays, which is technically a tag mounted on a substrate that is ready to be converted into a smart label which

carries a transmitting antenna, a receiving antenna and a data storing element such as integrated circuit chip. Sensors can be coupled with a tag to detect the surrounding environmental conditions such as pressure, temperature, the presence of a gas, moisture contents, and location. A reader typically referred to as an RFID interrogator is basically a radio frequency transceiver, that sends the interrogation signals to an RFID tag, which is to be identified. Firmware maintains the interface between the software protocol needed to encode and decode the identification data from the reader and the mainframe or personal computer.

1.2 RFID Applications

RFID has a variety of applications in industrial field where identification is needed. By affixing RFID to an object we can use and manage it to track goods, persons, animals etc. [?, ?, ?, ?, ?, ?, ?, ?, ?, ?]. RFID can be affixed to vehicles, electronic gadgets, books etc. We can use RFID to wirelessly identify something beyond line of sight operations. It stores a small amount of information and can change the information dynamically. The data can be altered during categorization or processing. It can communicate without human intervention and see an object from far away in the case of UHF RFID. In punitive atmospheres with severe filth, dust, moisture and excessive temperature conditions, it will work commendably without failure.

American armed forces used RFID in World War II (1948) to discriminate between friend or enemy aircraft and tanks. The enhanced versions of these systems are still used in defense fields. Years later from World War II the modules of the system were further technologically advanced and applications enhanced. The 1960s were the stage of premature explorations of RFID technology and laboratory experiments. In the early stage of 1970's developers, researchers, corporations, academic institutions and government laboratories were enthusiastically working on RFID and prominent advances were being made at research laboratories and academic institutions like Los Alamos Scientific Laboratory, Northwestern University and the Microwave Institute Foundation in Sweden. During the mid-1970's, large companies such as Raytheons Ray tag and Richard Klensch of RCA were also developing the technology. The development signaled the creation of practical, entirely

passive tags with an operational range of tens of meters. Illustrations of animal tagging examples with microwave systems are available at Los Alamos, Identronix and the inductive systems Europe. After the electronic article surveillance appeared, on the market, it was the first large-scale system of this kind.

In 1980's RFID reached commercial applications i.e, it was the decade of full implementation of RFID technology. In U.S. it was extensively used for transportation and personal access purposes. In Europe the greatest attentions were for short range systems for animals, engineering and commercial applications. Toll roads in Italy, France, Spain, Portugal and Norway were fortified with RFID. Vital to the rapid development of RFID applications was the development of personal computer that permitted, suitable and economical collection and management of data from these systems. 1990's were a significant epoch for RFID i.e, the development of standards. It was widely set up and became a part of daily life. Both inductive and microwave technologies were employed which discovered a wide variety of other applications in commerce. Companies such as Microdesign, CGA, Alcatel, Bosch and Philips were among them. At the end of the 20th century RFID was used not only for the electronic toll collection but also for parking lot access, fare collection, gated public access, campus access, as implants for animal identification and as an electronic immobilizer. The 21st century opened immense area of applications such as access / security cards, tracking, management, transactions, ticketing, labeling, logistics and distribution etc., with the smallest RFID tags.

1.3 RFID Classifications

RFID systems are commonly categorized, or differentiated, in one or more of the following ways, which includes describing the differences, advantages and disadvantages of the different types of tags that are commercially available. The following topics are covered in detail in this chapter.

- How RFID tag is powered
- Frequency of operation
- With or without an electronic chip

1.3.1 How RFID Tag is Powered

The tag requires power for communicating information to the reader through the antenna. Based on the way the RFID tags are powered, they can be classified as passive tags, semi-passive tags and active tags. Each type of tag has its own advantages and disadvantages that should be carefully considered when designing an RFID system.

Passive RFID Tags

Passive RFID tags are excited by the RFID reader. To power the tag circuitry, the tag relies on electromagnetic power obtained from the RFID reader antenna. Since the passive tags do not have their own power sources, the designs can be simple and inexpensive. Passive tags should be in close proximity to the reader antenna in order to obtain sufficient power to transmit a signal. The advantages of passive RFID Tag include:

- Less expensive
- Compact sizes
- Greater operational life
- Environmental robustness

Nowadays, very small size RFID tag approximately the size of a rice grain is used for different applications. The small size of passive tags also means that they are thin and very light. The compact size of RFID allows great flexibility in applications like animal tracking and individual sports competitions. Greater operational life is achieved by the lack of an internal power source. Since no internal power source is necessary, the tag cannot become non-operational due to battery depletion. In contrast, active tags must have their batteries replaced every three to four years, depending on the exact nature of usage. Passive tags can last for decades, depending on how they are treated. Since passive RFID tags do not have a provision for a battery, they may be hermetically sealed during manufacturing. So this makes passive RFID tags inherently environmentally robust. Since the tag is sealed, moisture cannot enter the tag.

The disadvantages of passive RFID Tag are

- Lower range
- Lesser Identification capability
- Low efficiency

The disadvantage of all kinds of passive tags is their extremely limited range. The lower range capabilities of passive tags have both advantage and disadvantage. From a blessing standpoint, the reduced range is advantageous for privacy reasons. The downside to lesser range is that a passive RFID system is much more sensitive to bad reads. The system must ensure that the tag is in closer proximity to the RFID reader antenna. A second major drawback of passive tags is their low identification capability.

Active RFID Tags

When compared to passive tags, active tags contain an on-board power source. It is usually in the form of a small power source, which powers both the tag's on-board antenna and internal circuitry.

These tags conserve battery power by normally existing in a sleep mode. The tag wakes up or is activated upon entrance into an RFID system interrogation zone. When the tag is powered it provides data to the RFID system as requested. The operational life of an active tag can be lengthened when it can be put in a sleep mode while not in use. The length of the battery life is dependent on the time the tag is activated. The existence of an internal power source yields both advantages and disadvantages to the RFID system designer. The major advantages are greater range and greater identification capability. The disadvantages are more expensive, lesser operational life and large physical size.

Semi-passive RFID Tags

RFID tags can also be designed with features found in both passive and active tags. These techniques are implemented to retain the advantages while eliminating the disadvantages of each type. These tags typically use an internal battery to power the circuits that are internal to the tag. Usually, circuitry on semi-active tags includes sensors for monitoring environmental conditions

such as humidity and temperature. When compared to active tags, the semi-active tag does not use its internal power source to communicate with the antenna. In the field of communications, this tag relies on electromagnetic field power received from the system's antenna. By preserving its internal power in this manner we can greatly extend the internal battery life.

1.3.2 Chip RFID and Chipless RFID

Chip RFID tag contains integrated circuits to store unique identification code. Chip RFID is further classified on the basis of how it is powered, whether the memory is re-writable or not, writing capabilities and frequency of operation. Due to the use of the silicon chip, the tag is more expensive than the other identification method.

Chipless RFID tag is less expensive due to the absence of power source and silicon microchip. Most chipless RFID systems use the electromagnetic properties of various designs of conductor layouts/ shapes and/or materials to achieve particular electromagnetic properties/ behavior. The major challenge in designing a chipless RFID tag is how to encode data, without the presence of a memory chip. To overcome this problem, two general types of RFID tags can be identified: Time Domain Reflectometry (TDR) based and spectral (frequency) signature-based chipless RFID tags. There have been some reported chipless RFID tag developments in recent years. The main focus of this thesis will be on chipless RFID systems.

The low cost chipless RFID has the potential to provide low cost item tagging and thus replace the optical barcode from markets. The solution is to make the tag chipless and printable on low cost substrate such as plastics and papers, realizing that the chipless RFID technology is the only way of competing with existing tagging technologies. Depending on the technology used chipless RFID tag classified into two types

1. Spectral Signature Based Chipless Tags
2. Time Domain Reflectometry Based Chipless Tags

Different types of spectral signature based chipless tags is overviewed in the next chapter. The following section gives a brief discussion of Time domain reflectometry based chipless tags.

1.3.3 Time Domain Reflectometry Based Chipless Tags

Time Domain Reflectometry (TDR) is a microwave measurement technique to evaluate the time domain response of any electromagnetic system. TDR is used to determine all the effects of the system, including geometry and electrical properties by observing the reflected waveform. Various chipless RFID tags have been reported using TDR-based technology for data encoding. Such tags are interrogated by sending a signal from the reader in the form of a pulse and observing the echoes of the pulse sent by the tag. A train of pulses is thereby generated, which can be used to encode data. Two different types of TDRs based tags are available in market. They are

1. Surface acoustic wave tag
2. Delay line based tag

Surface acoustic wave tag

Surface Acoustic Wave (SAW) tag was first developed by RFSAW Inc., [?]. SAW tags are based on the piezoelectric effect and on the surface related dispersion of acoustic(elastic) waves at low speed. If a crystal is elastically deformed in a certain direction, surface charges will be produced and hence electric voltages are developed. Conversely, the application of a surface charge to a crystal leads to an elastic deformation in the crystal grid. Usually Surface acoustic wave devices are operated at microwave frequencies, normally at ISM bands.

Surface acoustic wave transducers are used for wireless label system [?,?]. The system consists of a pulsed transmitter, time gated receiver, phase detector and surface acoustic wave tag. SAW tag consists of interdigital electro-acoustic transducers and reflectors fabricated on piezoelectric substrates such as Lithium niobate ($LiNbO_3$) or lithium tantalate using planar electrode structures. The interdigital transducer is positioned at the end of a long piezoelectrical substrate, and a suitable dipole antenna operating at the required frequency is attached to its busbar. The interdigital transducer is used to convert electrical signals to acoustic surface waves and vice versa.

A high frequency pulse generated by the reader is send through its transmitting antenna. The dipole antenna of the transponder receives this interrogating signal, is supplied to the interdigital transducer and it converts the RF

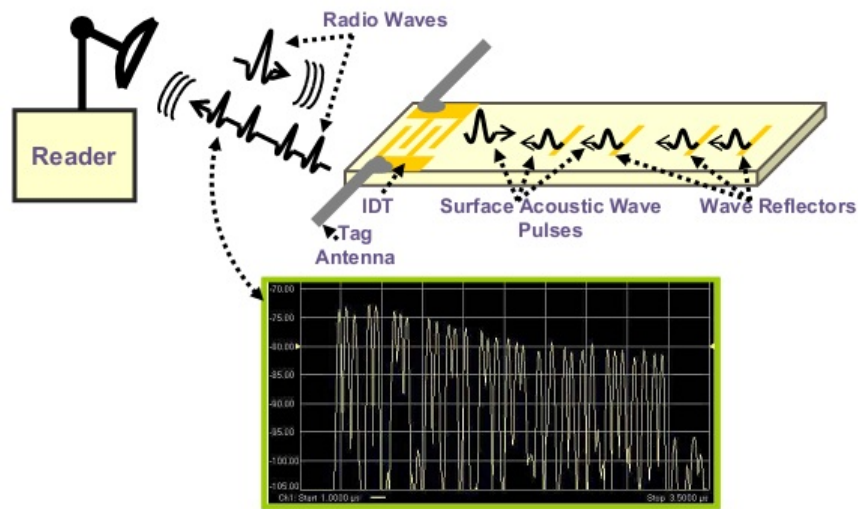


Figure 1.1: 128-Bit Global SAW tag and reader system (Courtesy: Clinton. S. Hartmann et. al.) [?]

signal into an acoustic surface wave, which flows through the substrate along the longitudinal direction. The frequency of the surface wave corresponds to the carrier frequency of the sampling pulse. The carrier frequency of the reflected and returned pulse sequence thus corresponds with the transmission frequency of the sampling pulse. A part of the surface wave is reflected by the reflective strips distributed across the substrate, while the remaining part of the surface wave travel to the end of the substrate and is absorbed there. The reflected parts of the wave travel back to the interdigital transducer, where they are converted into a high frequency pulse sequence and are radiated by the dipole antenna. This pulse sequence can be received by the reader. The number of pulses received corresponds with the number of reflective strips on the substrate as depicted in Figure 1.1. Likewise, the delay between the individual pulses is proportional to the spatial distance between the reflector strips on the substrate. The spatial layout of the reflector strips can represent a binary sequence of digits. Due to the slow speed of the surface waves on the substrate the first response pulse is only received by the reader after a dead time of around 1.5ms relative to the transmission of the scanning pulse. This gives decisive advantages for the reception of the pulse. The data storage capacity and data transfer speed of a surface wave transponder depend upon

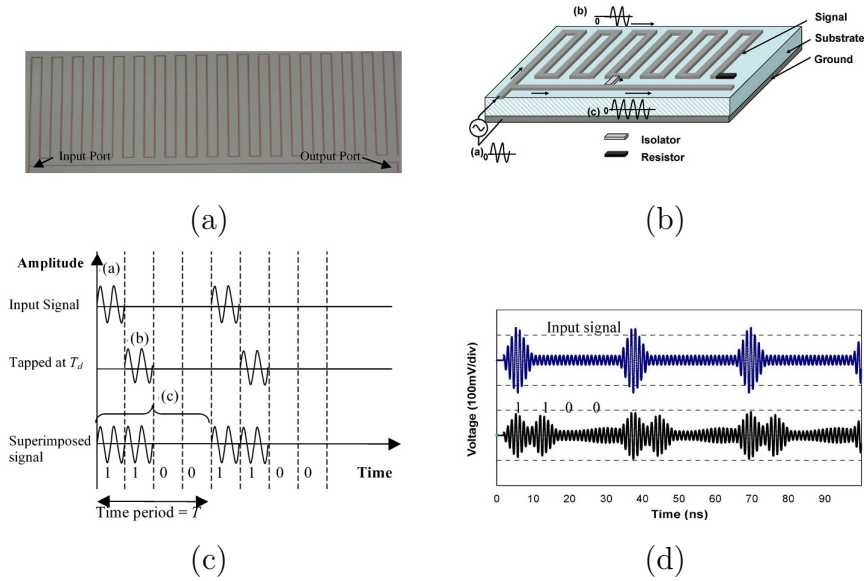


Figure 1.2: (a) Transmission delay line based ID generation circuit (b) Schematic diagram of transmission delay line based ID generation circuit (c) Binary code generation by the superimposition of delayed signals and (d) Input and output waveforms of the ID (Courtesy: Aravind Chamarti) [?]

the size of the substrate and the realizable minimum distance between the conducting strips on the substrate.

Delay line based tag

Transmission delay line based ID generation circuit is presented for Radio Frequency Identification (RFID) [?, ?, ?, ?, ?, ?]. The concept of binary code generation by the superimposition of the delayed signals is illustrated [?] and depicted in Figure 1.2. Obtainable delays, dependent on the frequency of operation, the length of the delay line and such circuits are sufficient for ID generation. This circuit receives the input signal from the antenna, generates the ID code, and sends the generated code back to the antenna.

1.4 Motivation of Thesis

Nowadays the barcode is being replaced by RFID tag. The cost of existing RFID tag is much higher than the price of barcode. In order to lowering the price of RFID tag, we have to do research in it. So the primary aim of the project is develop a fully printable chipless RFID tag for low cost item tagging.

Spectral signature based chipless RFID tag requires compact, narrow band, planar multiresonator circuit. The multiresonator is an essential component of all types of spectral signatures based chipless tag. Hence the thesis is completely focused on multiresonator circuits with a narrow band. The bistatic radar principle or monostatic radar principle is used for reading the spectral signature based tag [?, ?, ?]. Depending on the technology, which is used by the reader the tag may consist of transmitting and receiving antennas, i.e, the spectral signature scattering based tag consists of multiresonators [?, ?, ?].

Preradovic et. al. presented a reading technique used for demonstrating the multiresonator circuit for chipless tag applications [?]. In this method the tag consists of two orthogonally polarized antennas connected with multiresonator. The multiresonating circuit modulates the interrogation signal and re-transmits to the reader through transmitting antenna.

The cascade spiral resonators and C-shaped resonators have low surface code density(bit/cm^2) [?, ?, ?, ?]. Here some techniques are proposed for improving compactness and quality factor with high surface code density. The different kinds of multiresonators such as coupled bunch hair pin resonator, open stub in the bifurcated transmission line and loop resonators on bifurcated transmission line shorted with via are discussed in the following chapters.

1.5 Thesis Organization

The thesis is organized as follows: Chapter 1: Introduction, The chapter gives a brief discussion of RFID tag applications and classifications.

Chapter 2: Literature Survey: This chapter presents a comprehensive review of available chipless RFID tags on the market and reported in the literature. Different types of chipless RFID tags based on different encoding techniques are reviewed with illustrations. Even though the technology is still

in its infancy, a number of developments have already been made in the industry, which are overviewed here. A comprehensive overview of the operating principle of spectral signature based chipless RFID systems is presented, followed by a description of different reading techniques used in the chipless tag reader. This chapter also covers a brief description of different types of planar resonators.

Chapter 3: Coupled bunch Hairpin Resonator Based Chipless Tag: A novel idea of coupled bunch hair pin resonator is introduced for realizing multiple resonances. Here a thorough study of parallel coupled line resonator, couple hairpin resonator and disc loaded monopole are carried out. Parametric studies and optimization of coupled bunch hair pin resonator is explained. It is noted that each resonance can be independently controlled by varying the length of the corresponding resonator and optimization of multiresonating circuit which is used for multiple bit data encoding. Finally, the chipless RFID tag using coupled bunch multiresonator is realized.

Chapter 4: Open Stub and Open Loop Multiresonator Based Chipless RFID Tag: This chapter explains the open stub and open loop multiple resonators placed in a bifurcated transmission line for creating multiple resonances. The chapter also describes the advantages and disadvantages of the same along with all the parametric studies and bistatic measurement results.

Chapter 5: Closed Loop Multi-resonator Based Chipless RFID Tag: The closed loop multiresonators placed in the bifurcated transmission line for creating multiple resonances is reported in this chapter. The theory behind closed loop multi resonator and its bistatic measurement results are also discussed.

Chapter 6: Conclusions and future scope of work: All the relevant points about the present research are concluded in the thesis with the insight to future studies. The thesis also includes the bibliography and a list of publications by the author in the related field.

REFERENCES

- [1] K. Ahsan, H. Shah, and P. Kingston, "RFID Applications : An Introductory and Exploratory Study," *IJCSI International Journal of Computer Science Issue*, vol. 7, no. 1, pp. 1–7, 2010.

- [2] Deborah Platt Majoras, Orson Swindle, Thomas B. Leary, Harbour, Pamela Jones and Jon Leibowitz, “Radio Frequency Identification : Applications and Implications for Consumers,” *A Workshop Report from the Staff of the Federal Trade Commission*, pp. 1–54, 2005.
- [3] Jeremy Landt, “ The History of RFID,” *IEEE Potentials*, pp. 8–11, 2005.
- [4] Martin Brandl, Karlheinz Kellner, Martin Miundlein, and Johann Nicolics , “Low-Cost wireless Transponder System for Industrial and Biomedical Applications ,” *ICICS 2005*, pp. 1444–1447, 2005.
- [5] Murali Kodialam, Thyaga Nandagopal, and Wing Cheong Lau, “Anonymous Tracking using RFID tags,” *proc.of IEEE Infocom 2007*, pp. 1217–1225, 2007.
- [6] Hui Tan , “The Application of RFID Technology in the Warehouse Management Information System,” *2008 International Symposium on Electronic Commerce and Security*, pp. 1063–1067, 2008.
- [7] Dianmin Vue, Xiaodan Wu, and Junbo Bai , “RFID Application Framework for Pharmaceutical Supply Chain,” *Service Operations and Logistics, and Informatics, 2008. IEEE/SOLI 2008. IEEE International Conference*, pp. 1125–1130, 2008.
- [8] Dong-liang Wu, Wing W Y Ng, Daniel S Yeung, and Hai-lan Ding , “A Brief Survey On Current Rfid Applications,” *Proceedings of the Eighth International Conference on Machine Learning and Cybernetics, Baoding 2009*, no. July, pp. 2330–2335, 2009.
- [9] Chia-Hung Huang, “An Overview of RFID Technology , Application , and Security / Privacy Threats and Solutions,” *Spring 2009*, pp. 1–20, 2009.
- [10] Tudor Ioan Cerlinca, Cristina Turcu, Cornel Turcu, and Marius Cerlinca , “RFID-based Information System for Patients and Medical Staff Identification and Tracking,” *Intech-Sustainable Radio Frequency Identification Solutions*, no. February, 2010.
- [11] C. Hartman, “Future High Volume Applications Of Saw Devices,” *IEEE Transactions on Sonics and Ultrasonics*, 1985.

- [12] Halvor Skeie, SanJose, Donald Armstrong, and Belmont, “Passive Interrogator Label System With A Surface Acoustic Wave Transponder Operating At Its Third Harmonic And Having Increased Bandwidth,” *United States Patent*, no. 19, 1988.
- [13] F. J. Herraiz-martínez, F. Paredes, and G. Z. González, “Printed Magnetoinductive-Wave (MIW) Delay Lines for Chipless RFID Applications,” *IEEE Transactions On Antennas And Propagation*, vol. 60, no. 11, pp. 5075–5082, 2012.
- [14] Aravind Chamarti, K.Varahramyan, “Transmission Delay Line Based ID Generation Circuit for RFID Applications,” *IEEE Microwave And Wireless Components Letters*, vol. 16, no. 11, pp. 588–590, 2006.
- [15] S. Hu, Y. Zhou, and C. L. Law, “Study of a Uniplanar Monopole Antenna for Passive Chipless UWB-RFID Localization System,” *IEEE Transactions On Antennas And Propagation*, vol. 58, no. 2, pp. 271–278, 2010.
- [16] J. Vemagiri, A. Chamarti, M. Agarwal, and K. Varahramyan, “Transmission line delay-based radio frequency identification (rfid) tag,” *Microwave And Optical Technology Letters*, vol. 49, no. 8, pp. 1900–1904, 2007.
- [17] Sudhir Shrestha, and Mercyma Balachandran, “A Chipless RFID Sensor System for Cyber Centric Monitoring Applications,” *IEEE Transactions On Microwave Theory And Techniques*, vol. 57, no. 5, pp. 1303–1309, 2009.
- [18] S. Shrestha, J. Vemagiri, M. Agarwal, and K. Varahramyan, “Transmission line reflection and delay-based ID generation scheme for RFID and other applications,” *Int. J. Radio Freq. Identification Tech*, vol. 1, no. 4, pp. 401–416, 2007.
- [19] S. Gupta, B. Nikfal, and C. Caloz, “Chipless RFID System Based on Group Delay Engineered Dispersive Delay Structures,” *IEEE Antennas And Wireless Propagation Letters*, vol. 10, no. 2, pp. 1366–1368, 2011.
- [20] Arnaud Vena, Etienne Perret, and Smail Tedjini , “Chipless RFID Tag Using Hybrid Coding Technique,” *IEEE Transactions on Microwave Theory and Techniques*, vol. 59, no. 12, pp. 3356–3364, Dec. 2011.

- [21] Arnaud Vena, Etienne Perret, and Smail Tedjini , “High-Capacity Chipless RFID Tag Insensitive to the Polarization,” *IEEE Transactions on Antennas and Propagation*, vol. 60, no. 10, pp. 4509–4515, Oct. 2012.
- [22] Arnaud Vena, Etienne Perret, and Smail Tedjini, “Design of Compact and Auto-Compensated Single-Layer Chipless RFID Tag,” *IEEE Transactions on Microwave Theory and Techniques*, vol. 60, no. 9, pp. 2913–2924, Sep. 2012.
- [23] A. Vena, A. A. Babar, L. Sydänheimo, M. M. Tentzeris, and L. Ukkonen, “A Novel Near-Transparent ASK-Reconfigurable Inkjet-Printed Chipless RFID Tag,” *IEEE Antennas and Wireless Propagation Letters*, vol. 12, pp. 753–756, 2013.
- [24] Arnaud Vena, Smail Tedjini, and Etienne Perret , “A Fully Printable Chipless RFID Tag With Detuning Correction Technique,” *IEEE Microwave and Wireless Components Letters*, vol. 22, no. 4, pp. 209–211, Apr. 2012.
- [25] Arnaud Vena, Etienne Perret, and Smail Tedjin, “A Depolarizing Chipless RFID Tag for Robust Detection and Its FCC Compliant UWB Reading System,” *IEEE Transactions on Microwave Theory and Techniques*, vol. 61, no. 8, pp. 2982–2994, Aug. 2013.
- [26] Stevan Preradovic, Isaac Balbin, and Nemaï Chandra Karmakar, and Gerhard F Swiegers , “Multiresonator-Based Chipless RFID System for Low-Cost Item Tracking,” *IEEE Transactions on Microwave Theory and Techniques*, vol. 57, no. 5, pp. 1411–1419, May 2009.
- [27] Shrestha, Sudhir and Balachandran, Mercyma, “A Chipless RFID Sensor System for Cyber Centric Monitoring Applications,” *IEEE Transactions on Microwave Theory and Techniques*, vol. 57, no. 5, pp. 1303–1309, May 2009.
- [28] Li Yang, Rongwei Zhang, and Daniela Staiculescu , “A Novel Conformal RFID-Enabled Module Utilizing Inkjet-Printed Antennas and Carbon Nanotubes for Gas-Detection Applications,” *IEEE Antennas and Wireless Propagation Letters*, vol. 8, pp. 653–656, Aug. 2009.

- [29] Won-seok Lee, Hyung-seok Jang, Kyung-sub and Jong-won Yu , “Design of Chipless Tag with Electromagnetic Code for Paper-based Banknote Classification,” *Microwave Conference Proceedings (APMC), 2011 Asia-Pacific*, pp. 1406–1409, 2011.

Chapter 2

Literature Review of Chipless Tags

-
1. Introduction
 2. Spectral Signature Based Chipless Tags
 3. Chipless RFID Tag Reading Technique
 4. Planar Resonators
-

This chapter presents a comprehensive review of chipless RFID tags available in the open literature. Different types of chipless RFID tags based on different encoding techniques are reviewed. Even though the technology is still in its infancy, a number of developments have already been made in the industry are overviewed here. Different kinds of data decoding technique and processing in reader are overviewed. Planar multiresonator is the basic component of spectral signature based chipless tags. So a detailed overview of the work on planar resonator is carried out.

2.1 Spectral Signature Based Chipless Tags

Most chipless RFID systems use the electromagnetic properties of materials and/or various conductor layouts to achieve particular electromagnetic signatures. The spectral signature of an object is a function of the incident electromagnetic wavelength and material interaction with it. Spectral signature modulation is performed by both material and layout printed on the substrate. The presence of a specific resonance is used to encode logic 1 and absence of the specific resonance is used to encode logic 0. The layout may consist of antennas with different resonant frequencies alone or an antenna associated with some other microwave circuits such as resonators, impedance varying structures etc., for making spectral signature. Modulation is performed either in magnitude, phase or group delay. The magnitude is modulated in the form of and phase are modulated in the form of magnitude attenuation and phase as phase variations at the resonant frequencies of the corresponding resonators.

Each data bit is usually associated with the presence or absence of a resonant peak at a predetermined frequency in the spectrum. Generally structures with high Quality factor are used for encoding data in spectrum so that it exhibits narrow bandwidth which helps to accommodate large number of bits in particular frequency range with distinct resonant frequency. This improves efficiency, readability and reliability of the tag. This section presents a comprehensive review of spectral signature based chipless RFID.

Capacitively tuned dipoles for RFID barcode is first reported by Jalaly and Robertson [?] shown in Figure 2.1. Here RF barcode technique is presented using arrays of identical planar dipoles capacitively tuned to be resonant at different frequencies within the desired frequency bands, which absorbs energy from a reader/interrogator corresponding to its resonance. This multi-bit read only tag exhibits 1:1 corresponding to a data bit. Both width and length of the dipole has good control over the resonant frequency, with high resolution.

Spectral signature based space filling curve RFID tags were first reported by McVay [?]. These tags are designed by Peano and Hilbert curves which acts as a compact resonator with high Q-factor and large scattering characteristics as illustrated in Figure 2.2. The compactness is achieved by higher order iteration of the space filling curves. But the tag requires significant structural modification for encoding different bit patterns.

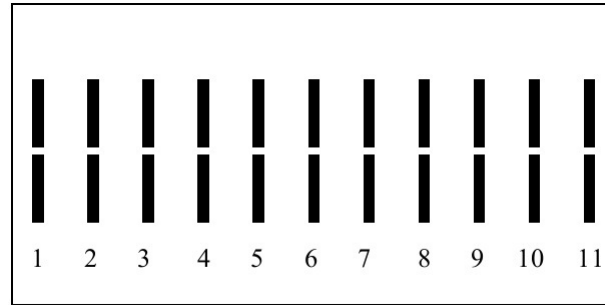


Figure 2.1: Capacitively-tuned planar dipoles for RFID Barcodes (Courtesy: I. Jalaly) [?]

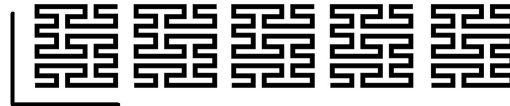


Figure 2.2: Five bit peano-curve based tag (Courtesy: John Mc Vay) [?]

A fully printable chipless RFID tags using multiresonators are proposed by Preradovic et.al. in [?, ?]. The working principle of the RFID system is based on retransmission of interrogated signal with encoded ID. The tag consists of multiresonators, transmitting and receiving antennas. The unique ID is encoded as the spectral signatures which is created by a set of cascaded spiral resonators designed to resonate at different frequencies with high Q-factor to create stop bands. Each data bit is represented by a particular frequency in the predetermined frequency spectrum and the variation of the amplitude or phase is used for data encoding. Wide band omnidirectional antenna is used in the tag. In order to avoid interference between interrogation signal and encoded signal, the antennas are cross-polarized in both transponder and reader. Spiral multi-resonators will perform band-stop filtering of the continuous wave interrogation signal and hence create the spectral signature. The signature can be decoded by the reader after being received. Here spectral signature modulation is performed in both magnitude and phase of the spectrum. The photograph of spiral resonator based spectral signature tag as shown in Figure 2.3.

Printable chipless RFID system on a 90- μm thin Taconic TF-290 laminate

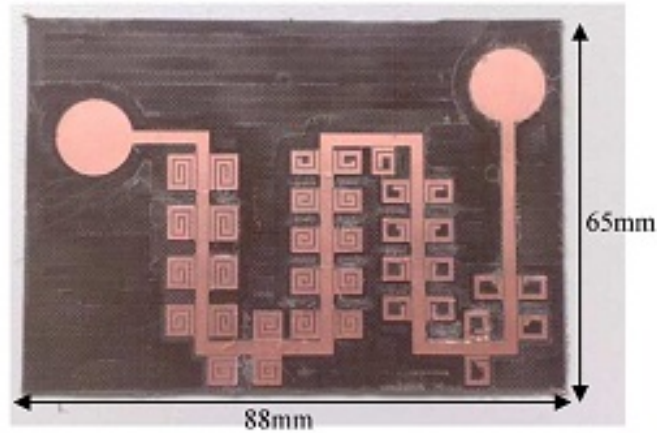


Figure 2.3: Spiral resonator based 35-bit spectral signature chipless tag (Courtesy: S. Predrovic et. al.) [?]

is presented in [?, ?, ?]. For the first time 35 spiral resonators with two cross-polarized transmitting and receiving antennas are used for spectral signature chipless RFID [?, ?]. The chipless tag [?] comprises of two multiresonating circuits and one broadband power divider to reuse the frequency band to yield more number of bits.

A back scatter based chipless RFID tag consisting of single UWB antenna and cascaded Electromagnetic Band Gap (EBG) spiral resonators with high Q-factor is described in [?, ?]. EBG structure is used for making multiple band notch filter circuit. The advantage of this type of tag is that it does not require strict alignment between the tag and the reader. It has an antenna which reduces the overall size.

Taeik Kim et al suggest a chipless RFID tag [?] as an alternative of barcode, that consists of transmitting antenna, receiving antenna and a single band stop resonator. The band stop frequency can be adjusted by changing the cutting position of the resonator and it has low data capacity. Saming Hu et. al., proposed a backscattering based chipless RFID tag which introduces meandrous time delay line integrated within the antenna for generating unique ID in both time domain and frequency domain [?].

Predarovic et.al. [?] propose a chipless tag that encode data into the spectral signature of millimeter wave range multiresonators. The millimeter chipless RFID tag [?] consists of orthogonally polarized slot loaded millimeter

UWB circular patch antennas. The slot on the patch determines individual resonant frequency signature hence the number of data bits.

Chipless tag with integrated sensor element is used to detect various automated monitoring applications. The sensor element is attached to dedicated resonator tag [?]. These sensor elements may be capacitive or resistive. The resistive sensor output changes the Q factor of the spiral resonator by effectively changing its insertion loss at the resonant frequency. The capacitive sensor can change the spiral resonator.

Real time temperature sensor using the dielectric property of temperature dependent high K polyamides is proposed in [?]. Introducing high K dielectric material changes the equivalent capacitance of the LC resonator which varies with environment temperature. Results verify that a dedicated resonator can perform the sensing whereas the other cascaded resonators resemble the ID of the tag. A multiresonator chipless RFID temperature sensor is proposed having dual performance of tagging and sensing temperature simultaneously.

Spectral signature based near field card using split ring resonators [?] exhibits frequency selective property with deep rejection in the vicinity of resonant frequency. The near field chipless card reader has a guiding wave structures such as waveguide or transmission line to detect the presence of tag with predetermined frequencies. Conductive ink is used for fabricating SRR on thin paper based materials [?]. The tag is made of two multiple slot-loaded rectangular patches [?]. Slots with adjacent frequencies are placed alternately into two patches to reduce the mutual coupling between the slot resonators. The tag measurements are done for both proximity reading and slot card reading techniques. The variable slot length influences the resonance frequency.

Chipless RFID system using Pulse Position Modulation (PPM) coding based on group delay is reported in [?]. This system employs transmission-type all-pass dispersive delay structures (DDSs) to assign the PPM code onto the interrogating signal.

If an impulse plane wave is incident on a structure, it scatters in a unique fashion. The structural information of an object can be extracted by analyzing the late-time scattered field as the impulse response of the structure [?]. The echo of scattered field, which represents the source-free response of the structure, contains a summation of damped sinusoids. The damping factor and

frequency of these damped sinusoids are uniquely associated with the structural information and can be used to identify an unknown object. To create uniquely identifiable scattered fields from an object by incorporating notches in the structure giving rise to specific damped sinusoids in the source free scattered field of the structure as shown in Figure 2.4. Data is encoded as complex natural resonant frequencies in the structure and is retrieved from the scattered field. Data retrieval is based on Singularity Expansion Method (SEM) analysis using target identification techniques. Each complex frequency pole provides two dimensional data (real and imaginary) which can be extracted from the echo impulse response of the structure using a numerical technique such as the Matrix Pencil Method.

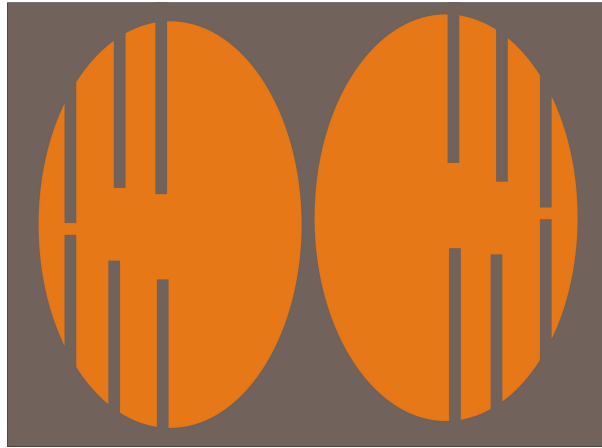


Figure 2.4: Notched elliptical dipole tag using SEM method (Courtesy: Andrew T. Blischak et. al.) [?]

A hybrid coding technique is introduced by combining phase deviation and frequency position encoding that proposed in [?]. The proposed tag has five hair pin resonators having resonance frequency within the band of 2.5 GHz to 7.5 GHz with 22 bit coding capacity.

A spectral signature tag integrated with a permittivity sensor which contains a dual-band capacitive loaded resonator [?]. The first resonance is used for identification and the second resonance is used for sensing the dielectric constant of the material attached to the tag.

Slot-loaded dual-polarized chipless radio frequency identification tag is presented in [?]. The tag comprises of four rectangular metallic patches loaded

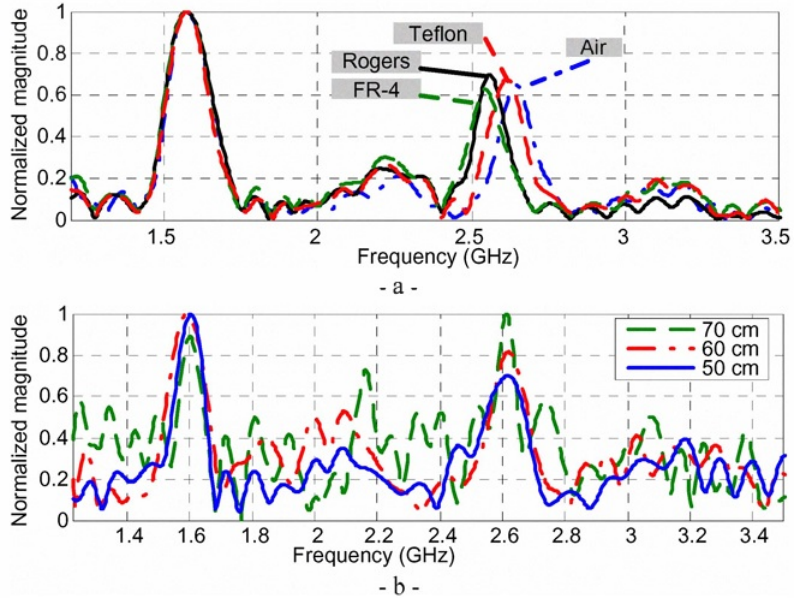


Figure 2.5: Normalized detected amplitude for five materials and for Teflon at several distances tag-reader (Courtesy: David Girbau et. al.) [?]

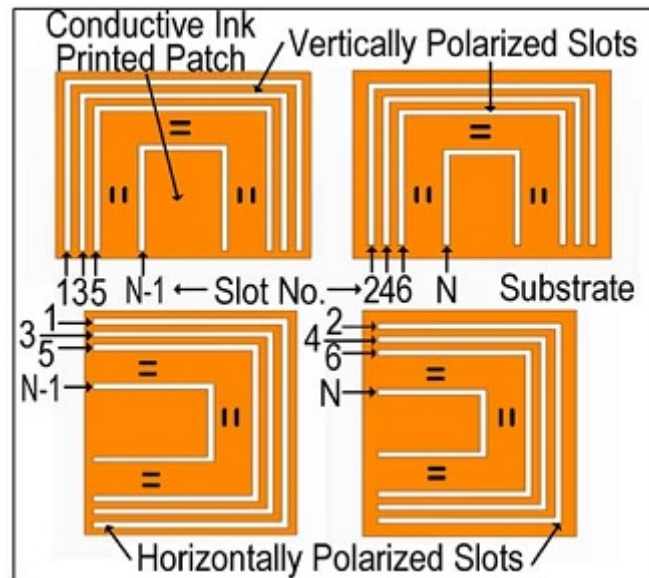


Figure 2.6: Dual polarization slotted tag (Courtesy: Md. Aminul Islam et. al.) [?]

with multiple slot resonators as shown in Figure 2.6. Slots with the same polarization for adjacent frequencies are placed alternately into two patches to reduce the mutual coupling between them. Then two similar sets are placed in horizontal and vertical polarization to double the number of bits within the same frequency bandwidth. The tag can be detected using dual-polarized antennas.

A UWB linear chirp signal is employed for reading multi-resonator based chipless RFID tags based on a bi-static coherent frequency modulated continuous wave (FMCW) radar technique [?]. Hilbert transform is used to extract the envelope and phase information of the received signal from the chipless tag.

3^n words can be coded in a tag when using n -stub-loaded dual-band resonators as shown in Figure 2.7. This can increase the number of bits coded in each resonator with increased the operational bandwidth [?]. Background subtraction and time gating technique have been used to extend the range of chipless tag.

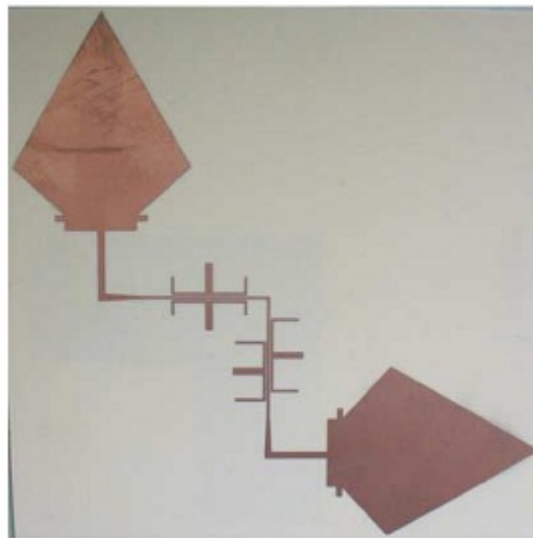


Figure 2.7: Spectral signature tag based on dual band resonators (Courtesy: David Girbau et.al.) [?]

An ultra-wideband impulse radar based reader interrogates the chipless tag with a UWB pulse and the received backscatter is analyzed in the time domain [?]. The backscattered signal constitutes the structural mode and the

antenna mode and their spectral contents are analyzed. Antenna mode back scattered signal contains the information carrying signal while the structural mode contains no information about the tag.

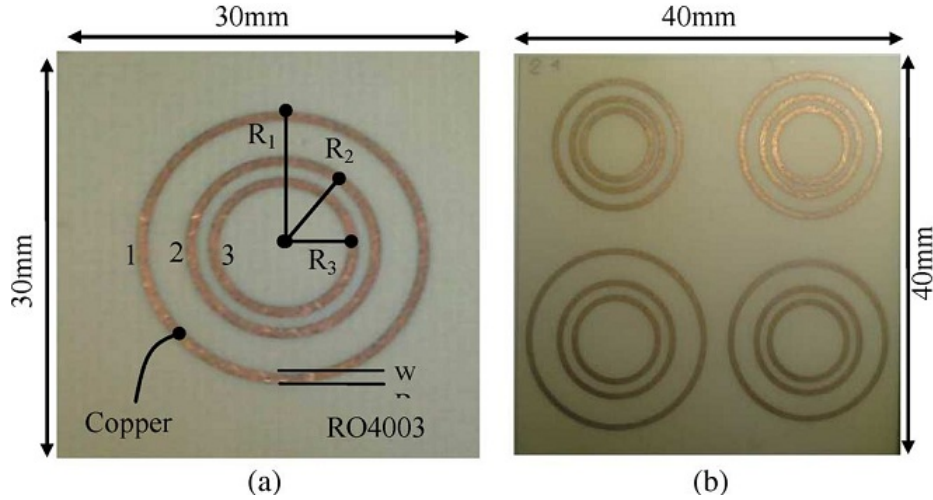


Figure 2.8: Concentric circular ring chipless tag (Courtesy: A. Vena et. al.) [?]

A polarization independent concentric ring structure is discussed in [?]. RCS from the tag is used to decode the spectral signature. The coding capacity of this tag reaches 19 bits within a compact structure $3 \times 3 \text{ cm}^2$ i.e. 2.1 bits/cm^2 as shown in Figure 2.8.

In order to separate a large number of frequency values in a particular bandwidth, the frequency band required to represent resonance has to be as small as possible. To achieve this condition, the quality factor of each resonance has to be sufficiently very high, but the large quality factor also causes a poor immunity to the surrounding environment. Increasing the number of resonators is an evident way to increase the capacity of coding. The number of coding resonators is limited by their size and mutual coupling [?]. The proposed tag depicted in Figure 2.9 is based on a multiple band co-planar strips resonator with open ended extremities.

Detuning correction technique is used for data encoding [?]. The structure consists of 20 hairpin resonators without ground plane. Absence of resonance is created by fill the slot of hairpin. Consequently, the predetermined resonant frequency shifts to higher frequency that is out of desired frequency spectrum and represent logic 0. Scattering technique is used for identifying the unique spectral ID.

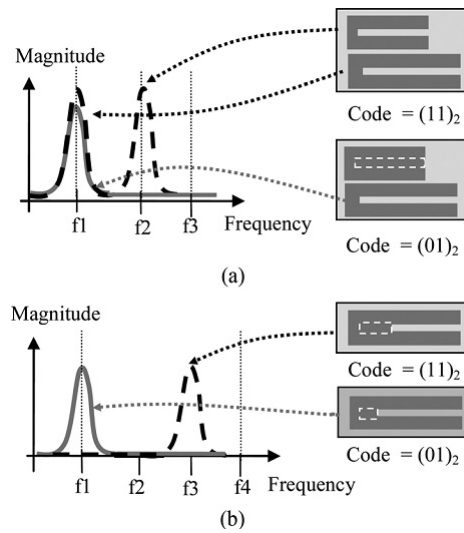


Figure 2.9: Chipless tag using two different coding approaches: (a) absence/presence of resonances and (b) frequency shift and absence/presence of resonances (Courtesy: A. Vena et. al.) [?]

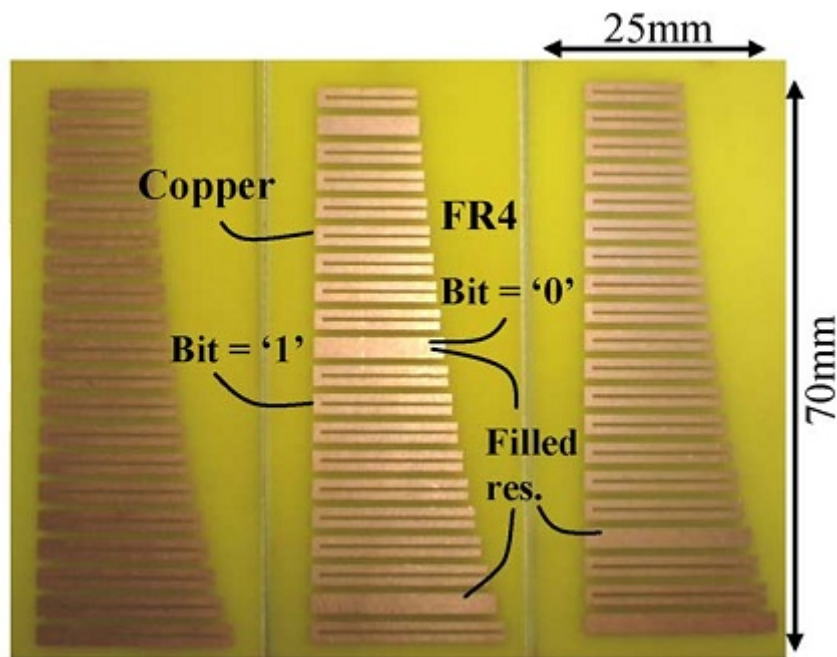


Figure 2.10: 20-bit chipless tags (Courtesy: A.Vena et. al.) [?]

Depolarized tag with dual L resonators and 45° tilted shorted dipoles as shown in Figure 2.11 are reported in [?]. When incident EM wave impinges the conductive strips of the tag, the resonator excites and creates some surface currents on the conducting strips. This is the first time response. Depending on the conductor layout, a standing wave mode can be created so that a resonant behaviour may appear. The EM response of a tag is usually dependent on the polarization of the incident wave as well as its direction. The polarization independency of L resonators and 45° tilted shorted dipoles are used. Substrate integrated cavity resonator based tag encodes the data by changing the effective permittivity which gives a unique frequency signature [?] as shown in Figure 2.12. In this work high quality factor of substrate integrated resonator is utilized for tag design.

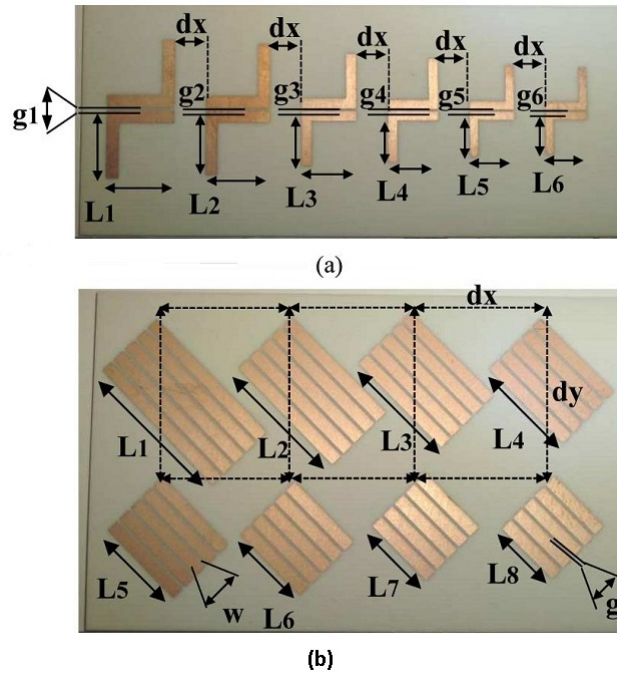


Figure 2.11: (a) Tag based on dual-L resonators (b) Tag based on shorted dipoles oriented at 45° (Courtesy: A. Vena et. al.) [?]

Planar multiresonating circuits are the main component of chipless tag design. In this thesis, different multiresonators for chipless tag application are employed. A deep knowledge in microwave resonator is essential for the design of these circuits.

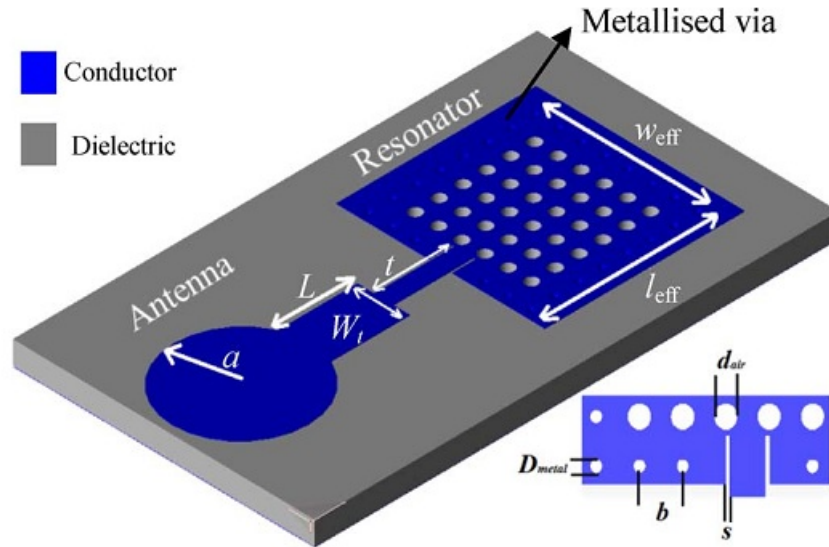


Figure 2.12: Substrate integrated tag (Courtesy: Hatem El Matbouly et. al.) [?]

2.2 Chipless Tag Reading Techniques

2.2.1 Reading Methods

There are different reading techniques used for identifying the tag ID. They are (1) Device under test (2) Bistatic radar measurement technique and (3) Monostatic radar measurement technique. The working principle and calibration methods are briefly explained in below.

Device Under Test (DUT)

Vector network analyzer is used as test equipment which has at least two ports. The ports should be calibrated before the measurement. The device to be tested is connected between these ports. Network analyzer can easily analyze electrical characteristics such as transmission characteristics, reflection characteristics phase, group delay, etc. They can be displayed in different formats. From the transmission characteristics the tag provides exact spectral signature by measuring magnitude attenuation or phase jump or group delay.

This technique can be extend to either microstrip transmission line based swipe card method. In swipe card method, the reader consists of transmis-

sion line with a swiping slot. The transmission line is connected between the calibrated two ports of reader or PNA E8362B and calibrated the system. Whenever, the tag swipes into the slot of reader, the multiresonating circuit touches the transmission line and it inhibits the propagation of some frequencies which determine a unique spectral signature.

The second method is a slotted waveguide reading system, where the guide is connected between two ports of Network analyzer or reading system and the system should be calibrated before reading the tag. The cut-off frequency of waveguide and size of tag are crucial parameters in this measurement. The resonating frequencies of tag should be greater than the cut-off frequency of waveguide. Whenever it is inserted into the waveguide, it exhibits transmission characteristics with a spectral signature of a particular tag. The former microstrip line swipe method and latter slotted waveguide method should technically provide the same response.

Bi-static Measurement Technique

The transmit and receive antennas are separated with a small angular distance but still appear to be at the same location when viewed from the target. Some RFID reader systems have two identical antennas to send continuous wave interrogating signals to the tag and receive the encoded returned signals from the chipless tag.

Monostatic Measurement Technique

Certain interrogator systems use an antenna for transmission and reception of the interrogating signal. Since a common antenna is used for transmission and reception, there must be a device that provides a solution between transmitted and received energy, also provides energy flow in the proper direction. Either a duplexer or circulator is used for controlling the direction of energy flow.

2.2.2 Different Types of Chipless RFID Tag Readers

Depending on the technique used to encode the data on the tag, the reading technique and architecture of the reader, there are different types of chipless RFID readers. There are four types of chipless RFID tag readers reported in [?].

1. Time domain chipless tag reader

2. Frequency domain chipless tag reader
3. Hybrid domain chipless tag reader
4. SAR based chipless tag reader

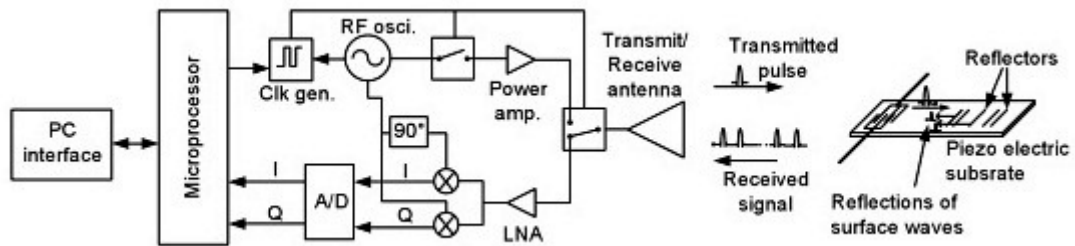


Figure 2.13: Block diagram of time domain based reader for SAW tags (Courtesy: Nemaï Karmakar et. al.) [?]

Time domain reader uses reflected echoes as a stream of pulses from the tag to decode the data. In spectral signature based tag, data encoded in the form of amplitude or phase of frequency response or both amplitude and phase. The basic steps of all kinds of reader are same. The hybrid domain combines both time domain and frequency domain techniques for encoding and decoding tag. Synthetic Aperture Radar (SAR) imaging technique used for reading the SAR based tag. The reading process involves generating interrogation signal, capturing the signals received from the tag, signal processing and decoding the tag data encoded in the tag.

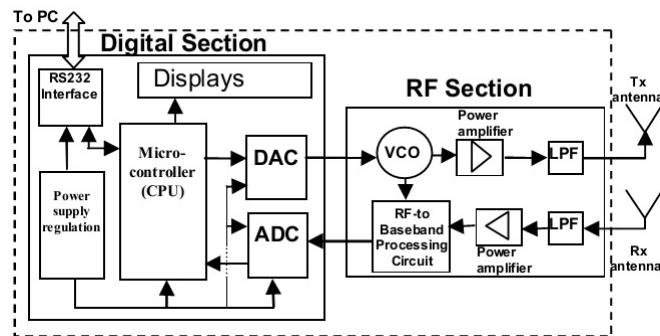


Figure 2.14: Block diagram of spectral signature based chipless RFID reader (Courtesy: Nemaï Karmakar . et. al.) [?]

2.2.3 Chipless RFID Reader

A chipless reader/interrogator is a device which sends the interrogating signal to transponder/tag and the re-transmitted signals from tag is received and processed to identify the tag. In open literature various types of reader architectures and different operating principles are used in chipless tag readers. The reader consists of following components.

1. Antenna
2. RF section
3. Digital control and data processing section

Reader system can have single or multiple antenna depending on the technology used in the RFID tags. Antennas are used for transmitting and receiving electromagnetic waves, which establish the communication between the tag and reader. Nowadays conventional RFID antennas are replaced by smart antennas in order to increase the capabilities antennas and enhance the performance of RFID systems.

RF section consists of RF signal source such as an oscillator, mixer, Low noise amplifier, power amplifier, filters and power dividers. This section consists of two channels: transmitting path and receiving path. The type of signal generator depend on the desired frequency band of operation. Usually, voltage controlled oscillator (VCO) is used as an oscillator for generating RF signal to be transmitted. A small portion of the transmitted signal is extracted by a directional coupler as a reference signal to be used for demodulation process in the receiver path. Low noise amplifier is used to amplify the received weak signals from tag. RF power amplifier is used for strengthening both the output of oscillator in transmitting path and output of LNA in receiving path. Designer should be aware of input power level of amplifier, otherwise the higher power level inputs might drive the RF amplifier into saturation. The mixer circuit is used in reader to down convert the incoming RF into an IF signal for demodulation. Microwave filters are essential component of demodulator that filter out the unwanted frequencies generated in the IF section.

The gain phase detector is a specialized RF component that compares the amplitude and phase of two RF signals. It is the main component of reader

circuit, the sensitivity of detector determines the both efficiency and accuracy of decoded data.

Digital section controls the transmission of the interrogation signal demodulated signal from the RF section. A powerful signal processing algorithms or anti-collision algorithms are also implemented in this section.

2.3 Planar Resonators

Resonators are key elements in RF and microwave engineering. Most microwave circuits and antennas contains resonant elements. There are different types of resonators used for RF and microwave applications, such as dielectric resonators, cavity resonators, lumped element resonators, acoustic wave resonators, transmission line resonators, quartz crystal resonators and semi-lumped resonators.

In this section, the focus is on different types of planar resonators. Planar resonators are most preferable for designing RF and microwave circuits such as filters, oscillators and tuned amplifiers. The advantages are, small size, light weight, high bandwidth, easy fabrication process by photo lithography and very good affinity with active circuit elements. However, a major disadvantage to the use of the resonator is a drastic increase in insertion loss compared to other types of resonators, making it difficult to apply such planar resonators to narrow band applications. Planar resonators are further classified as planar transmission line resonator and stepped impedance resonator.

2.3.1 Transmission Line Resonator

Transmission line resonators are also planar resonators, but their dimensions scale with the resonance frequency . This resonant structure is transmission line possessing uniform characteristic impedance with an electrical length of π radian. Such transmission line resonators will be referred as uniform impedance resonator (UIR) [?]. In the case of conventional UIR, the resonant condition is determined solely on transmission line length. The most typical planar transmission line resonators are operating in transverse electromagnetic modes (quasi-TEM modes). These resonators have a wide applicable frequency range starting from several hundred MHz extending to around 100

GHz and presently exist the most common choice for filters in wireless communication. They are simple in structure, small size, light weight and capability of wide application to various devices. Moreover, the most attractive feature of planar resonator is that they can be easily integrated with active circuits such as MMICs, because they are manufactured by photolithography of metalized film on a dielectric substrate. In this section we discuss the use of transmission line sections with various lengths and terminations (open or short) to form resonators.

Short Circuit $\lambda/2$ Resonator

Figure 2.15 shows the fundamental structure of a short circuited planar microstrip half-wavelength resonator which fabricated on dielectric substrate of low loss-tangent, high permittivity and high temperature stability. The resonator structure consists of a conductor strip of uniform width with an overall length equivalent to half-wavelength of resonant frequency and a rectangular ground plane is printed on the other side of the substrate parallel and symmetric to the strip. This resonator can be expressed in electrical parameters as a transmission line possessing uniform characteristic impedance with an electrical length of π radian. Such transmission line resonators will be referred to as uniform impedance resonator [?, ?].

The line exhibits series resonance and it has a attenuation constant α , propagation constant β and characteristic impedance Z_0 . At the frequency $\omega = \omega_0$ the length of line is $l = \lambda/2$ where $\lambda = \frac{2\pi}{\beta}$, the input impedance is,

$$Z_{in} = Z_0 \tanh(\alpha + j\beta)l \quad (2.1)$$

Using an identity for the hyperbolic tangent gives

$$Z_{in} = Z_0 \frac{\tanh \alpha l + j \tan \beta l}{1 + j \tan \beta l \tanh \alpha l} \quad (2.2)$$

if lossless transmission line $\alpha = 0$

$$Z_{in} = jZ_0 \tan \beta l$$

The values of resistance R , inductance L and capacitance C of equivalent series RLC resonant circuit to be calculated. In practical application, most transmission line have very small loss,

$$\tanh \alpha l \approx \alpha l$$

i.e., $\alpha l \ll 1$

Now let $\omega = \omega_0 + \Delta\omega$,

$$\beta l = \frac{\omega l}{v_p} = \frac{\omega_0 l}{v_p} + \frac{\Delta\omega l}{v_p}$$

where v_p is the phase velocity of the transmission line. Since $l = \frac{\lambda}{2} = \frac{\pi v_p}{\omega_0}$ for $\omega = \omega_0$

$$\beta l = \pi + \frac{\Delta\omega\pi}{\omega_0}$$

then

$$\tan \beta l = \tan\left(\pi + \frac{\Delta\omega\pi}{\omega_0}\right) = \tan\left(\frac{\Delta\omega\pi}{\omega_0}\right) \approx \frac{\Delta\omega\pi}{\omega_0} \quad (2.3)$$

using these results in 2.2 gives

$$Z_i n \approx Z_0 \frac{\alpha l + j \frac{(\Delta\omega\pi)}{\omega_0}}{1 + j \frac{(\Delta\omega\pi)}{\omega_0} \alpha l} \approx Z_0 \left(\alpha l + j \frac{\Delta\omega\pi}{\omega_0} \right) \quad (2.4)$$

since $\frac{\Delta\omega\alpha l}{\omega_0} \ll 1$

$$Z_i n = R + 2jL\Delta\omega \quad (2.5)$$

which is the input impedance of series RLC resonant circuit, we can distinguish the resistance of the equivalent circuit as

$$R = Z_0 \alpha l \quad (2.6)$$

the inductance of the equivalent circuit as

$$L = \frac{Z_0 \pi}{2\omega_0} \quad (2.7)$$

and capacitance of the equivalent circuit as

$$C = \frac{1}{\omega^2 L} \quad (2.8)$$

the Q of this resonator can be found from the above equation as

$$Q = \frac{L\omega_0}{R} = \frac{\pi}{2\alpha l} \approx \frac{\beta}{2\alpha} \quad (2.9)$$

since, $\beta l = \pi$ at the first resonance. This result shows that the Q decreases as the attenuation of the line increases.

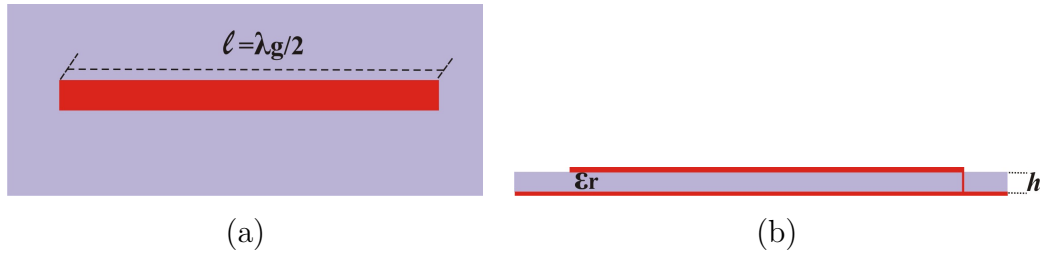


Figure 2.15: (a) Top view (b) Side view of shorted half wave microstrip resonator (Courtesy: David M. Pozar) ([?])

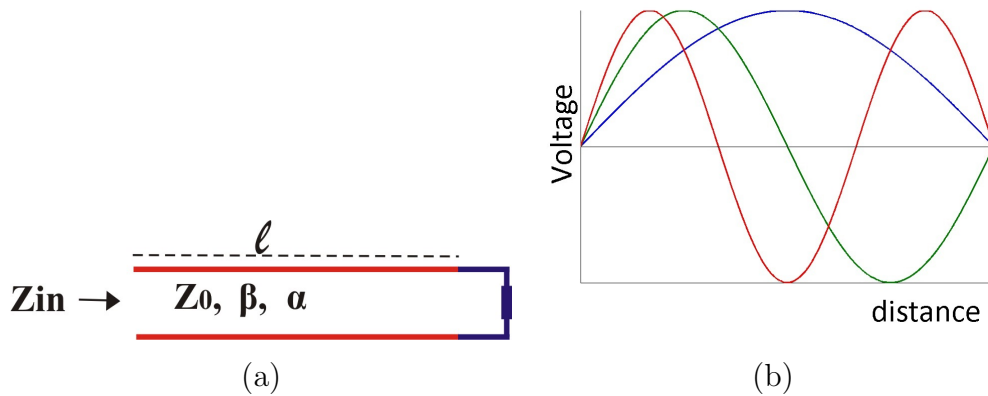


Figure 2.16: (a) Shorted circuit half wave length transmission line (b) Voltage distributions for $n = 1(l = \frac{\lambda}{2})$; $n = 2(l = \lambda)$ and $n = 3(l = 3\frac{\lambda}{2})$ (Courtesy: David M. Pozar) ([?])

Resonance also occurs for $l = n\frac{\lambda}{2}$, $n = 1, 2, 3, \dots$ the voltage distribution for the $n = 1$, $n = 2$ and $n = 3$ the resonant modes are shown in Figure 2.16.

Open Circuit $\lambda/2$ Resonator

Figure 2.17 shows the structure of an open circuited planar microstrip half-wavelength resonator with two open circuited ends which is fabricated on

dielectric substrate of low loss-tangent and high permittivity [?].

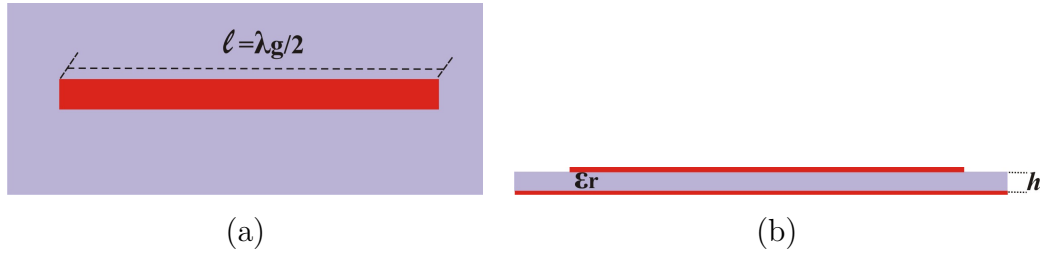


Figure 2.17: (a) Top view (b) Side view of half wave microstrip resonator (Courtesy: David M. Pozar) ([?])

$$Q = \omega_0 RC = \frac{\pi}{2\alpha l} \approx \frac{\beta}{2\alpha} \quad (2.10)$$

since, $\beta l = \pi$ at resonance.

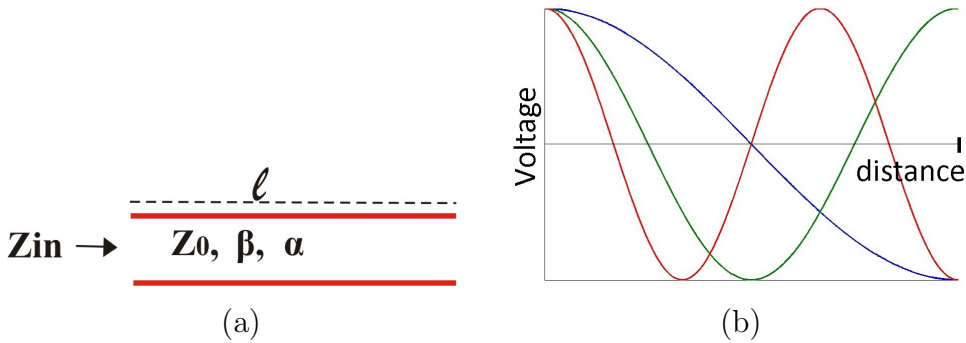


Figure 2.18: (a) Open circuited half wave length transmission line (b) Voltage distributions for $n = 1 (l = \frac{\lambda}{2})$; $n = 2 (l = \lambda)$ and $n = 3 (l = 3\frac{\lambda}{2})$ (Courtesy: David M. Pozar) ([?])

Antiresonance also occurs for $l = n\frac{\lambda}{2}$, $n = 1, 2, 3, \dots$ the voltage distribution for the $n = 1$, $n = 2$ and $n = 3$ the resonant modes are shown in Figure 2.18.

Short Circuit $\lambda/4$ Resonator

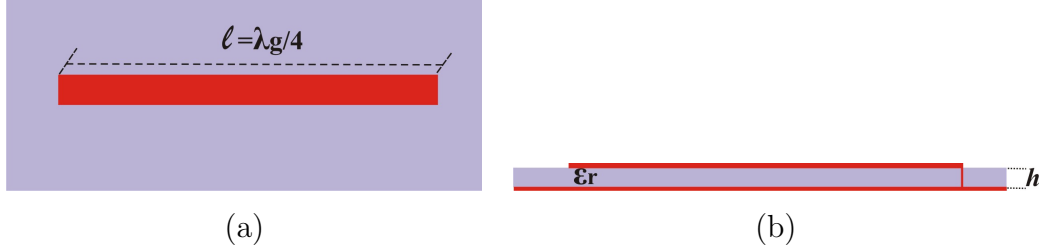


Figure 2.19: (a) Top view (b) Side view of short circuited quarter wavelength microstrip resonator (Courtesy: David M. Pozar) ([?])

An antiresonance can be achieved by using short circuited transmission line of $\frac{\lambda}{4}$.

$$Q = \omega_0 RC = \frac{\pi}{4\alpha l} \approx \frac{\beta}{2\alpha} \quad (2.11)$$

since, $\beta l = \pi$ at resonance.

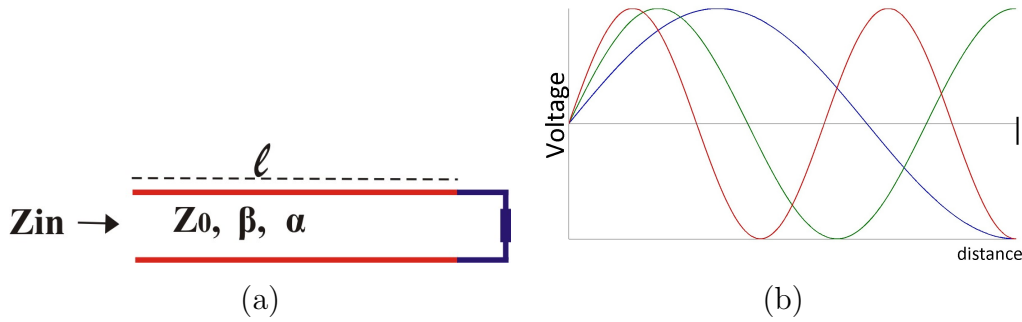


Figure 2.20: (a) Short circuited quarter wave length transmission line (b) Voltage distributions for $n = 1 (l = 3\frac{\lambda}{4})$; $n = 2 (l = 5\frac{\lambda}{4})$ and $n = 3 (l = 7\frac{\lambda}{4})$ (Courtesy: David M. Pozar) ([?])

Open Circuit $\lambda/4$ Resonator

Open circuited quarter wavelength resonator act as a series RLC resonator.

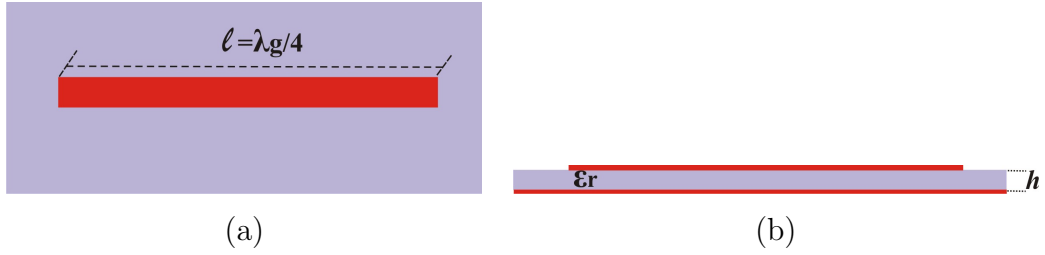


Figure 2.21: (a) Top view (b) Side view of open circuited quarter wave microstrip resonator (Courtesy: David M. Pozar) ([?])

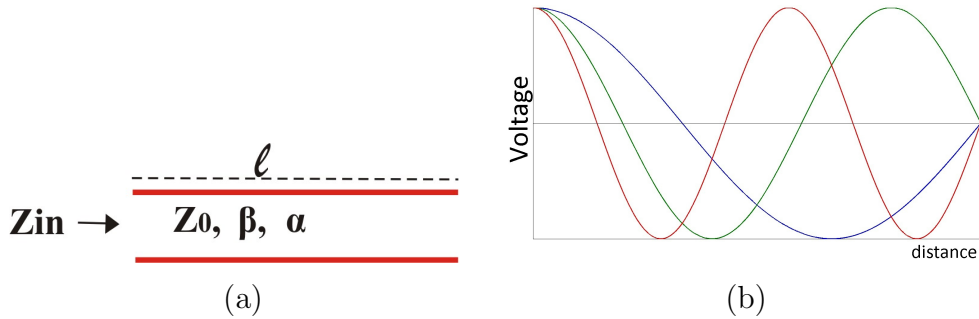


Figure 2.22: (a) Open circuited quarter wave length transmission line (b) Voltage distributions for $n = 1 (l = 3\frac{\lambda}{4})$; $n = 2 (l = 5\frac{\lambda}{4})$ and $n = 3 (l = 7\frac{\lambda}{4})$ (Courtesy: David M. Pozar) ([?])

$$Z_{in} = Z_0 \coth(\alpha + j\beta)l \approx Z_0 \frac{1 + j \tan \beta l \tanh \alpha l}{\tanh \alpha l + j \tan \beta l} \quad (2.12)$$

Since $l = \frac{\lambda}{4}$ at $\omega = \omega_0$

the Q of this resonator can be found from the above equations as

$$Q = \frac{L\omega_0}{R} = \frac{\pi}{4\alpha l} \approx \frac{\beta}{2\alpha} \quad (2.13)$$

2.3.2 Stepped Impedance Resonator

Basic Structure of SIR

The planar stepped impedance resonator is a quasi-TEM mode resonator which is composed of more than two transmission line with dissimilar characteristic impedance [?]. Figure 2.23 shows different SIR structures, Z_1 and Z_2

are characteristic impedance corresponding to electrical length θ_1 and θ_2 of transmission line. An important electrical parameter which characterizes the SIR is impedance ratio K defined by

$$K = \frac{Z_2}{Z_1} \quad (2.14)$$

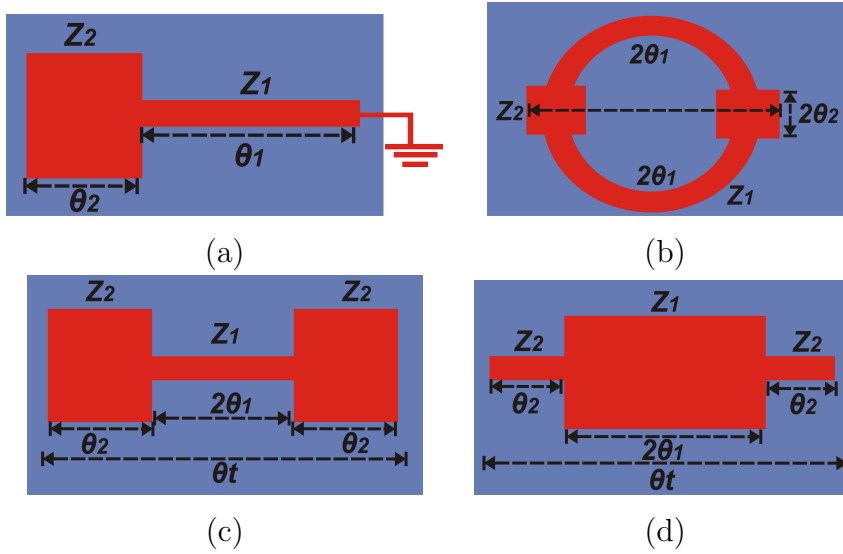


Figure 2.23: Basic structure of SIR (a) Quarter wavelength SIR (b) Full wavelength SIR (c) Half wavelength SIR $K = \frac{Z_2}{Z_1} < 1$ (d) Half wavelength SIR $K = \frac{Z_2}{Z_1} > 1$ (Courtesy: Makimoto) ([?])

The knowledge in impedance ratio (K) of SIR and electrical length θ_1 , θ_2 help to predict the basic properties such as the resonator length, resonance conditions and spurious resonance [?].

Resonance Conditions

The input impedance of SIR Z_i can be expressed as

$$Z_i = jZ_2 \frac{Z_1 \tan \theta_1 + Z_2 \tan \theta_2}{Z_2 - Z_1 \tan \theta_1 \tan \theta_2} \quad (2.15)$$

Let $Y_i = \frac{1}{Z_i} = 0$, then the parallel resonance condition can be obtained as $Z_2 - Z_1 \tan \theta_1 \tan \theta_2 = 0$

thus

$$\tan \theta_1 \tan \theta_2 = \frac{Z_2}{Z_1} = K \quad (2.16)$$

From this equation 2.16, the resonant condition is determined by electrical length θ_1, θ_2 and impedance ration K . The overall electrical length $\theta_T A$ is expressed as

$$\theta_T A = \theta_1 + \theta_2 = \theta_1 + \tan^{-1}\left(\frac{K}{\tan \theta_1}\right) \quad (2.17)$$

In the case of Quarter wavelength SIR, the normalized resonator length is defined by

$$L_n = \frac{\theta_T A}{\frac{\pi}{2}} = \frac{2\theta_T A}{\pi} \quad (2.18)$$

Overall electrical length of $\frac{\lambda_g}{2}$ and λ_g type SIR, defined, respectively, as $\theta_T B$ and $\theta_T C$, can be expressed as

$$\theta_T B = 2\theta_T A$$

$$\theta_T C = 4\theta_T A$$

These electrical length can be normalized by corresponding Uniform Impedance Resonator (UIR) length $\frac{\pi}{2}$ radians, π radians and 2π radians, providing following equations

$$\frac{\theta_T A}{\frac{\pi}{2}} = \frac{2\theta_T A}{\pi} = L_n \quad (2.19)$$

$$\frac{\theta_T B}{\pi} = \frac{2\theta_T A}{\pi} = L_n \quad (2.20)$$

$$\frac{\theta_T C}{2\pi} = \frac{4\theta_T A}{2\pi} = L_n \quad (2.21)$$

The above equations suggest that the resonance conditions of all three types of SIR can be expressed using the same equation.

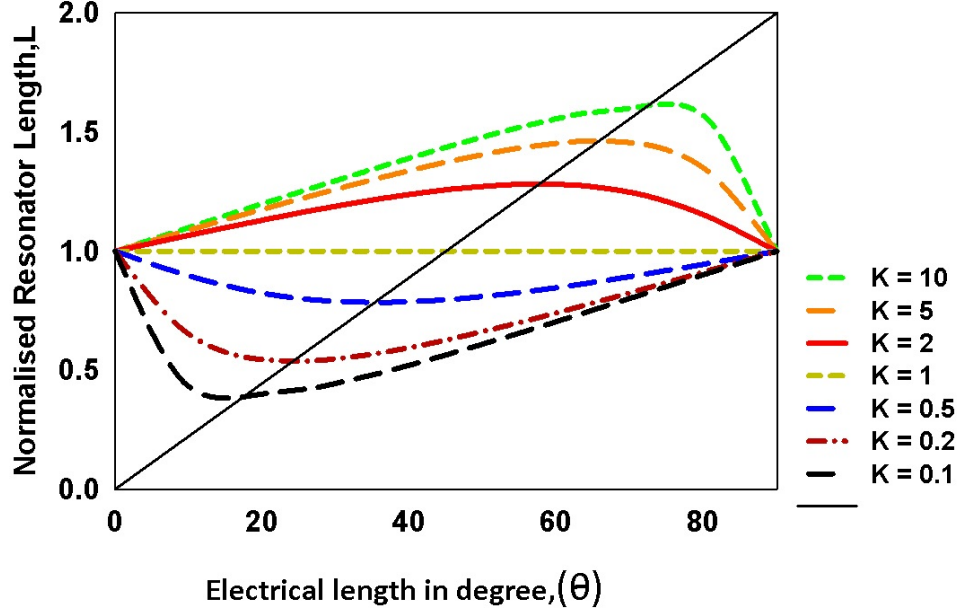


Figure 2.24: Relationship between electrical length θ_1 and normalized resonator length L_n taking R_z as parameter (Courtesy: M.Makimoto et al)

From Figure 2.24 it depicts that normalized resonator length L_n attains a maximum value when $K \geq 1$ and a minimum value when $K < 1$.

$$K = \frac{\tan \theta_1 (\tan \theta_T A - \tan \theta_1)}{1 + \tan \theta_T A \tan \theta_1} \quad (2.22)$$

when $0 < R_z < 1$ and $0 < \theta_T A < \pi/2$,

$$\tan \theta_T A = \frac{1(\tan \theta_1 + \frac{K}{\tan \theta_1})}{1 - K} \quad (2.23)$$

$$= \frac{\sqrt{K}(\frac{\tan \theta_1}{\sqrt{K}} + \frac{\sqrt{K}}{\tan \theta_1})}{1 - K} \quad (2.24)$$

$$\geq \frac{2\sqrt{K}}{1 - K} \quad (2.25)$$

this equation is equated $\frac{\tan \theta_1}{\sqrt{K}} = \frac{\sqrt{K}}{\tan \theta_1}$ thus

$$\theta_1 = \theta_2 = \tan^{-1} \sqrt{K} \quad (2.26)$$

$\theta_T A$ attains minimum value of

$$(\theta_T A)_{min} = \tan^{-1}\left(\frac{2\sqrt{K}}{1-K}\right) \quad (2.27)$$

similarly, if $K > 1$ and $\pi/2 < \theta_T < \pi$, we obtain the following equation.

$$\tan \theta_T A = -\frac{\sqrt{K}\left(\frac{\tan \theta_1}{\sqrt{K}} + \frac{\sqrt{K}}{\tan \theta_1}\right)}{K-1} \quad (2.28)$$

Due to $0 < \theta_1 < \pi/2$, $\theta_T A$ attains a maximum value of

$$(\theta_T A)_{max} = \tan^{-1}\left(\frac{2\sqrt{K}}{1-K}\right) \quad (2.29)$$

Spurious Resonance

A distinct feature of the SIR is that the resonator length and corresponding spurious resonance frequencies can be adjusted by changing the impedance ratio K of the SIR. In discussion, the fundamental resonance frequency is represented as f_0 , while the lowest spurious frequencies of $\frac{\lambda_g}{4}$, $\frac{\lambda_g}{2}$ and λ_g -type SIR are represented as f_{SA} , f_{SB} and f_{SC} respectively. Resonator electrical lengths corresponding to spurious frequencies f_{SA} , f_{SB} and f_{SC} are expressed as θ_{SA} , θ_{SB} and θ_{SC} , respectively.

$$\tan \theta_{SA} = \tan(\pi - \theta_0) = -\tan^{-1} \sqrt{K} \quad (2.30)$$

$$(K \tan \theta_1 + \tan \theta_2)(K - \tan \theta_1 \tan \theta_2) \quad (2.31)$$

let $\theta_1 = \theta_2 = \theta$

$$\tan \theta(K+1)(K - \tan^2 \theta) = 0 \quad (2.32)$$

the solution is

$$\theta_0 = \tan^{-1} \sqrt{K} \quad (2.33)$$

$$\theta_{SB} = \theta_{SC} = \frac{\pi}{2} \quad (2.34)$$

spurious resonance frequencies are obtained as follows:

$$\frac{f_{SA}}{f_0} = \frac{\theta_{SA}}{\theta_0} = \frac{\pi - \theta_0}{\theta_0} = \frac{\pi}{\tan^{-1} \sqrt{K}} - 1 \quad (2.35)$$

$$\frac{f_{SB}}{f_0} = \frac{f_{SC}}{f_0} = \frac{\theta_{SB}}{\theta_0} = \frac{\pi}{2 \tan^{-1} \sqrt{K}} \quad (2.36)$$

The ratios of the first spurious frequency f_{s1} to the fundamental frequency f_0 of SIRs are shown in Figure 2.25. It is obvious that $\frac{f_{s1}}{f_0} < 2$ for the cases $K > 1$. As the impedance ratio K increases, the fundamental and the first spurious frequencies are close to each other. The most interesting observation is that for a given impedance ratio K , it is better to choose $\alpha \sim 0.7$ in order to obtain the smaller values of $\frac{f_{s1}}{f_0}$. On the contrary, if $\frac{f_{s1}}{f_0} > 2$ is required, then the cases of $K < 1$ must be chosen.

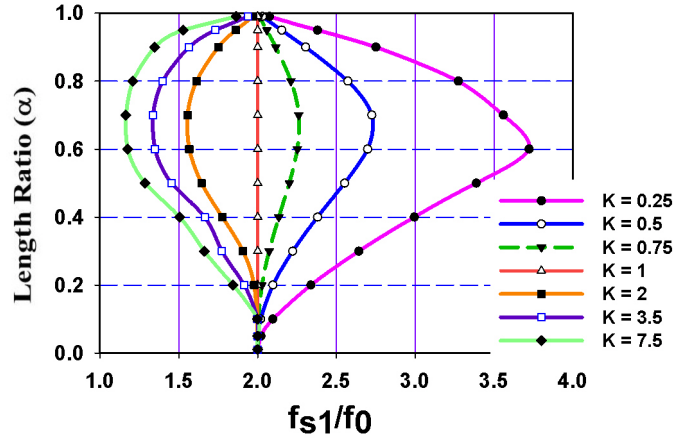


Figure 2.25: Ratios of the first higher order resonant frequency to the fundamental resonant frequency of SIRs (Courtesy: M. Makimoto et. al.) [?]

2.3.3 Semi-lumped Resonators

Semilumped resonators are small resonant elements and fully planar, which utilized for special interest in applications where size reduction and cost are important. To reduce device size, a possible strategy is to replace transmission line resonators with semilumped resonators. However, as the size of resonator is reduced, the quality factor Q , is also degraded. In semilumped resonators the inductance and capacitance can be associated to a certain element of the resonator topology.

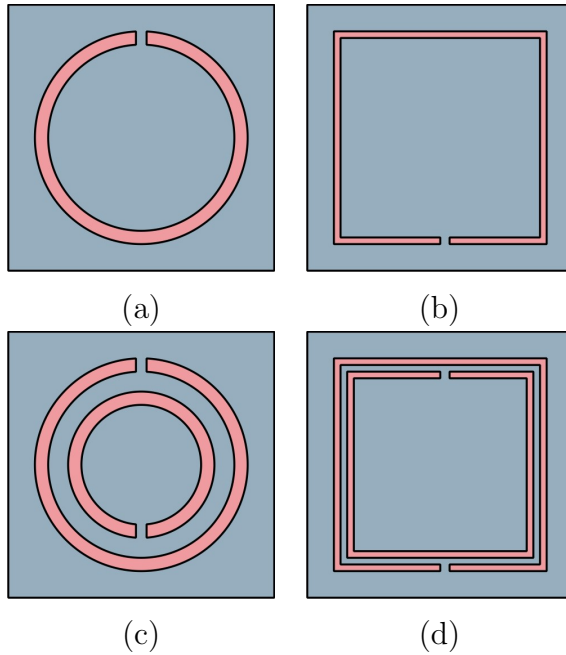


Figure 2.26: (a) Circular open ring (b) Square open ring (c) Circular split ring resonator (d) Rectangular split ring resonator

Open ring resonator can be excited by means of an axial time varying magnetic field, or even by means of an electric field in the plane of the particle. The electrical length of the open ring is $\frac{\lambda}{2}$ at resonance. However, this ring resonator is a distributed element since it operates under the same principle of unfolded counterpart, as shown in Figure 2.26(a) and (b). In order to miniaturize the size of a split ring, one possible solution is to add an inner ring with the slit on the opposite side, as depicted in Figure 2.26(c) and (d) which is known as Split Ring Resonator(SRR) [?, ?]. By virtue of the mutual coupling between both rings, the fundamental resonance of the resulting element is lower than the fundamental resonance of any of the individual rings and thus the element is electrically smaller than a single ring resonator. According to the Lenz's law, the magnetic field generated by the induced currents in the SRR is opposite to the incident magnetic field and this element is useful for the synthesis of negative effective permeability media. Most microwave circuits and antennas based on metamaterial concepts are implemented by means of electrically small resonators like the SRR have been reported.

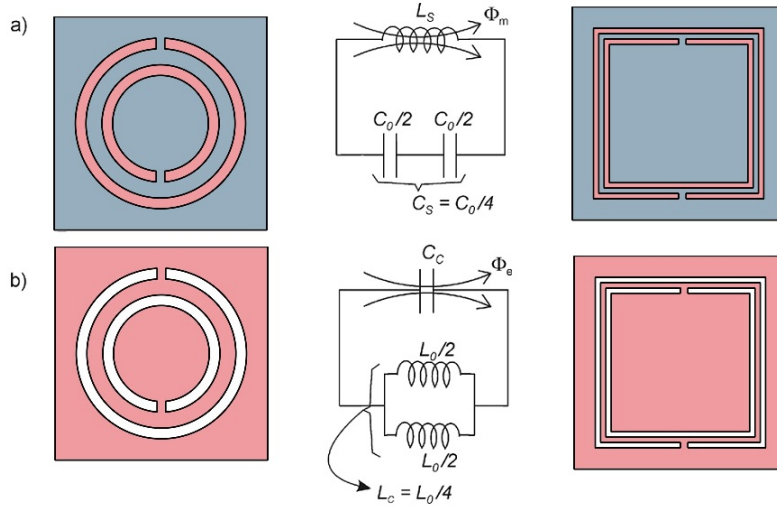


Figure 2.27: Equivalent circuit of SRR and CSRR

When the SRR is excited by an external time-varying magnetic field directed along the SRR axis, the slot on each ring forces the electric current to flow from one ring to another across the slot between them, taking the form of a strong displacement current. The slot between the rings therefore behaves as a distributed capacitance. The SRR topology and its equivalent circuit are shown in Figure 2.27. where L_s is the SRR self-inductance and $\frac{C_0}{2}$ is the capacitance associated with each SRR half. The total capacitance of this circuit is the series connection of the capacitance of both SRR halves, that is, $\frac{C_0}{4}$. Therefore, the resonance frequency ω_0 is given by [?, ?].

$$\omega_0 = \frac{2}{\sqrt{L_s C_0}} = \sqrt{\frac{2}{\pi r_0 L_s C}} \quad (2.37)$$

where C is capacitance per unit length.

Complimentary split ring resonator (CSRR) is a negative image of SRR and it exhibits duality character of conventional SRR as shown in Figure 2.27(b). It is excited by time varying axial electric field rather than axial magnetic field. Different SRR structures that do not exhibit cross-polarization effects hence, these effects are also absent in their complementary counterparts.

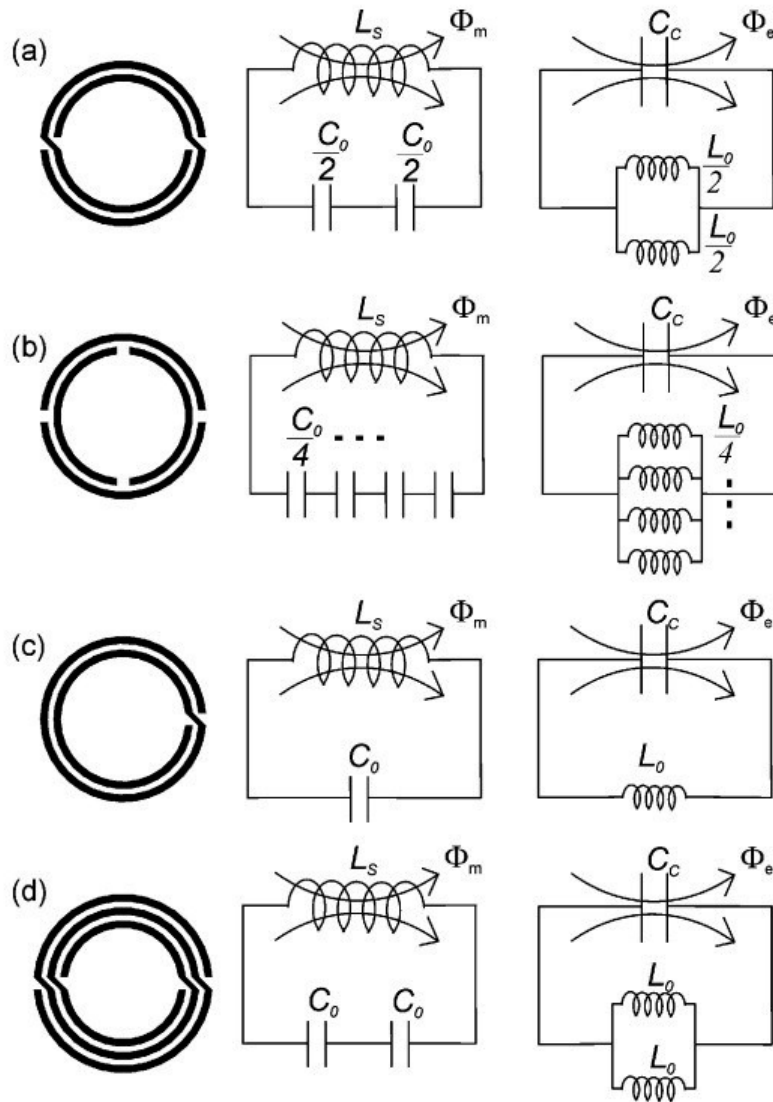


Figure 2.28: Different types SRR with equivalent circuits

The equivalent circuits for these topologies, as well as for their complementary configurations, are also shown in Figure 2.28. This is known as Non-bianisotropic Split ring Resonator (NB SRR). The equivalent circuit model and resonant frequency of the NB SRR are identical to those of the SRR [?, ?]. The double-split SRR (D SRR) exhibits symmetry but does not exhibit cross polarization. However, the D-SSR equivalent circuit differs from that of the SRR, being the frequency of resonance twice than that of the SRR. Broadside

coupled split ring resonators (BC-SRR), charges in the upper half are also images of charges in the lower half, but this charge distribution does not result in a net dielectric dipole. Thus, the BC-SRR is non-bianisotropic.

REFERENCES

- [1] I. D. Robertson and I. Jalaly, "Capacitively-Tuned Split Microstrip Resonators for RFID Barcodes," *2005 European Microwave Conference, France*, vol. 2, pp. 5–6, Oct. 2005.
- [2] I. Jalaly and I. D. Robertson, "Capacitively-Tuned Split Microstrip Resonators for RFID Barcodes," pp. 5–6.
- [3] J. McVay, A. Hoorfar, and N. Engetha, "Space filling curve RFID tags," *2006 IEEE Radio and Wireless Symposium, San Diego, USA*, vol. 2, pp. 199–202, Jan. 2006.
- [4] S. Preradovic, I. Balbin, N. C. Karmakar, and G. Swiegers, "A Novel Chipless RFID System Based on Planar Multiresonators for Barcode Replacement," *IEEE International Conference on RFID The Venetian, Las Vegas, Nevada, USA*, vol. 3169, pp. 289–296, Apr. 2008.
- [5] S. Preradovic, I. Balbin, and N. Karmakar, "The development and design of a novel chipless RFID system for low-cost item tracking," *2008 Asia-Pacific Microwave Conference*, pp. 1–4, Dec. 2008.
- [6] S. Preradovic, S. Member, I. Balbin, N. C. Karmakar, S. Member, and G. F. Swiegers, "Multiresonator-Based Chipless RFID System for Low-Cost Item Tracking," *IEEE Transactions on Microwave Theory and Techniques*, vol. 57, no. 5, pp. 1411–1419, May 2009.
- [7] S. Preradovic, I. Balbin, N. C. Karmakar, and G. Swiegers, "Chipless Frequency Signature Based RFID Transponders," *Proceedings of the 38th European Microwave Conference Chipless*, no. 38, pp. 1723–1726, Oct. 2008.
- [8] S. Preradovic, S. Roy, and N. Karmakar, "Fully printable multi-bit chipless RFID transponder on flexible laminate," *2009 Asia Pacific Microwave Conference*, pp. 2371–2374, Dec. 2009.

- [9] S. Preradovic and N. C. Karmakar, "Design of Chipless RFID Tag for Operation on Flexible Laminates," *IEEE Antennas and Wireless Propagation Letters*, vol. 9, pp. 207–210, Sep. 2010.
- [10] S. Preradov, M. Roy, and C. Karmakar, "RFID System Based on Fully Printable Chipless Tag for Paper-/Plastic-Item Tagging," *IEEE Antennas and Propagation Magazine*, vol. 53, no. 5, Oct. 2011.
- [11] S. Preradovic and N. C. Karmakar, "Design of Fully Printable Planar Chipless RFID Transponder with 35-bit Data Capacity," *Proceedings of the 39th European Microwave Conference*, pp. 13–16, Oct. 2009.
- [12] S. Bhuiyan, R.-e. Azim, and N. Karmakar, "A Novel Frequency Reused Based ID Generation Circuit for Chipless RFID Applications," *Proceedings of the Asia-Pacific Microwave Conference 2011*, pp. 1470–1473, Dec. 2011.
- [13] S. Preradovic and N. C. Karmakar, "Design of short range chipless RFID reader prototype," *2009 International Conference on Intelligent Sensors, Sensor Networks and Information Processing (ISSNIP)*, pp. 307–312, Dec. 2009.
- [14] N. C. Karmakar and S. Preradovic, "Multiresonator Based Chipless RFID Tag and Dedicated RFID Reader," *proceedings of IMS 2010*, no. iv, pp. 1520–1523, Jun. 2010.
- [15] S. Preradovic and N. Karmakar, "4 th Generation Multiresonator-Based Chipless RFID Tag Utilizing Spiral EBGs," *Proceedings of the 40th European Microwave Conference*, no. September, pp. 1746–1749, Sep. 2010.
- [16] N. Karmakar and S. Preradovic, "Chipless RFID tag with integrated sensor," *2010 IEEE Sensors conference*, pp. 1277–1281, Nov. 2010.
- [17] T. Kim, U. Kim, J. Kwon, and J. Choi, "Design of a Novel Chipless RFID Tag Using a Simple Bandstop Resonator," *Proceedings of Asia-Pacific Microwave Conference 2010*, pp. 2264–2267, Dec. 2010.

- [18] S. Hu, S. Member, Y. Zhou, C. L. Law, and S. Member, "Study of a Uniplanar Monopole Antenna for Passive Chipless UWB-RFID Localization System," *IEEE Transactions on Antennas and Propagation*, vol. 58, no. 2, pp. 271–278, Feb. 2010.
- [19] L. Reichardt, G. Adamiuk, G. Jereczek, and T. Zwick, "Chipless RFID Systems for Car-to-Infrastructure Communication," *2010 IEEE International Conference on Communications Workshops*, pp. 1–5, May 2010.
- [20] R. Koswatta and N. C. Karmakar, "Investigation into Antenna Performance on Read Range Improvement of Chipless RFID Tag Reader," *Proceedings of Asia-Pacific Microwave Conference 2010*, pp. 1300–1303, Dec. 2010.
- [21] S. Preradovic and N. C. Karmakar, "Chipless RFID : Bar Code of the Future," *IEEE Microwave Magazine*, no. December, pp. 87–97, Dec. 2010.
- [22] S. Preradovic and N. Karmakar, "Chipless Millimeter Wave Identification (MMID) Tag at 30 GHz," *Proceedings of the 41st European Microwave Conference Chipless*, no. October, pp. 123–126, Oct. 2011.
- [23] N. C. Karmakar and C. K. Pern, "mm-wave chipless RFID tag for low-cost item tagging," *Proceedings of the Asia-Pacific Microwave Conference 2011*, pp. 1462–1465, Dec. 2011.
- [24] S. Preradovic, N. Kamakar, and E. Amin, "Chipless RFID Tag with Integrated Resistive and Capacitive Sensors," *Proceedings of the Asia-Pacific Microwave Conference 2011*, pp. 1354–1357, Dec. 2011.
- [25] M. Polivka, J. Havlíek, M. Svanda, and J. Machá, "Detection of Spiral Resonator Array for Chipless RFID," *6th European Conference on Antennas and Propagation (EUCAP)*, pp. 3001–3004, Mar. 2011.
- [26] E. M. Amin and N. Karmakar, "Development of a chipless RFID temperature sensor using cascaded spiral resonators," *2011 IEEE SENSORS Proceedings*, pp. 554–557, Oct. 2011.
- [27] P. Kalansuriya, N. Karmakar, and E. Viterbo, "Signal Space Representation of Chipless RFID Tag Frequency Signatures," *2011 IEEE Global Telecommunications Conference - GLOBECOM 2011*, pp. 1–5, Dec. 2011.

- [28] R. V. Koswatta and N. C. Karmakar, “A Novel Method of Reading Multi-Resonator Based Chipless RFID Tags Using an UWB Chirp Signal,” *Proceedings of the Asia-Pacific Microwave Conference 2011*, pp. 1506–1509, Dec. 2011.
- [29] S. Preradovic and N. Karmakar, “Chipless RFID for intelligent traffic information system,” *2011 IEEE International Symposium on Antennas and Propagation (APSURSI)*, pp. 992–995, Jul. 2011.
- [30] S. Preradov, M. Roy, and C. N. Karmakar, “RFID System Based on Fully Printable Chipless Tag for Paper-/Plastic-Item Tagging,” *IEEE Antennas and Propagation Magazine*, vol. 53, no. 5, Oct. 2011.
- [31] S. Preradovic and A. Menicanin, “Chipless Wireless Sensor Node,” *MIPRO 2012, Opatija, Croatia*, pp. 179–182, May 2012.
- [32] R. V. Koswatta and N. C. Karmakar, “A Novel Reader Architecture Based on UWB Chirp Signal Interrogation for Multiresonator-Based Chipless RFID Tag Reading,” *IEEE Transactions on Microwave Theory and Techniques*, vol. 60, no. 9, pp. 2925–2933, Sep. 2012.
- [33] C. M. Nijas, R. Dinesh, U. Deepak, A. Rasheed, S. Mridula, K. Vasudevan, and P. Mohanan, “Chipless RFID Tag Using Multiple Microstrip Open Stub Resonators,” *IEEE Transactions on Antennas and Propagation*, vol. 60, no. 9, pp. 4429–4432, Sep. 2012.
- [34] H.-S. Jang, W.-G. Lim, K.-S. Oh, S.-M. Moon, and J.-W. Yu, “Design of Low-Cost Chipless System Using Printable Chipless Tag With Electromagnetic Code,” *IEEE Microwave and Wireless Components Letters*, vol. 20, no. 11, pp. 640–642, Nov. 2010.
- [35] W.-s. Lee, H.-s. Jang, K.-s. Oh, and J.-w. Yu, “Design of Chipless Tag with Electromagnetic Code for Paper-based Banknote Classification,” *Proceedings of the Asia-Pacific Microwave Conference 2011*, pp. 1406–1409, Dec. 2011.
- [36] A. Islam, S. Bhuiyan, and N. Karmakar, “A Novel Compact Chipless RFID Tag and Near-Field Reader,” *Proceedings of the Asia-Pacific Microwave Conference 2011*, no. 1, pp. 1518–1521, Dec. 2011.

- [37] S. Gupta, B. Nikfal, and C. Caloz, “Chipless RFID System Based on Group Delay Engineered Dispersive Delay Structures,” *IEEE Antennas and Wireless Propagation Letters*, vol. 10, no. 2, pp. 1366–1368, Sep. 2011.
- [38] a. T. Blischak and M. Manteghi, “Embedded Singularity Chipless RFID Tags,” *IEEE Transactions on Antennas and Propagation*, vol. 59, no. 11, pp. 3961–3968, Nov. 2011.
- [39] A. Vena, E. Perret, and S. Tedjini, “Chipless RFID Tag Using Hybrid Coding Technique,” *IEEE Transactions on Microwave Theory and Techniques*, vol. 59, no. 12, pp. 3356–3364, Dec. 2011.
- [40] D. Girbau, A. Lazaro, and R. Villarino, “Passive wireless permittivity sensor based on frequency-coded chipless RFID tags,” no. 2, pp. 2–4, 2012.
- [41] A. Islam and N. C. Karmakal, “A Novel Compact Printable Dual-Polarized Chipless RFID System,” *IEEE Transactions on Microwave Theory and Techniques*, vol. 60, no. 7, pp. 2142–2151, Jul. 2012.
- [42] D. Girbau, J. Lorenzo, A. Lázaro, and C. Ferrater, “Frequency-Coded Chipless RFID Tag Based on Dual-Band Resonators,” *IEEE Antennas and Wireless Propagation Letters*, vol. 11, no. 4, pp. 126–128, 2012.
- [43] P. Kalansuriya, N. C. Karmakar, and E. Viterbo, “On the Detection of Frequency-Spectra-Based Chipless RFID Using UWB Impulsed Interrogation,” *IEEE Transactions on Microwave Theory and Techniques*, vol. 60, no. 12, pp. 4187–4197, Dec. 2012.
- [44] A. Vena, E. Perret, S. Tedjini, and S. Member, “High-Capacity Chipless RFID Tag Insensitive to the Polarization,” *IEEE Transactions on Antennas and Propagation*, vol. 60, no. 10, pp. 4509–4515, Oct. 2012.
- [45] A. Vena, E. Perret, and S. Tedjini, “Design of Compact and Auto-Compensated Single-Layer Chipless RFID Tag,” *IEEE Transactions on Microwave Theory and Techniques*, vol. 60, no. 9, pp. 2913–2924, Sep. 2012.

- [46] E. Perret, A. Vena, and S. Tedjini, “A Fully Printable Chipless RFID Tag With Detuning Correction Technique,” *IEEE Microwave and Wireless Components Letters*, vol. 22, no. 4, pp. 209–211, Apr. 2012.
- [47] A. Vena, E. Perret, and S. Tedjini, “A Depolarizing Chipless RFID Tag for Robust Detection and Its FCC Compliant UWB Reading System,” *IEEE Transactions on Microwave Theory and Techniques*, vol. 61, no. 8, pp. 2982–2994, Aug. 2013.
- [48] H. E. Matbouly, N. Boubekeur, and F. Domingue, “A Novel Chipless Identification Tag Based on a Substrate Integrated Cavity Resonator,” *IEEE Microwave and Wireless Components Letters*, vol. 23, no. 1, pp. 52–54, Jan. 2013.
- [49] N. C. Karmakar, R. v. Koswatta, P. kalansuriya, and R. E-Azim, *Chipless RFID Reader Architecture*, 2013.
- [50] M. Makimoto and S. Yamashita, *Microwave Resonators and Filters for Wireless Communication*.
- [51] D. Pozar, *Microwave and Rf Design of Wireless Systems*, 2000.
- [52] J. D. Baena, J. Bonache, F. Martín, R. M. Sillero, F. Falcone, T. Lopetegi, M. A. G. Laso, J. G. García, I. Gil, M. F. Portillo, and M. Sorolla, “Equivalent-Circuit Models for Split-Ring Resonators and Complementary Split-Ring Resonators Coupled to Planar Transmission Lines,” vol. 53, no. 4, pp. 1451–1461, 2005.
- [53] J. Carbonell and V. E. Boria, “Study of equivalent circuits for open-ring and split-ring resonators in coplanar waveguide technology,” no. 1, pp. 170–176, 2007.

Chapter 3

Coupled Bunch Hairpin Resonator Based Chipless RFID Tags

-
1. Characteristics of Hairpin Resonators
 2. Coupled Bunch Hairpin Resonators
 3. Disc Loaded Monopole Antenna
 4. Operating Principle of Spectral Signature Based Chipless RFID Tags
 5. Result and Discussions
 6. Conclusion

Multiresonator is an essential component of spectral signature based chipless RFID tags [4–33]. This chapter deals with the design and development of coupled bunch hairpin resonator for multiresonating circuit. A brief discussion on hairpin resonator and evolution of coupled bunch hairpin resonator are presented. The data encoding technique applied is also illustrated in detail. Two disc monopole antennas are connected to the proposed multiresonator for transmission and reception purpose. The complete tag system and its measured characteristics are discussed in detail.

3.1 Characteristics of Hairpin Resonator

The resonators used for printable chipless tag applications should be compact, fully planar and narrow bandwidth (high Q-factor) for optimum performance. Various resonators which are coupled to the microstrip transmission lines can be found in the open literature. Some of which are etched in the ground plane [15], some inside the microstrip line [8] or coupled to the microstrip line [6]. This section presents the detailed investigation of planar hairpin resonator which is the fundamental component of the coupled bunch hairpin resonator tag. The discussion starts with the microstrip line design.

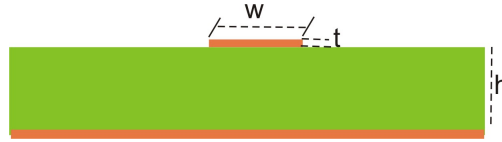


Figure 3.1: Cross section of microstrip line ($W = 3.4\text{mm}$, $h = 1.6\text{mm}$ and $\epsilon_r = 3.7$)

Microstrip line is a channel for electromagnetic waves, which consists of three layers. The layers are conducting strip, lossless dielectric substrate and infinite ground plane as shown in Figure 3.1. The effective permittivity and characteristic impedance of microstrip line are determined by physical parameters such as width of conducting strip (W), height of substrate (h) and relative permittivity of substrate (ϵ_r). According to Ross and Howes [?],

for $\frac{W}{h} \leq 2$

$$\epsilon_{eff} = \frac{\epsilon_r + 1}{2} + \frac{\epsilon_r - 1}{2} \left(1 + \frac{10h}{w}\right)^{-\frac{1}{2}} + 0.468 \frac{\epsilon_r + 0.5}{1.5} \sqrt{\frac{t}{w}} \quad (3.1)$$

for $\frac{W}{h} \geq 2$

$$\epsilon_{eff} = \frac{\epsilon_r + 1}{2} + \frac{\epsilon_r - 1}{2} \left(1 + \frac{10h}{w}\right)^{-\frac{1}{2}} \quad (3.2)$$

for $\frac{W}{h} \leq 1$

$$Z_0 = 60 \ln \left[\frac{8h}{w} + \frac{w}{4h} \right] \quad (3.3)$$

for $\frac{w}{h} \geq 1$

$$Z_0 = \frac{120\pi}{\left[\frac{w}{h} + 2.42 - 0.44 \frac{h}{w} + \left(1 - \frac{h}{w}\right)^6 \right]} \quad (3.4)$$

Usually 50Ω impedance line is used for RF/ microwave application. 30Ω cables have higher power handling capacity, whereas the lowest attenuation could be achieved by using 77Ω coaxial cables. Thus, 50Ω co-axial cable is selected as the ideal compromise which offers both power handling capacity and minimum attenuation. It is also used to design and fabricate microwave components such as resonators, filters, antennas, directional couplers and power divider etc. The advantage of microstrip line is less expensive and light weight compared to waveguide.

Parallel coupled line resonator consists of a conducting strip of width 0.2mm and electrical length $\frac{\lambda_g}{2}$ of particular frequency placed parallel to the conducting strip of microstrip line as shown in Figure 3.2. Such a resonator behaves as a shunt RLC resonator when the length $l =$ is multiples of $\frac{\lambda_g}{2}$ [51].

$$\lambda_g = \frac{\lambda_0}{\sqrt{\epsilon_{eff}}} \quad (3.5)$$

where λ_g is guided wavelength, λ_0 is free space wavelength and ϵ_{eff} is effective relative permittivity.

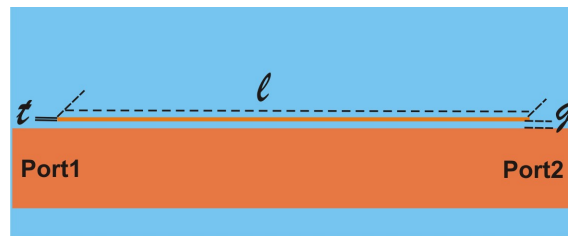


Figure 3.2: Microstrip coupled line resonator($l = 34\text{mm}$, $t = 0.2\text{mm}$, $g = 0.35\text{mm}$, $W = 3.4\text{mm}$ and $\epsilon_r = 3.7$)

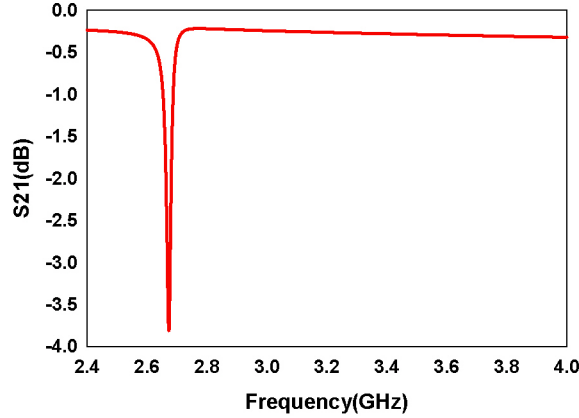


Figure 3.3: Simulated insertion loss of the coupled line resonator ($l = 34\text{mm}$, $t = 0.2\text{mm}$, $W = 3.4\text{mm}$, $h = 1.6\text{mm}$, $g = 0.35\text{mm}$ and $\epsilon_r = 3.7$)

A parametric study of coupled line resonator is carried out by using Ansoft HFSS software. Resonant frequency is determined by both physical dimension of resonator and substrate used for fabrication. As the length of resonator increases, the resonant frequency shifts towards lower side. A small frequency shift towards the lower side can be observed when the width of the resonator is large and this is due to the increased electrical length. To a certain extent, coupling strength can be increased by decreasing the coupling gap between transmission line and resonator.

Coupled parallel line resonator of length 34mm , width 0.2mm and gap between transmission line and resonator of 0.35mm is shown in Figure 3.2. The structure is simulated using Ansoft HFSS and the transmission characteristic exhibits resonance at 2.6828 GHz . The insertion loss at resonance is about -3.5dB and fractional bandwidth 0.12114 as depicted in Figure 3.3. The coupled line resonator inhibits the propagation of particular frequency (2.6828 GHz) through transmission line. The coupled resonator structure exhibits anti-resonance which attenuates energy at particular frequency. This attenuation technique is utilized to create band notch effect.

The disadvantages of coupled line resonator are large physical dimension and less energy coupling between transmission line and resonator. Due to these reasons, it is not a good candidate for chipless RFID tag applications. The coupling strength between resonator and transmission line can be enhanced by reducing the spacing between them, or by using high Q resonators.

The spacing between resonator and transmission line cannot be reduced beyond a limit due to fabrication problem. In such cases high Q resonators are the best option. High Q resonant structure has low band width and high coupling capacity.

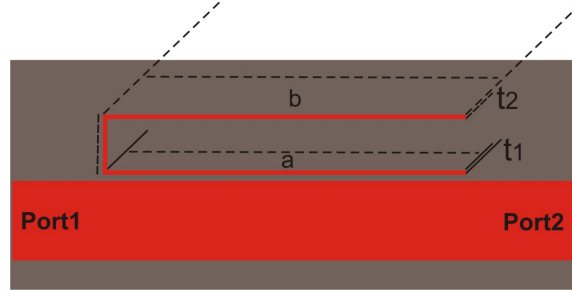


Figure 3.4: Coupled hairpin resonator ($a = b; t_1 = t_2$)

Line resonator is modified to a hairpin resonator to achieve compactness and to enhance energy coupling. Hairpin resonators have been used for microwave filters and Transversed Electromagnetic Waves (TEM) printed circuit realization [?]. The coupling characteristics and transmission characteristics of hairpin resonator is investigated in this section.

The wave propagation through the line is inhibited in the vicinity of the resonant frequency. It is obvious that the coupling in these structure is proximity coupling, which is basically through fringe fields. Strength of coupling has to be improved for better band rejection of band stop filter. Length of open loop resonator L_1

$$L_1 = \frac{\lambda_g}{2} = \frac{c}{2 * f_r * \sqrt{\epsilon_{reff}}}$$

where L_1 is total length of resonator, c is the velocity of light in free space, λ_g is guided wavelength of microstrip line and ϵ_{reff} is the effective dielectric constant of the microstrip line.

The geometry of coupled hairpin resonator is shown in Figure 3.4. Here resonator is printed on the same side parallel to the transmission line. The transmission characteristics of coupled hairpin resonator is shown in Figure 3.5. It resonates at 2.74GHz with 17dB insertion loss and act as a band stop filter. The open ended $\frac{\lambda_g}{2}$ hairpin resonator act as a parallel RLC circuit which

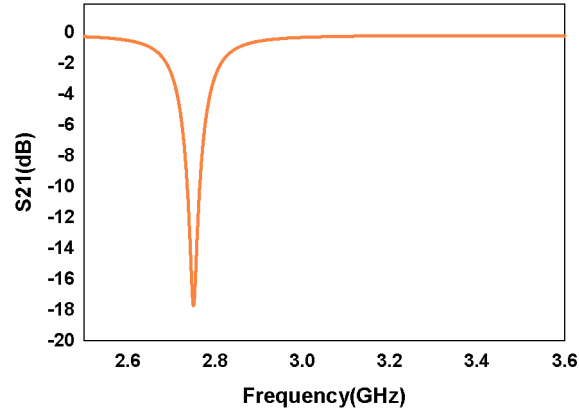


Figure 3.5: Simulated Insertion loss of the coupled hairpin resonator ($l = 34\text{mm}$, $t_1 = 0.2\text{mm}$, $t_2 = 0.2\text{mm}$, $W = 3.4\text{mm}$, $h = 1.6\text{mm}$, $g = 0.35\text{mm}$ and $\epsilon_r = 3.7$)

produces high impedance to transmission line at its resonance. The equivalent circuit of transmission line consist of lumped parameters such as series resistance (R), series inductance (L), parallel conductance (G) and parallel capacitance (C) [?]. The resonator circuit consists of inductive and capacitive parameters. The mutual coupling between resonator and transmission line provides band notch effect in circuit.

Surface Current Distribution

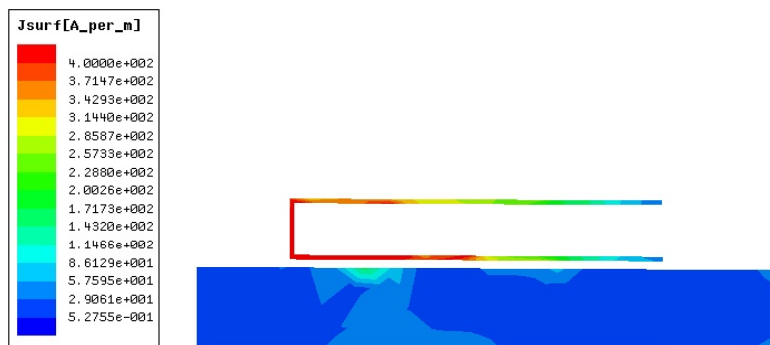


Figure 3.6: Surface current distribution at resonance at 2.74 GHz

Surface current distribution of hairpin resonator is shown in Figure 3.6, it is obvious that current distribution is greater at its resonant frequency and

the resonant length is about $\frac{\lambda_g}{2}$. Resonator absorbs electromagnetic energy from transmission line at its resonance. Consequently, the system act as a band notch filter and there is no current propagation from port 1 to port 2 of transmission line. Variation in electrical length of coupled symmetric hairpin resonator causes change in resonant frequency as shown in Figure 3.7. The relation between physical length(L) and wavelength (λ_g) are related to the following design equation.

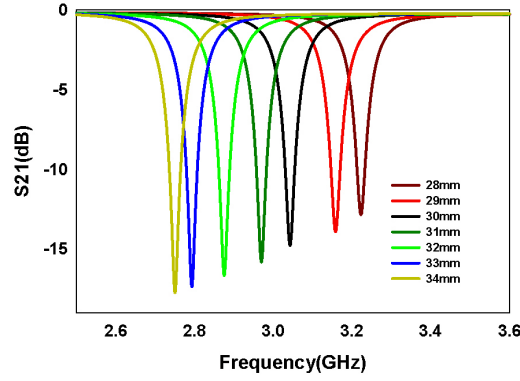


Figure 3.7: Effect of the variation in total length (L_1) of hairpin line resonator ($L_1 = a + b + c$)

$$L_1 = (a + b + c) \approx \frac{\lambda_g}{2}$$

where a , b and c are sectional length of hairpin.

Next we investigated asymmetric hairpin resonator as shown in Figure 3.8. The impedance and the electrical length of each section of asymmetric hairpin resonator is different, which acts as Stepped Impedance Resonator (SIR). Even electrical length is kept constant at $34mm$, the resonant frequency is shifted due to the variation length and width of the resonator as depicted in Figure 3.8 and Table.3.1. The fractional bandwidth of asymmetric hairpin resonator is smaller than the both symmetric hairpin resonator and coupled line resonator is shown in Table 3.2.

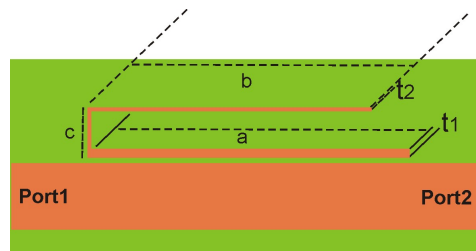


Figure 3.8: Geometry of asymmetric hairpin resonator ($a \neq b; t_1 \neq t_2$), ($L_i = a + b + c = 34\text{mm}$)

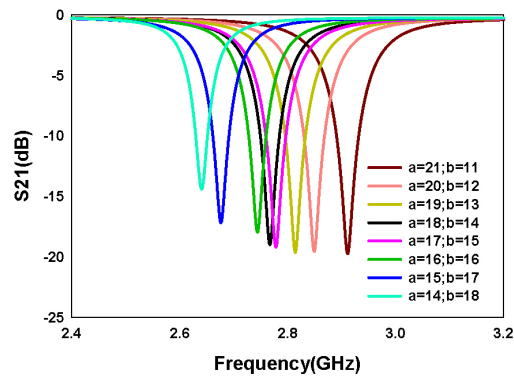


Figure 3.9: Effect of length and width variation in the asymmetric hairpin resonator ($a \neq b; t_1 \neq t_2$), ($L_i = a + b + c = 34\text{mm}$)

Table 3.1: Effect of variation in arm length (a, b) and width (w)

Arm length(mm)	Resonance(GHz)	Insertion loss(dB)
a=21;b=11	2.9968	-18.5064
a=20;b=12	2.9248	-18.9258
a=19;b=13	2.9168	-19.012
a=18;b=14	2.8736	-18.5205
a=17;b=15	2.7872	-18.0782
a=16;b=16	2.7616	-16.647
a=15;b=17	2.748	-15.5364
a=14;b=18	2.6952	-15.126

Table 3.2: Fractional bandwidth comparison

Resonator type	Bandwidth	Resonant frequency	FBW
Coupled line resonator	0.3236	2.6713	0.12114
Symmetric hairpin resonator	0.1058	2.7429	0.038572
Asymmetric hairpin resonator	0.0915	2.7607	0.033144

The characteristics of coupled line resonator, symmetric hairpin resonator and asymmetric hairpin resonator are investigated in this section. Hairpin resonators are suitable for narrow bandwidth application. Hence, hairpin resonator is modified to form a multiresonator. The evolution of bunch resonator from hairpin resonator is explained in the following section.

3.2 Coupled Bunch Hairpin Resonator

Enhancing the data encoding capacity is an important factor in the development of chipless RFID tag. In the previous section, a conventional coupled hairpin resonator is discussed. However, the main goal is to design a multiresonating circuit for encoding spectral signature. The geometry of the proposed coupled bunch hairpin resonator for chipless tag as shown in Figure 3.10 and the dimensions are given in Table.3.3. The coupled hairpin resonator is modified to form a bunch hairpin resonators. One section of hairpin resonators is common to all resonators. One part of hairpin resonator L_i ($i = 1, 2, 3...8$) along with common section will act as individual hairpin resonator at different frequencies. Here frequency can be independently controlled by varying the length of the corresponding section L_i . Here each bunch offers four resonance. In order to encode a data byte, two bunches are used. The bunches are placed on upper and lower side of the transmission line. The multiresonator circuit is printed on a substrate of relative permittivity (ϵ_r) = 3.7, loss tangent ($\tan \delta$) = 0.003 and height (h) = 1.6mm .

Generally, multiresonators are formed by multiple resonators which are placed in a cascaded manner. Predrovic et al. presented cascaded spiral resonator based multiresonator circuit for chipless tag applications [5]. In cascading, each resonator does not have any physical contact with other and they

work independently. Whereas, in our design a single structure exhibits multiple resonances and each resonator in this structure work independently. The novelty of proposed multiresonating circuit is that, it is designed by bunching the resonators instead of cascading resonators to achieve compactness. Each resonator in this structure has different resonant frequencies due to different electrical length. The common section of bunch resonator is placed very near to microstrip line to achieve maximum coupling and maximum attenuation at resonant frequencies. The coupled bunch hairpin resonator exhibits very low fractional bandwidth that helps to encode data very accurate with unique spectral signature.

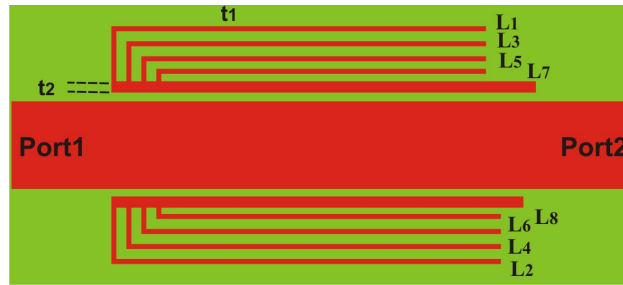


Figure 3.10: Coupled bunch hairpin resonator($L_1 = 34.15mm$, $L_2 = 34mm$, $L_3 = 32.35mm$, $L_4 = 32mm$, $L_5 = 30.5mm$, $L_6 = 30.2mm$, $L_7 = 28.55mm$, $L_8 = 28mm$, $h = 1.6mm$, $t_1 = 0.2mm$, $t_2 = 0.45mm$ and $g = 0.2mm$)

The two bunch resonators are electromagnetically coupled to the microstrip transmission line. Each bunch exhibits four resonant frequencies. When a sweep of electromagnetic energy propagates along the transmission line, the electromagnetic energy is coupled by these resonators and it inhibits the propagation of the resonant frequencies. Consequently, it shows eight notches in their transmission characteristics as shown in Figure 3.11. The resonant frequencies are found to be 2.6784GHz, 2.744GHz, 2.8552GHz, 2.9576GHz, 3.1296GHz, 3.2312GHz, 3.3832GHz and 3.4856GHz. The bandwidth required for presenting eight resonant frequency is 807.2MHz. Each band notch has very low value 3-dB bandwidth and hence Fractional bandwidth(FBW) which is helpful to accommodate more number of bits in a small frequency spectrum. These resonant frequencies, bandwidth and FBW are shown in Table.3.4.

The surface current of each resonator at its eight resonant frequencies are shown in Figure 3.12. Each resonator is excited when its length is approximately equal to $\frac{\lambda_g}{2}$. The current distribution is minimum at both ends and

Table 3.3: Geometric parameters of the coupled bunch hairpin multiresonator

Parameter	Physical dimension (mm)
Hieght, h	1.6
Length of the resonator, L1	34.15
Length of the resonator, L2	34
Length of the resonator, L3	32.35
Length of the resonator, L4	32
Length of the resonator, L5	30.5
Length of the resonator, L6	30.2
Length of the resonator, L7	28.55
Length of the resonator, L8	28
width,t1	0.2
width,t2	0.45

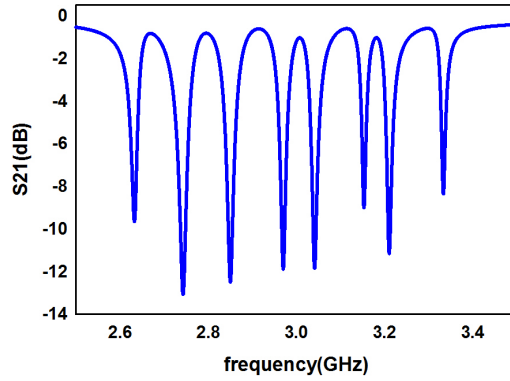


Figure 3.11: Simulated insertion loss of 8-bit coupled bunch hairpin multiresonator based band stop filter ($L_1 = 34.15\text{mm}$, $L_2 = 34\text{mm}$, $L_3 = 32.35\text{mm}$, $L_4 = 32\text{mm}$, $L_5 = 30.5\text{mm}$, $L_6 = 30.2\text{mm}$, $L_7 = 28.55\text{mm}$, $L_8 = 28\text{mm}$, $h = 1.6\text{mm}$, $t_1 = 0.2\text{mm}$, $t_2 = 0.45\text{mm}$ and $g = 0.2\text{mm}$)

maximum at center of the resonator that means apparent half wavelength variation of surface current at resonance. The mutual coupling between resonators is very low since, the performance of each resonator is not affected by nearest resonators.

The proposed structure is a good candidate for multiresonator based chipless tag applications due to its narrow bandwidth, less mutual coupling, compact structure, less complexity in structure with an added advantage of easy printing on substrate.

Table 3.4: Bandwidth, fractional bandwidth and Q at different resonances

Lenth of resonator	frequency(GHz)	BW (MHz)	FBW
34.15mm	2.6784	31.4716	0.011750149
34 mm	2.744	31.256	0.011390671
32.35mm	2.8552	29.4948	0.010330205
32 mm	2.9576	29.0424	0.009819583
30.5mm	3.1296	27.3704	0.008745654
30.2mm	3.2312	26.9688	0.008346373
28.55mm	3.3832	25.1668	0.007438756
28 mm	3.4856	24.5144	0.00703305

3.3 Data Encoding Technique

One of the main challenges faced during development of chipless RFID tag is how to encode digital code on passive microwave circuits. Each bit is usually associated with the presence or absence of a resonant peak at a predetermined frequency in the spectrum. The presence of resonance is used to encode logic 1 and the absence of resonance is used to encode logic 0. In order to avoid a particular resonance from predetermined spectrum to form a unique spectral signature, open the corresponding resonator by removing a small portion of metal near the common section of bunch resonator as shown in Figure 3.13. Consequently, the effect will be same as absence of that particular resonator. The absence of a specific resonator will cause minimum attenuation at that particular frequency i.e, the particular notch will be disappeared from the

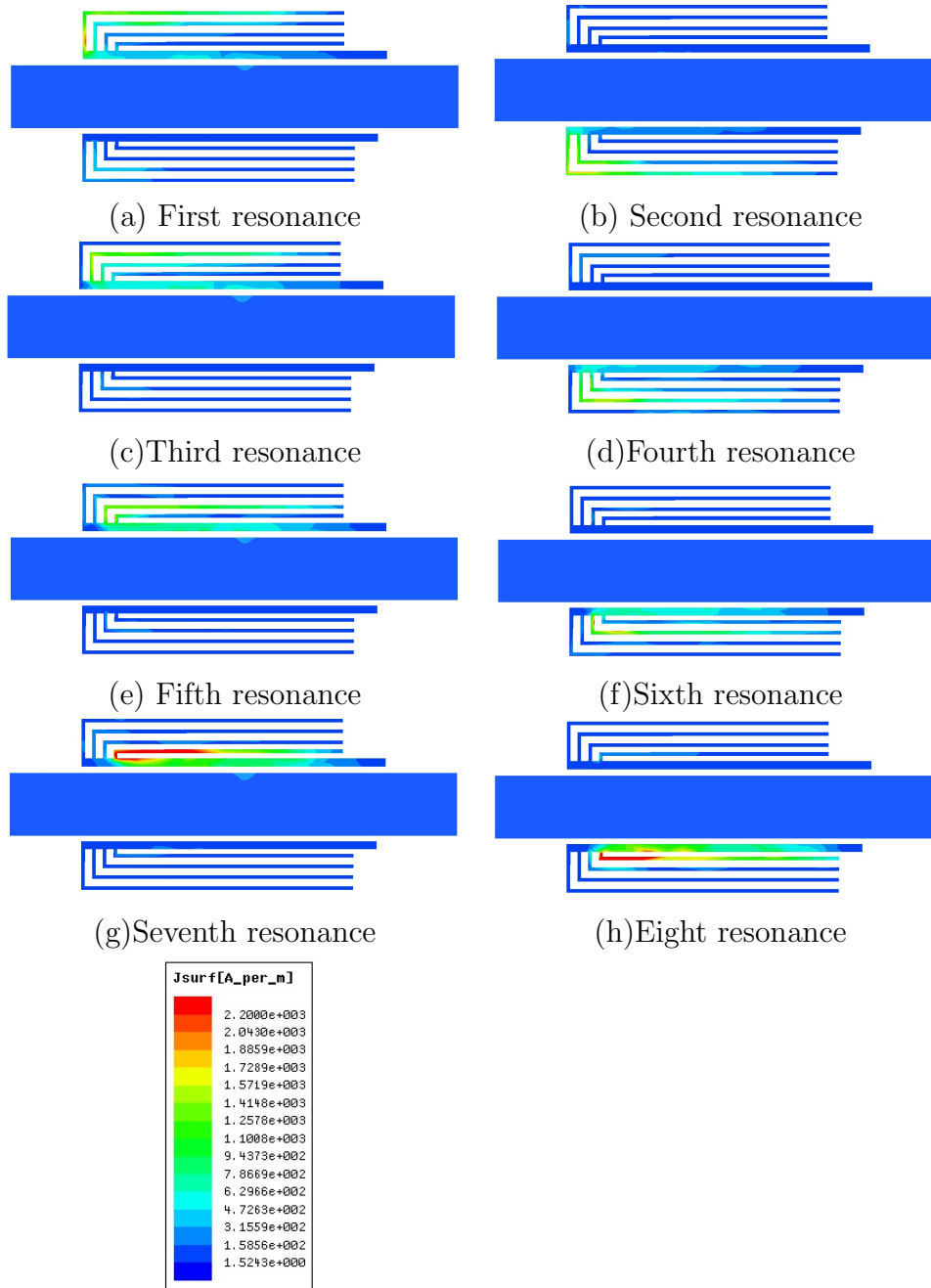


Figure 3.12: Surface current distribution at each resonance

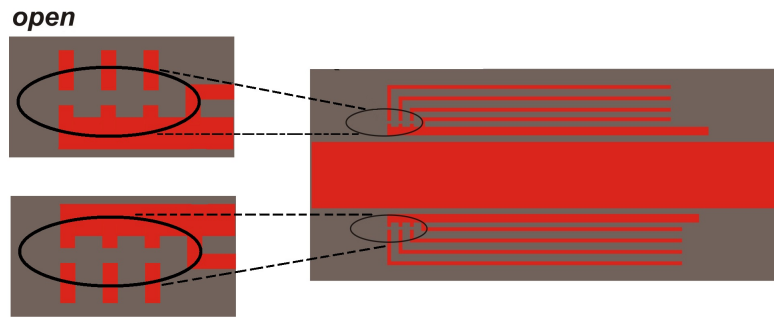


Figure 3.13: Data encoding technique

tag. This encoding method is used here. Different bit combinations of multiresonator based hairpin tag are shown in Figure 3.14. Another technique to avoid a particular resonance is either increase or decrease electrical length of specific resonator and it will resonate at a resonant frequency outside the frequency spectrum of tag.

3.4 Disc-Loaded Monopole Antennas

Spectral signature based chipless RFID requires two UWB antennas to be connected to the multiresonator circuit. High bandwidth antennas are required for chipless tag applications. A circular shaped patch is placed at the top of monopole to achieve large bandwidth. The geometry of disc loaded microstrip fed monopole UWB antenna is shown in Figure 3.15.

The antenna should have good impedance matching over entire frequency band and also needs linear polarization characteristics to achieve good reception and retransmission of interrogation signal. The antenna characteristics are mainly determined by the layout parameters such as ground size $L_g \times W_g$ and radius of circular disc structure. The ground parameter both $L_g \times W_g$ provides impedance matching, omni direction radiation pattern, high efficiency and gain for entire frequency band. But diameter of circular disc determines the fundamental resonance of antenna. It is approximately

$$\frac{\lambda_{g1}}{4} \approx 2R$$

where λ_{g1} is guided wavelength at fundamental resonance.

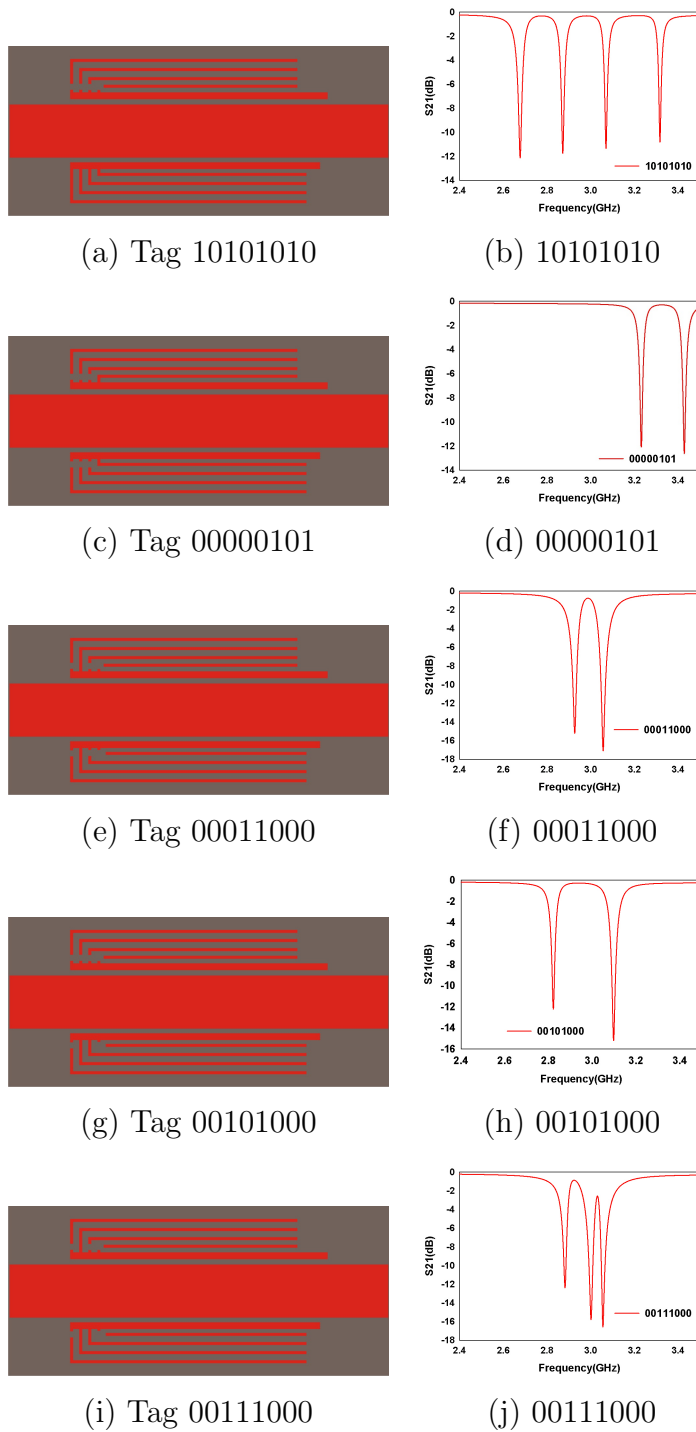


Figure 3.14: Generation of different spectral signature

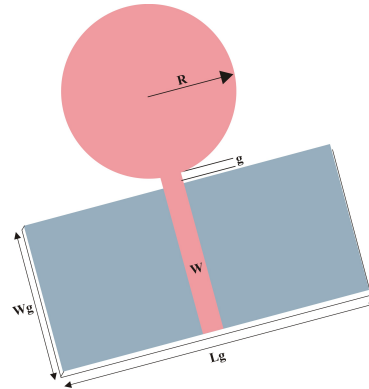


Figure 3.15: Geometry of UWB antenna ($L_g = 40\text{mm}$, $W_g = 20\text{mm}$, $W = 3\text{mm}$, $R = 15\text{mm}$, $\epsilon_r = 4.3$ and $h = 1.6\text{mm}$)

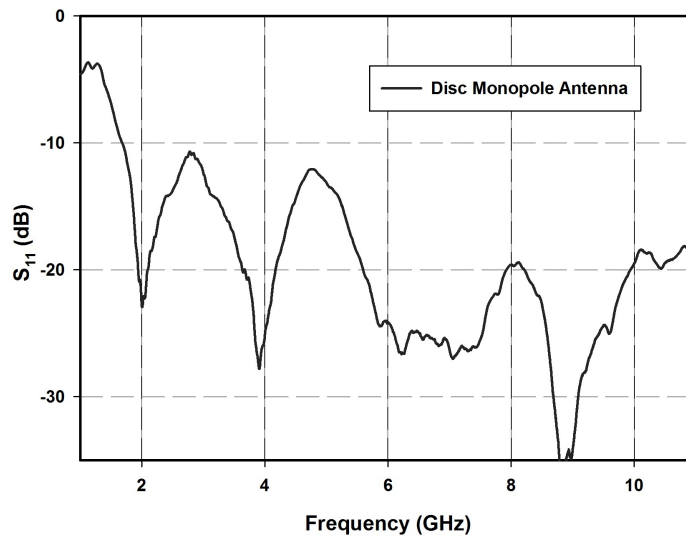


Figure 3.16: Measured returnloss of microstrip fed disc loaded monopole antenna

Circular disc structure supports multiple resonant modes. The band width enhancement is achieved by overlapping of these multiple resonant modes which are shown in Figure 3.16. The disc monopole antenna operates in a hybrid mode of standing wave and traveling wave. Standing wave and traveling wave dominate at low and high frequencies respectively. The bandwidth is limited at higher frequency due to poor structural support to traveling wave.

The radiation behavior of antenna is analyzed by using return loss, sur-

face current distributions and radiation patterns. The radiation patterns are plotted by using PNA E 8362B by placing antenna in anechoic chamber. The surface current distribution of the antenna at different frequencies are plotted by using Ansoft HFSS software as shown in Figure 3.17. There are different energy modes excited in this structure. At lower frequencies, they are purely standing wave modes but in higher frequencies they are traveling wave modes.

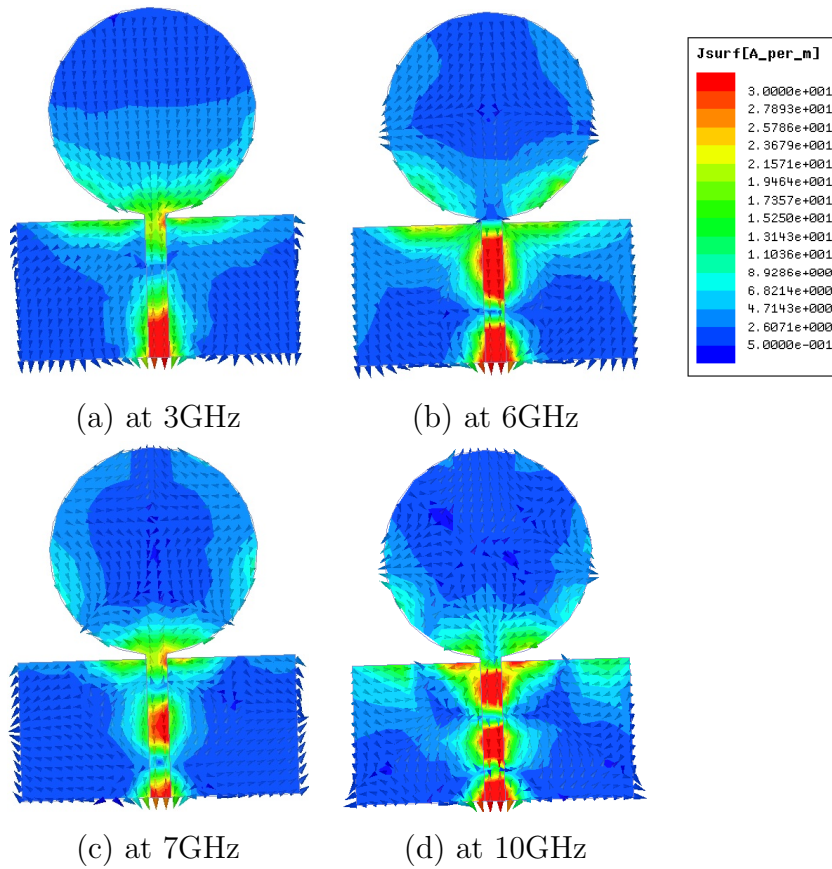


Figure 3.17: Surface current distribution of UWB monopole antenna at different frequencies

The measured radiation pattern at different frequencies are plotted in Figure 3.18. The UWB antenna exhibits omnidirectional radiation pattern. The antenna exhibits good isolation between co-polarization and cross polarization. Above 7GHz, deterioration is due to the excitation of higher order modes.

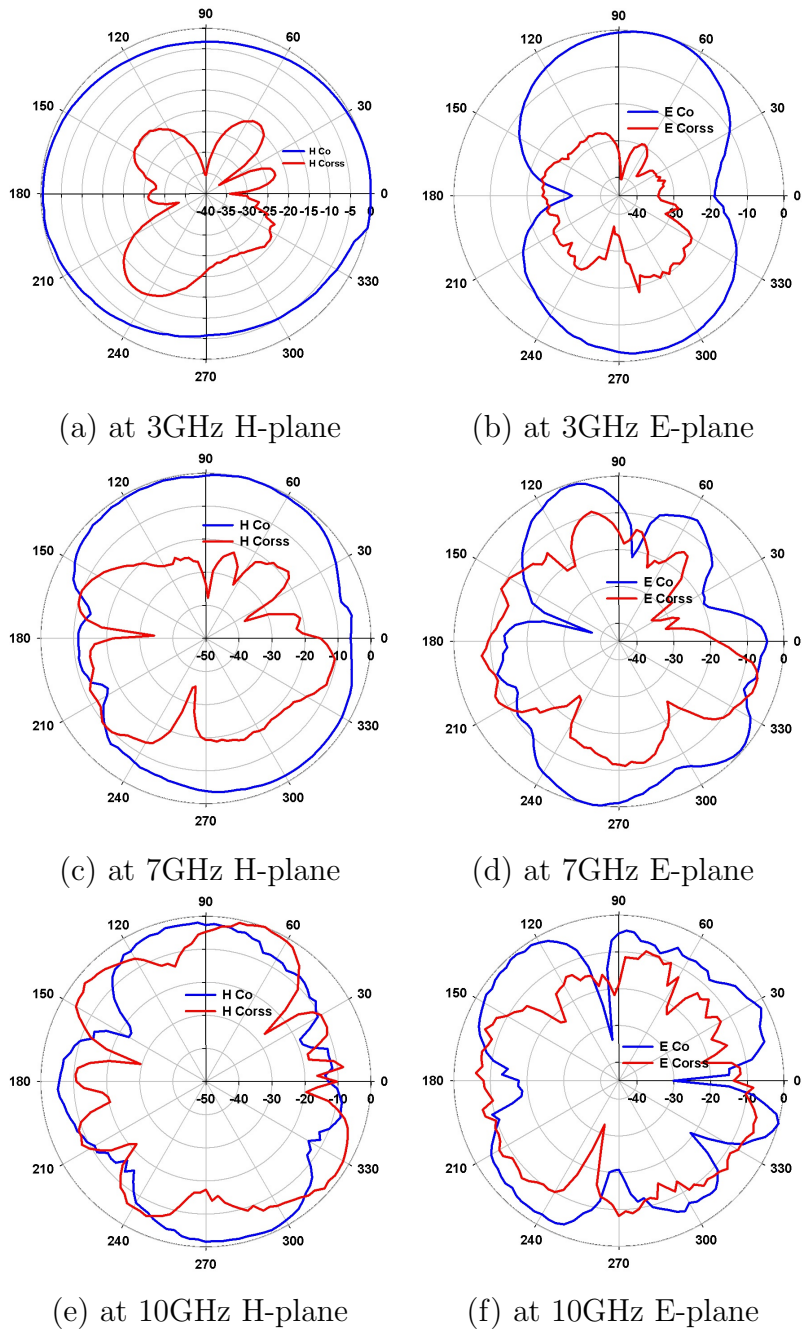


Figure 3.18: Measured radiation pattern of UWB monopole antenna

The disc loaded monopole antenna is used for wide band applications. The wide bandwidth is achieved by different modes overlapped together. The

overall gain of disc loaded monopole antenna is about 3 dBi and it offers high efficiency of about 85%. The gain of both Horn antenna and disc loaded monopole antenna are shown in Figure 3.19. Two wide band antennas connected to the tag with opposite polarization to achieve isolation between interrogative signals and re-transmitted signals.

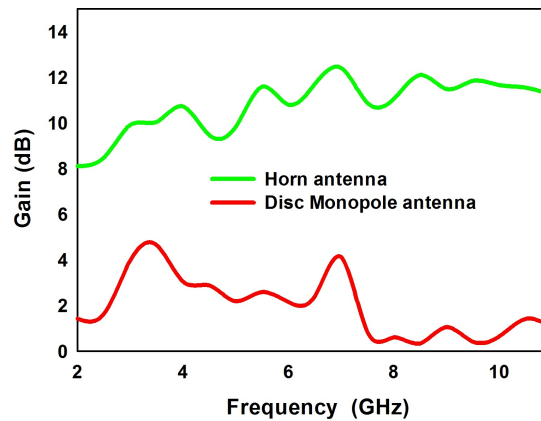


Figure 3.19: Measured gain of both horn antenna and microstrip fed disc loaded monopole antenna

3.5 Operating Principle of Spectral Signature Based Chipless Tags

The preceding sections explain how the wide band antennas are incorporated to a multiresonating circuit to form a complete chipless RFID tag. The data bits are encoded using the bunch hairpin resonators based multiresonator circuit as a unique spectral signature. The disc loaded monopole antennas are used for transmitting the signal from the tag and receiving signal from the reader. The tag antennas are cross polarized, in order to avoid the interference between them as shown in Figure 3.20. The two wide band antennas are incorporated to a multiresonating circuit to form a complete chipless tag. The reader sends a multifrequency interrogation signal to the tag. The receiving interrogation signal passes through the multiresonating circuit, which encodes the unique spectral signature to it and the output is re-transmitted.

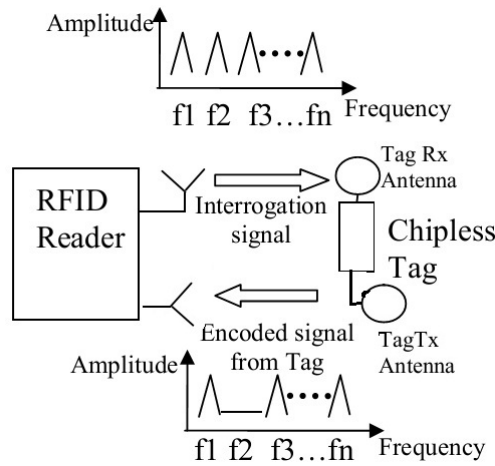


Figure 3.20: Block diagram of Spectral signature based chipless RFID reader system (Courtesy: S.Predrovic et.al.) [6]

3.6 Results and Discussions

There are two bunch resonators with four resonance printed on the same plane of the substrate. Each bunch resonator is arranged on opposite side of microstrip feed line. The photograph of coupled bunch hairpin multiresonator is shown in Figure 3.21. The prototypes are fabricated on different substrates. One made of dielectric constant (ϵ_r) 3.7, loss tangent ($\tan \delta$) 0.003 and height of substrate (h) 1.6mm. The other on a substrate with dielectric constant (ϵ_r) 4.3, loss tangent ($\tan \delta$) 0.0018 and height 1.6mm. The length of resonators are $L_1 = 34.15mm$, $L_2 = 34mm$, $L_3 = 32.35mm$, $L_4 = 32mm$, $L_5 = 30.5mm$, $L_6 = 30.2mm$, $L_7 = 28.55mm$, $L_8 = 28mm$ and width $t_1 = 0.2mm$, $t_2 = 0.45mm$. All experimental measurements are carried out by using PNA E8362B analyzer.



Figure 3.21: Photograph of the proposed multiresonator compared with INR 10 coin

Two probes of analyzer are calibrated to get exact measurement of transmission characteristics. Then, the multiresonating circuit fabricated on a substrate of dielectric constant, (ϵ_r 3.7) is connected between them. There are eight notches in transmission characteristics as shown in Figure 3.22. These resonant frequencies are found to be 2.73 GHz, 2.81 GHz, 2.9072 GHz, 3.04 GHz, 3.18 GHz, 3.25 GHz, 3.44 GHz and 3.52 GHz. The measured insertion loss and group delay of multiresonator is shown in Table. 3.5. The presence or absence of resonance are utilized to encode data on multiresonator. Spectral signature can be decoded from transmission characteristic parameters such as S_{21} , group delay, phase and SWR. These parameters are correlated with each other by their amplitude and phase. Both amplitude attenuation and phase jump are used to encode data on multiresonator.

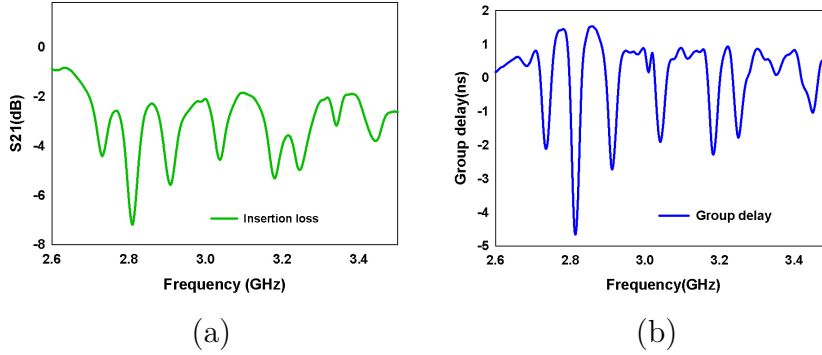


Figure 3.22: Measured (a) Insertion loss (b) Group delay of bunch hairpin resonator

Table 3.5: Measured transmission characteristics of bunch hairpin resonator on a substrate with ϵ_r 3.7

Resonant frequency(GHz)	Insertion loss(dB)	Group dealay(ns)
2.73	-4.4185	1.83
2.81	-7.1953	4.3383
2.90	-5.5622	2.6659
3.04	-4.521	1.8979
3.18	-5.3262	2.1754
3.25	-4.8737	1.7812
3.44	-3.1	0.6
3.52	-3.7981	1.0335

The bit combination 1111 1110 is shown in Figure 3.23. These resonant frequencies are found to be 2.1237 GHz, 2.27 GHz, 2.4072 GHz, 2.54 GHz, 2.77 GHz, 2.9385 GHz and 3.0879 GHz. The highest resonant frequency, 3.21 GHz vanishes in this result because, one of the resonators is detached from the bunch resonator. The highest resonance at 3.21 GHz is considered as Least Significant Bit (LSB) and the lowest resonant frequency 2.1237 GHz is known as Most Significant Bit (MSB). The circuit carries encoded data 1111 1110. The LSB becomes zero. Here presence of resonance in predetermined spectrum is considered as logic 1 and absence of resonance as logic 0. The measured insertion loss and group delay at resonance are shown in Table.3.6.

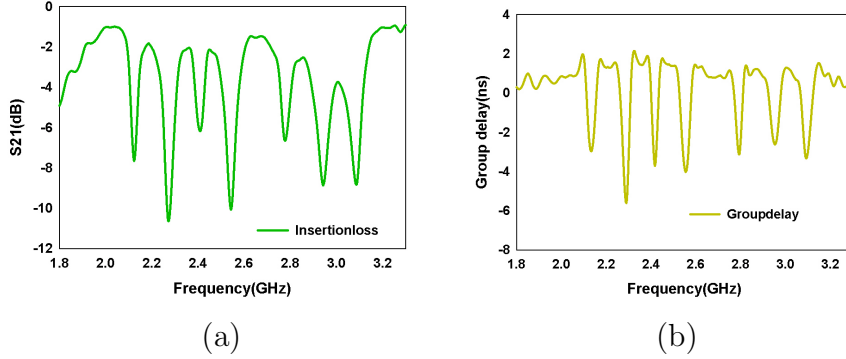


Figure 3.23: Bunch hairpin resonator fabricated on a substrate of ϵ_r 4.3 : Measured (a) Insertion loss (b) Group delay of the multiresonator

Table 3.6: Measured transmission characteristics of bunch hairpin resonator on a substrate with ϵ_r 4.3

Resonant frequency(GHz)	Insertion loss(dB)	Group dealay(ns)
2.1237	-7.66	2.3233
2.27	-10.5916	5.5432
2.4072	-5.8126	3.7177
2.54	-10.0781	3.1428
2.77	-6.5782	3.1018
2.9835	-8.8672	2.2156
3.0879	-8.7727	3.2387

3.6.1 Field Trials

Two cross polarized horn atennas are connected with analyzer to make a chipless tag reader. The tag mounted on a stand 35cm apart from the reader antenna. The measurement set up as shown in Figure 3.24. The system is calibrated with a microstrip line connected with two orthogonal polarized antennas. The microstrip line is replaced with coupled bunch hairpin resonator to read the unique spectral signature. The magnitude attenuation and group delay of the multiresonator are depicted in Figure 3.25. The field response

of different bit combinations are shown in Figure 3.26. The Figure 3.26(a) represents the ID 1111 1111. Here, eight resonators are embedded. ID 1111 1110 is shown in Figure 3.26(b). The highest frequency (LSB) 3.52 GHz is disappeared by put an open in that particular resonator from multiresonator circuit. The ID 1110 1110 and 1110 1100 responses are shown in Figure 3.26(c) and (d) respectively.

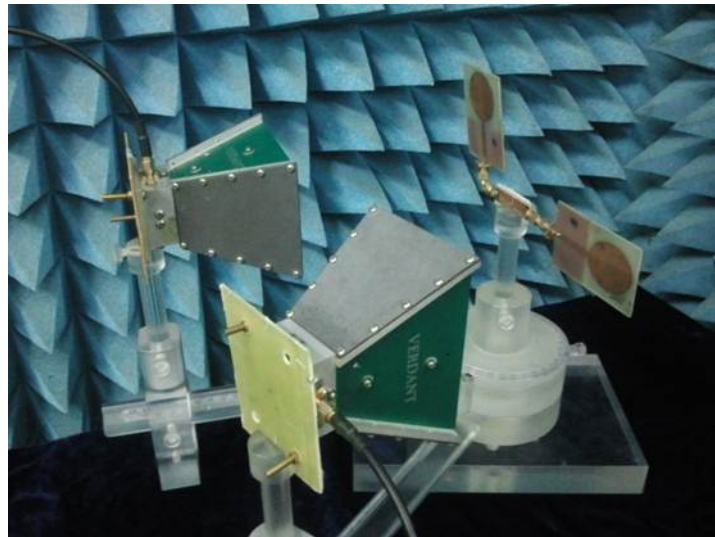


Figure 3.24: Bistatic measurement set up

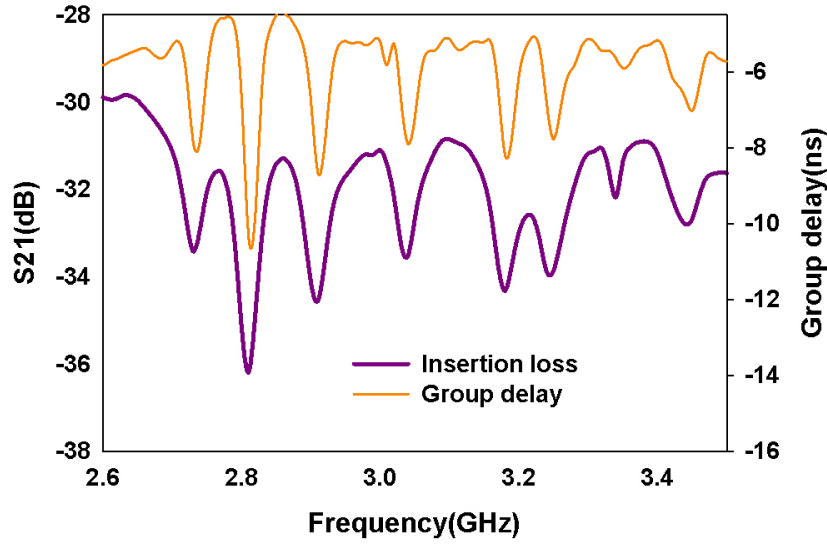
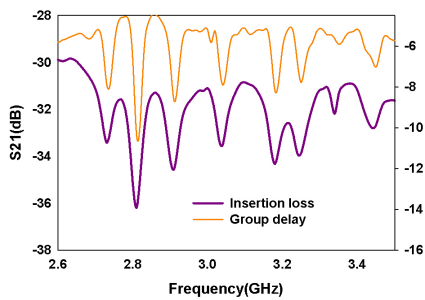
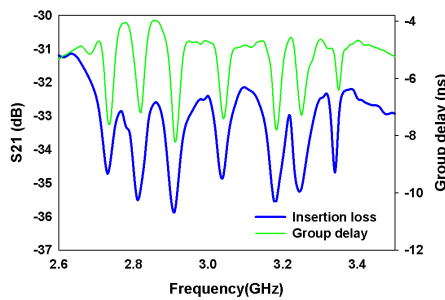


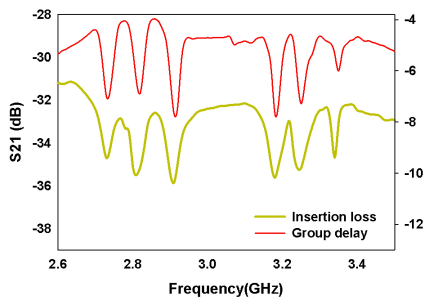
Figure 3.25: Tag response 1111 1111



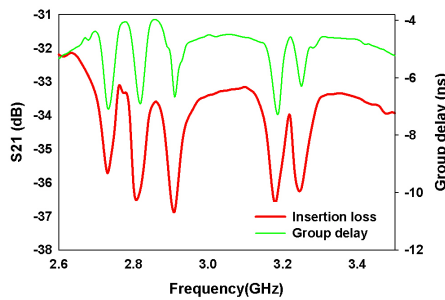
(a) Tag response 1111 1111



(b) Tag response 1111 1110



(c) Tag response 1110 1110



(d) Tag response 1110 1100

Figure 3.26: Different tag response of coupled bunch hairpin multiresonator based tag

3.7 Conclusion

The bunch resonator is highly compact different from ordinary coupled hairpin resonator. One arm of the hairpin section is made common to all resonators, thus achieving compactness. Section L_i ($i=1,2,3,8$) along with common section will act as individual hairpin resonator. Here frequency can be independently controlled by varying the length of the corresponding section L_i . The proposed multiresonator is good candidate for spectral signature based chipless tag.

REFERENCES

- [1] S. Preradovic, I. Balbin, N. C. Karmakar, and G. Swiegers, "Chipless Frequency Signature Based RFID Transponders," *Proceedings of the 38th European Microwave Conference Chipless*, no. 38, pp. 1723–1726, Oct. 2008.
- [2] S. Preradovic, I. Balbin, and N. Karmakar, "The development and design of a novel chipless RFID system for low-cost item tracking," *2008 Asia-Pacific Microwave Conference*, pp. 1–4, Dec. 2008.
- [3] S. Preradovic, I. Balbin, N. C. Karmakar, S. Member, and G. F. Swiegers, "Multiresonator-Based Chipless RFID System for Low-Cost Item Tracking," *IEEE Transactions on Microwave Theory and Techniques*, vol. 57, no. 5, pp. 1411–1419, May 2009.
- [4] S. Preradovic, S. Roy, and N. Karmakar, "Fully printable multi-bit chipless RFID transponder on flexible laminate," *2009 Asia Pacific Microwave Conference*, pp. 2371–2374, Dec. 2009.
- [5] S. Preradovic and N. C. Karmakar, "Design of Chipless RFID Tag for Operation on Flexible Laminates," *IEEE Antennas and Wireless Propagation Letters*, vol. 9, pp. 207–210, Sep. 2010.
- [6] S. Preradovic, M. Roy, and N. C. Karmakar, "RFID System Based on Fully Printable Chipless Tag for Paper-/Plastic-Item Tagging," *IEEE Antennas and Propagation Magazine*, vol. 53, no. 5, Oct. 2011.

- [7] S. Preradovic and N. C. Karmakar, "Design of Fully Printable Planar Chipless RFID Transponder with 35-bit Data Capacity," *Proceedings of the 39th European Microwave Conference*, pp. 13–16, Oct. 2009.
- [8] S. Bhuiyan, R.-e. Azim, and N. Karmakar, "A Novel Frequency Reused Based ID Generation Circuit for Chipless RFID Applications," *Proceedings of the Asia-Pacific Microwave Conference 2011*, pp. 1470–1473, Dec. 2011.
- [9] S. Preradovic and N. C. Karmakar, "Design of short range chipless RFID reader prototype," *2009 International Conference on Intelligent Sensors, Sensor Networks and Information Processing (ISSNIP)*, pp. 307–312, Dec. 2009.
- [10] S. Preradovic, "Multiresonator Based Chipless RFID Tag and Dedicated RFID Reader," *proceedings of IMS 2010*, no. iv, pp. 1520–1523, Jun. 2010.
- [11] S. Preradovic and N. Karmakar, "4 th Generation Multiresonator-Based Chipless RFID Tag Utilizing Spiral EBGs," *Proceedings of the 40th European Microwave Conference*, no. September, pp. 1746–1749, Sep. 2010.
- [12] S. Preradovic and Karmakar, "Chipless RFID tag with integrated sensor," *2010 IEEE Sensors conference*, pp. 1277–1281, Nov. 2010.
- [13] T. Kim, U. Kim, J. Kwon, and J. Choi, "Design of a Novel Chipless RFID Tag Using a Simple Bandstop Resonator," *Proceedings of Asia-Pacific Microwave Conference 2010*, pp. 2264–2267, Dec. 2010.
- [14] S. Hu, Y. Zhou, C. L. Law, and S. Member, "Study of a Uniplanar Monopole Antenna for Passive Chipless UWB-RFID Localization System," *IEEE Transactions on Antennas and propagation*, vol. 58, no. 2, pp. 271–278, Feb. 2010.
- [15] L. Reichardt, G. Adamiuk, G. Jereczek, and T. Zwick, "Chipless RFID Systems for Car-to-Infrastructure Communication," *2010 IEEE International Conference on Communications Workshops*, pp. 1–5, May 2010.

- [16] R. Koswatta and N. C. Karmakar, "Investigation into Antenna Performance on Read Range Improvement of Chipless RFID Tag Reader," *Proceedings of Asia-Pacific Microwave Conference 2010*, pp. 1300–1303, Dec. 2010.
- [17] S. Preradovic and N. C. Karmakar, "Chipless RFID : Bar Code of the Future," *IEEE Microwave Magazine*, no. December, pp. 87–97, Dec. 2010.
- [18] S. Preradovic and N. Karmakar, "Chipless Millimeter Wave Identification (MMID) Tag at 30 GHz," *Proceedings of the 41st European Microwave Conference Chipless*, no. October, pp. 123–126, Oct. 2011.
- [19] N. C. Karmakar and C. K. Pern, "mm-wave chipless RFID tag for low-cost item tagging," *Proceedings of the Asia-Pacific Microwave Conference 2011*, pp. 1462–1465, Dec. 2011.
- [20] S. Preradovic, N. Kamakar, and E. Amin, "Chipless RFID Tag with Integrated Resistive and Capacitive Sensors," *Proceedings of the Asia-Pacific Microwave Conference 2011*, pp. 1354–1357, Dec. 2011.
- [21] M. Polivka, J. Havlíek, M. Svanda, and J. Machá, "Detection of Spiral Resonator Array for Chipless RFID," *6th European Conference on Antennas and Propagation (EUCAP)*, pp. 3001–3004, Mar. 2011.
- [22] E. M. Amin and N. Karmakar, "Development of a chipless RFID temperature sensor using cascaded spiral resonators," *2011 IEEE SENSORS Proceedings*, pp. 554–557, Oct. 2011.
- [23] P. Kalansuriya, N. Karmakar, and E. Viterbo, "Signal Space Representation of Chipless RFID Tag Frequency Signatures," *2011 IEEE Global Telecommunications Conference - GLOBECOM 2011*, pp. 1–5, Dec. 2011.
- [24] R. V. Koswatta and N. C. Karmakar, "A Novel Method of Reading Multi-Resonator Based Chipless RFID Tags Using an UWB Chirp Signal," *Proceedings of the Asia-Pacific Microwave Conference 2011*, pp. 1506–1509, Dec. 2011.
- [25] S. Preradovic and N. Karmakar, "Chipless RFID for intelligent traffic information system," *2011 IEEE International Symposium on Antennas and Propagation (APSURSI)*, pp. 992–995, Jul. 2011.

- [26] S. Preradov, M. Roy, and C. N. Karmakar, "RFID System Based on Fully Printable Chipless Tag for Paper-/Plastic-Item Tagging," *IEEE Antennas and Propagation Magazine*, vol. 53, no. 5, Oct. 2011.
- [27] S. Preradovic and A. Menicanin, "Chipless Wireless Sensor Node," *MIPRO 2012, Opatija, Croatia*, pp. 179–182, May 2012.
- [28] R. V. Koswatta and N. C. Karmakar, "A Novel Reader Architecture Based on UWB Chirp Signal Interrogation for Multiresonator-Based Chipless RFID Tag Reading," *IEEE Transactions on Microwave Theory and Techniques*, vol. 60, no. 9, pp. 2925–2933, Sep. 2012.
- [29] C. M. Nijas, R. Dinesh, U. Deepak, A. Rasheed, S. Mridula, K. Vasudevan, and P. Mohanan, "Chipless RFID Tag Using Multiple Microstrip Open Stub Resonators," *IEEE Transactions on Antennas and Propagation*, vol. 60, no. 9, pp. 4429–4432, Sep. 2012.
- [30] S. Preradovic, I. Balbin, N. C. Karmakar, and G. Swiegers, "A Novel Chipless RFID System Based on Planar Multiresonators for Barcode Replacement," *IEEE International Conference on RFID The Venetian, Las Vegas, Nevada, USA*, vol. 3169, pp. 289–296, Apr. 2008.
- [31] J.A.G Malherbe, "Microwave transmission line filters," *Artech House*, 1979.
- [32] D. Pozar, "Microwave and Rf Design of Wireless Systems ," 2000.
- [33] E. G. Cristal and S. Frankel, "Hairpin line and hybrid hairpin line/ Halfwave parallel coupled line filters," no. 11, pp. 719–728, 1972.

Chapter 4

Open stub Multiresonator Based Chipless RFID Tag

1. Open Stub Resonators
 2. Modified Transmission Line
 3. Open Stub Multiresonator in the Modified Transmission Line
 4. Spectral Signature Coding Technique
 5. Chipless RFID Tag Development
 6. Conclusion
-

This chapter describes the detailed experimental and simulation studies about the usage of microwave open stubs for RFID applications. The fundamental microstrip transmission line is modified to accommodate resonators inside the line for achieving compact high Q operating mode. The multiresonator is compact and the data encoding capacity is about $2.85 \text{ bit}/\text{Cm}^2$.

4.1 Open Stub Resonator

Resonators are the most important elements in Radio Frequency (RF) and microwave engineering. To enhance the data coding capacity in spectral signature based tags it requires large number of resonances in a limited bandwidth. The successive resonant frequencies of the resonators should be closed spaced in the frequency domain. In order to achieve spectral separation, the quality factor of each resonance needs to be very high. It cannot be extended beyond a limit, since the enhanced quality factor causes a poor immunity to the surrounding environment. Moreover, increasing the number of resonators is an efficient way to increase the capacity of coding, but the coupling effect has to be taken into consideration.

Here we investigate open stub resonators for chipless tag applications. Basically, open stub shunt resonators [31] are quarter wavelength unit impedance resonator with one end connected to either feed line or ground which acts as a parallel RLC resonant circuit. Chipless tag application requires high-Q planar resonant structures.

4.2 Modified Microstrip Transmission Line

The conventional microstrip line is a guided wave structure for microwave applications which consists of three layers, conducting strip on top layer, lossless dielectric substrate and infinite ground plane at the bottom side. The cross sectional and top view of microstrip line are shown in Figure 4.1 and its transmission characteristics are plotted in Figure 4.2. The wavelength corresponding to a frequency is different in different media due to change in effective dielectric constant. Effective permittivity and characteristic impedance of microstrip line are determined by combining the effect of physical parameters such as width of conducting strip w , height of substrate h and relative permittivity of substrate ϵ_r . The related empirical formulas have been explained in the equation 3.1 and 3.2 in previous chapter. Here 50Ω impedance is chosen for achieving moderate power handling capacity and reduce the signal attenuation level. It can be inferred from the graph that the line shows negligible insertion loss over the band. The physical dimensions of microstrip line are

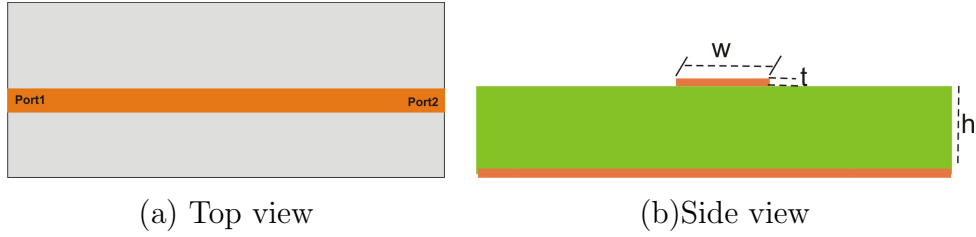


Figure 4.1: Conventional microstrip transmission line ($w = 3.4mm$, $h = 1.6mm$ and $\epsilon_r = 3.7$)

strip width, $w = 3.4mm$ ground size $L_g \times W_g$ is $28 \times 13.8 mm^2$ and height $h = 1.6mm$. The characteristics impedance of the line is about 50Ω .

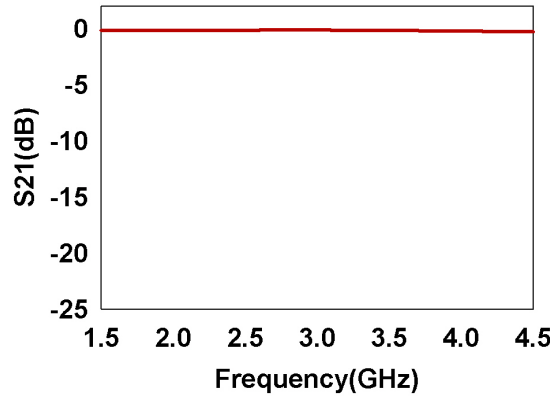


Figure 4.2: Transmission characteristics of the microstrip line ($w = 3.4mm$, $h = 1.6mm$ and $\epsilon_r = 3.7$)

The open stub shunt resonators are already employed for chipless tag applications [?, ?] but it has only moderate fractional bandwidth. i.e. Q-factor of open circuited shunt stub resonator is low. In order to enhance the Q-factor, the open stub resonators are placed inside the modified microstrip transmission line. The microstrip transmission line has to be modified by bifurcating and then the line has to be rejoined to form an island like structure to accommodate multiple resonators inside the line as shown in Figure 4.3. The slot size is $L_s \times W_s$ which accommodates open stub resonators. The transmission characteristics of the modified microstrip transmission line is shown in Figure 4.4. It is observed that the performance of proposed transmission line is de-

teriorated as compared to the conventional microstrip transmission line due to the reflections offered by the two 90° bends in the structure.

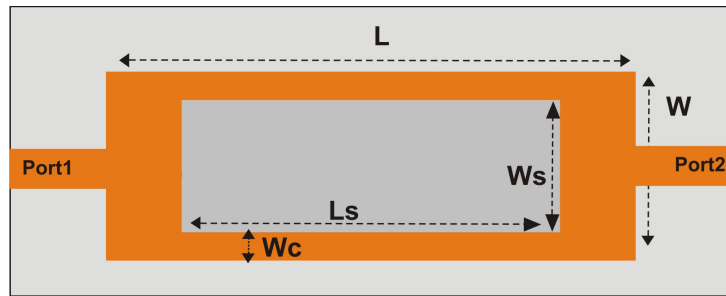


Figure 4.3: Modified transmission line ($L = 28\text{mm}$, $W = 13.8\text{mm}$, $h = 1.6\text{mm}$, $L_s = 20\text{mm}$, $W_s = 7\text{mm}$, $L_g = 28\text{mm}$, $W_g = 13.8\text{mm}$, $\epsilon_r = 3.7$ and $\tan\delta = 0.003$)

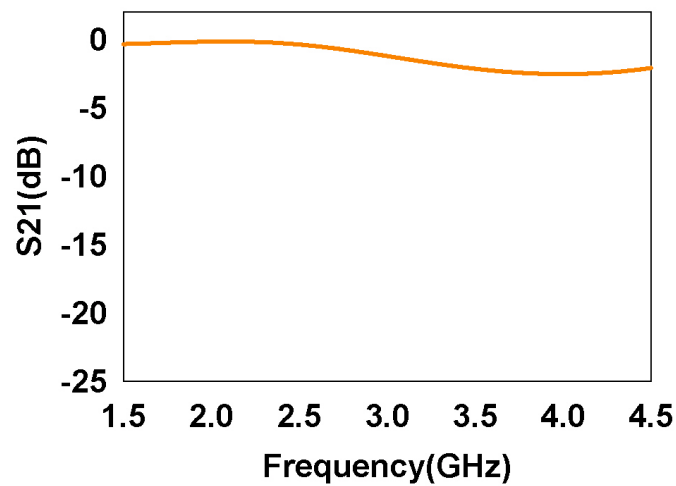


Figure 4.4: Insertion loss of the modified transmission line ($L = 28\text{mm}$, $W = 13.8\text{mm}$, $h = 1.6\text{mm}$, $L_s = 20\text{mm}$, $W_s = 7\text{mm}$, $L_g = 28\text{mm}$, $W_g = 13.8\text{mm}$, $\epsilon_r = 3.7$ and $\tan\delta = 0.003$)

4.3 Open Stub resonators Incorporated the Modified Transmission Line

In this section, the effect of placing a single open stub resonator inside the Modified Microstrip Transmission Line (MMTL) is discussed. The open stub resonators of size $L_1 \times t_1$ is placed inside the modified transmission line as shown in Figure 4.5. The structure exhibits excellent band rejection characteristics at resonance as shown in Figure 4.6. Open circuited shunt stub resonator is a $\frac{\lambda_g}{4}$ short circuit and it offers parallel resonance which was discussed in previous chapter. The transmission characteristics of an open stub shows resonance at 2.896 GHz as shown in Figure 4.6(a) and (b). The surface current distributions confirms the presence of quarter wave resonance. This quarter wave uniform impedance resonator act as a parallel lumped resonator. The design equation for fundamental frequency f_r of an open stub resonator can be expressed as

$$f_r = \frac{c}{\lambda_g} \quad (4.1)$$

$$\lambda_g \approx 4(L_1 + \Delta l) \quad (4.2)$$

where λ_g is guided wavelength, L_1 is resonator length, Δl extended length due to microstrip fringing which depends on thickness of substrate and c is velocity of light in vacuum.

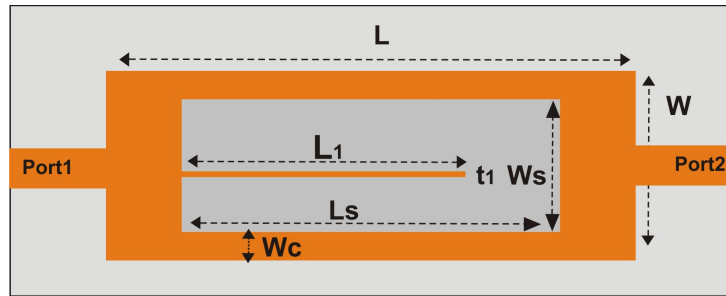


Figure 4.5: Open stub resonator in the bifurcated transmission line $L = 28mm$, $W = 13.8mm$, $h = 1.6mm$, $L_s = 20mm$, $W_s = 7mm$, $L_1 = 15mm$, $t_1 = 0.3mm$, $L_g = 28mm$, $W_g = 13.8mm$, $W_c = 3.4mm$, $\epsilon_r = 3.7$ and $\tan\delta = 0.003$

The structure consists of an open stub placed inside the bifurcated line as shown in Figure 4.5. The stub is on top side of the substrate with an infinite

ground plane on the bottom side. The open stub structure works as a quarter wave resonator. All the frequencies except open stub resonant frequency propagate through the transmission line from port 1 to port 2 confirms the band rejection mode of operation. The resonator prevents the transmission of particular frequency and creates a band notch filter response. The overall size of the filter ($W \times L$) is about $28 \times 13.8\text{mm}^2$, where W and L are width and length of the filter, respectively. The bifurcated line metal strip width is $W_c = 3.4\text{mm}$, open stub metal strip thickness $t_1 = 0.3\text{mm}$ and open stub length $L_1 = 20\text{mm}$ are the values selected for the simulation studies.

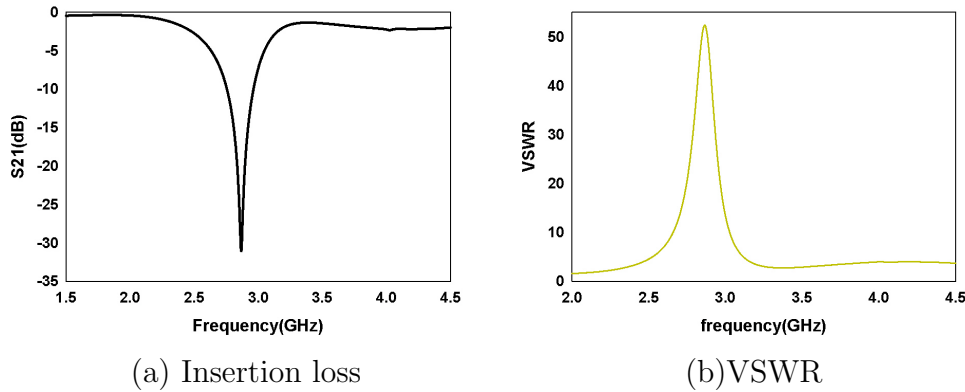
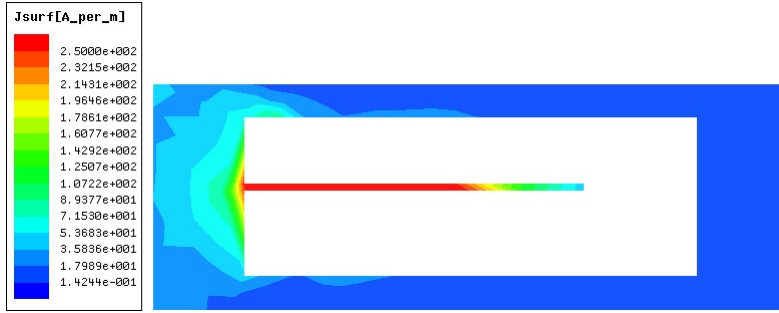


Figure 4.6: Transmission and reflection characteristics of open stub resonator in the modified microstrip transmission line ($L = 28\text{mm}$, $W = 13.8\text{mm}$, $h = 1.6\text{mm}$, $L_s = 20\text{mm}$, $W_s = 7\text{mm}$, $L_1 = 15\text{mm}$, $t_1 = 0.3\text{mm}$, $L_g = 28\text{mm}$, $W_g = 13.8\text{mm}$, $W_c = 3.4\text{mm}$, $\epsilon_r = 3.7$ and $\tan\delta = 0.003$)

The simulated transmission characteristics of open stub resonator is shown in Figure 4.6(a) and (b). The surface current distribution at the resonant and non-resonant frequency are plotted in Figures.4.7 (a) and (b) respectively. Current distribution is minimum at non-resonant condition, whereas surface current maximum occurs at its resonance i.e, one quarter wavelength variation. Equivalent circuit of open stub resonator is a parallel RLC tank circuit which offers high impedance at its resonance. The propagation of resonant frequency is prevented by the tank circuit.

The theoretical and experimental investigations provides an insight into band notch mechanism and effect of various filter parameters on the transmission characteristics. Inferences from these studies lead to the formation of



(a) Surface current distribution at resonance(2.896 GHz)



(b) Surface current distribution at non-resonant frequency (2 GHz)

Figure 4.7: Surface current distribution of open stub resonator in the modified microstrip transmission line ($L = 28\text{mm}$, $W = 13.8\text{mm}$, $h = 1.6\text{mm}$, $L_s = 20\text{mm}$, $W_s = 7\text{mm}$, $L_1 = 15\text{mm}$, $t_1 = 0.3\text{mm}$ $L_g = 28\text{mm}$, $W_g = 13.8\text{mm}$, $W_c = 3.4\text{mm}$, $\epsilon_r = 3.7$ and $\tan\delta = 0.003$)

design equations for the open stub resonator in modified transmission line. In order to find out the effect of various parameters on resonant characteristics thorough parametric analysis has been done. The influence of length of the resonator on the insertion loss characteristics is depicted in Figure 4.8. In the present study the length of the resonator is varied from 11mm to 19mm while maintaining other parameters constant. The resonances occurs at 3.884GHz and 2.3GHz respectively. It is clear from Figure 4.8 that the length of the resonator is responsible for the resonance. Resonant frequency decreases with increase in the length of resonator and vice versa. A slight variation in resonance due to the increase in the width of the resonator is depicted in Figure 4.9.

The multiple open stub resonators are attractive for band notch response owing their high Q-factor and simple structure. The open stub structures placed inside the microstrip line decreases the system complexity without any

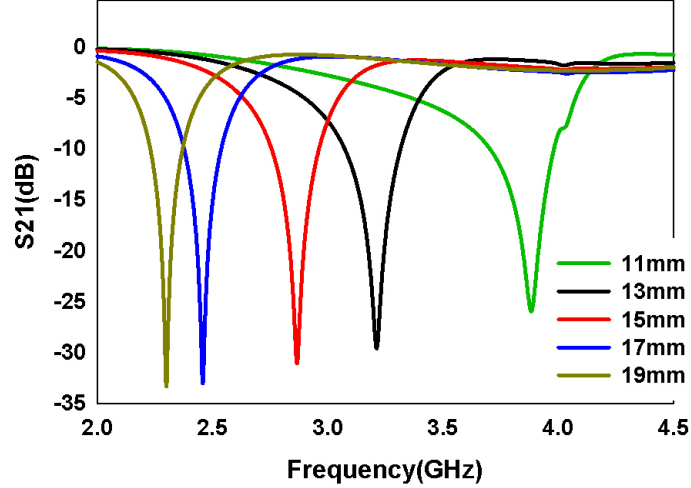


Figure 4.8: Effect of the length variation (L_1) on the insertion loss ($L = 28mm$, $W = 13.8mm$, $h = 1.6mm$, $L_s = 20mm$, $W_s = 7mm$, $t_1 = 0.3mm$, $\epsilon_r = 3.7$, $L_g = 28mm$, $W_g = 13.8mm$, $W_c = 3.4mm$ and $\tan\delta = 0.003$)

change in physical size. This property of the open stub resonator is effectively utilized for the design of a multiresonator based chipless RFID tag.

The proposed multi-resonator consists of eight open stub resonators placed inside the modified transmission line which reunites at the far end of the transmission line as shown in Figure 4.10. A prototype of the multiresonating circuit is fabricated on a substrate of $\epsilon_r = 3.7$ and $h = 1.6mm$ with parameters in Table:4.1. The length of each resonator is different for different exciting frequencies.

One end of each resonator is contact electrically with transmission line and it inhibits the propagation of a particular resonant frequency. Consequently, the multiresonator shows eight notches in their transmission characteristics as shown in Figure 4.11. The resonant frequencies are found to be 2.476GHz, 2.648GHz, 2.888GHz, 3.076GHz, 3.184GHz, 3.432GHz, 3.796GHz and 4.204GHz. The frequency difference between higher band notch frequency and lower band notch frequency is 1.728 GHz. i.e, eight resonant frequencies are accommodated within this range. The band notch is very sharp so as to accommodate more number of resonances within a small frequency band. The resonant frequencies, bandwidth and Fractional Bandwidth (FBW) are

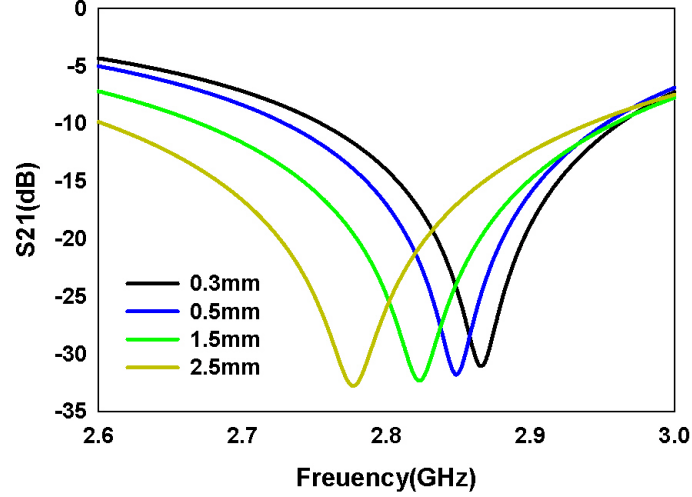


Figure 4.9: Effect of thickness Variation(t_1) on insertion loss($L = 28mm$, $W = 13.8mm$, $h = 1.6mm$, $L_s = 20mm$, $W_s = 7mm$, $L_1 = 15mm$, $\epsilon_r = 3.7$ $L_g = 28mm$, $W_g = 13.8mm$, $W_c = 3.4mm$ and $\tan\delta = 0.003$)

Table 4.1: Geometric parameters of the Open stub multiresonators inside the modified transmission line

Parameter	Physical dimension (mm)
Length x Breadth	28 x 13.8
Hieght, h	1.6
Slot size, (L_s x W_s)	20 x 7
Length of the resonator, L1	18
Length of the resonator, L2	17
Length of the resonator, L3	16
Length of the resonator, L4	15
Length of the resonator, L5	14
Length of the resonator, L6	13
Length of the resonator, L7	12
Length of the resonator, L8	11
Spacing between resonator,s	0.5
Width of the resonating element,t	0.3

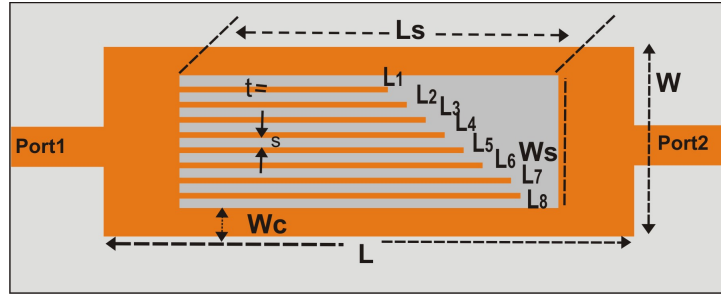


Figure 4.10: Multiresonator circuit in the modified transmission line ($L = 28\text{mm}$, $W = 13.8\text{mm}$, $h = 1.6\text{mm}$, $L_s = 20\text{mm}$, $W_s = 7\text{mm}$, $L_1 = 18\text{mm}$, $L_2 = 17\text{mm}$, $L_3 = 16\text{mm}$, $L_4 = 15\text{mm}$, $L_5 = 14\text{mm}$, $L_6 = 13\text{mm}$, $L_7 = 12\text{mm}$, $L_8 = 11\text{mm}$, $s = 0.5\text{mm}$, $t = 0.3\text{mm}$ $\epsilon_r = 3.7$ and $\tan\delta = 0.003$)

shown in Table.4.2. The resonators are designed in such a way that they work independent of each other. Figure 4.11 shows transmission characteristics and VSWR of multiresonator incorporated MMTL. From figures it is evident that the multiresonator exhibits narrow bandwidth.

Table 4.2: Resonator length and corresponding frequency

Lenth of resonator (mm)	fr (GHz)	BW (GHz)	FBW
18	2.476	0.1688	0.068263
17	2.6482	0.1502	0.05672
16	2.888	0.1458	0.05048
15	3.076	0.1465	0.04762
14	3.184	0.1825	0.05731
13	3.432	0.1825	0.05317
12	3.796	0.1045	0.02753
11	4.204	0.0932	0.02217

In order to confirm this the surface current at different resonances have been taken in HFSS and are shown in Figure 4.12. Each resonator excites at its own frequency. The equivalent circuit consists of multiple tank circuit connected in a series. Each tank circuit has different resonance as the lumped electrical parameter of each distributed open stub is different. These electrical parameters determine all the characteristics of open stub such as resonant

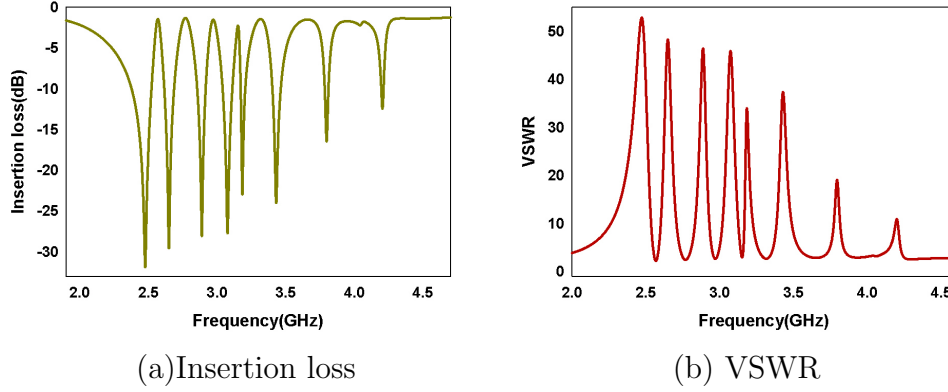


Figure 4.11: Transmission and reflection characteristics of open stub multiresonators in the modified line ($L = 28\text{mm}$, $W = 13.8\text{mm}$, $h = 1.6\text{mm}$, $L_s = 20\text{mm}$, $W_s = 7\text{mm}$, $L_1 = 18\text{mm}$, $L_2 = 17\text{mm}$, $L_3 = 16\text{mm}$, $L_4 = 15\text{mm}$, $L_5 = 14\text{mm}$, $L_6 = 13\text{mm}$, $L_7 = 12\text{mm}$, $L_8 = 11\text{mm}$, $s = 0.5\text{mm}$, $t = 0.3\text{mm}$, $\epsilon_r = 3.7$, $L_g = 28\text{mm}$, $W_g = 10\text{mm}$, $W_c = 3.4\text{mm}$ and $\tan\delta = 0.003$)

frequency, bandwidth and Q -factor.

Simulation studies are carried out using different substrates with the same physical dimensions. The outcome of these studies are tabulated in Table.4.3. As relative permittivity increases, the resonant frequency decreases in accordance with the variation of effective permittivity. Here the effective permittivity ϵ_{reff} is determined by the combined effect of physical parameters such as the width of the conducting strip w , height of the substrate h and relative permittivity of the substrate ϵ_r . Simulation studies are carried out for different substrate heights and the results are shown in Table.4.4. The cause of Variation of resonant frequency while changing substrate height is due to variation in effective permittivity, ϵ_{reff} of the structure.

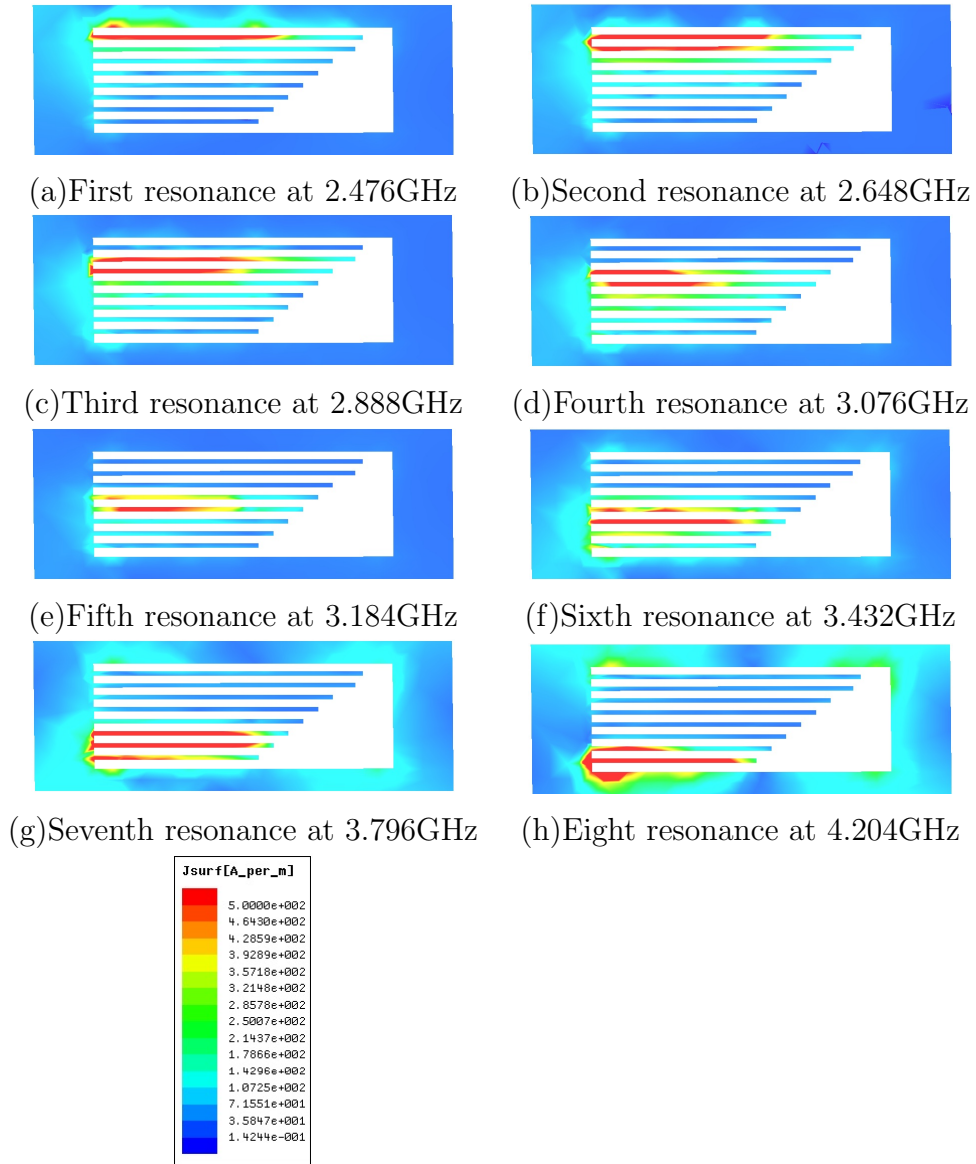


Figure 4.12: Surface current distribution

Table 4.3: Parametric studies of relative permittivity of resonator medium and corresponding resonance

Relative permittivity(F/m)	1	1.7	2.2	2.7	3.2	3.7	4.2	4.7
First resonance(LSB)(GHz)	3.8585	3.415	3.076	2.82	2.644	2.476	2.364	2.272
Second resonance (GHz)	4.0455	3.675	3.264	2.964	2.744	2.648	2.496	2.396
Third resonance (GHz)	4.1995	3.74	3.424	3.192	3	2.888	2.708	2.612
Fourth resonance (GHz)	4.535	4.1	3.664	3.488	3.308	3.076	2.896	2.828
Fifth resonance (GHz)	4.788	4.39	3.948	3.696	3.492	3.184	3.048	3.084
Sixth resonance (GHz)	5.1345	4.57	4.156	3.864	3.68	3.432	3.36	3.44
Seventh resonance (GHz)	5.8055	5.025	4.6	4.296	4.056	3.796	3.648	3.696
Eighth resonance(MSB)(GHz)	6.1905	5.415	4.984	4.896	4.412	4.204	3.948	3.752

Table 4.4: Parametric studies of height variations of substrate

Height 0.4mm		Height 0.8mm		Height 1.2mm		Height 1.6mm	
Resonant frequencies (GHz)	Insertion loss (dB)	Resonant frequencies (GHz)	Insertion loss (dB)	Resonant frequencies (GHz)	Insertion loss (dB)	Resonant frequencies (GHz)	Insertion loss (dB)
2.34	-48.2023	2.44	-40.4155	2.512	-35.1325	2.476	-31.8859
2.54	-34.1712	2.632	-33.0363	2.688	-13.074	2.648	-29.5529
2.6	-45.4922	2.84	-38.0559	2.796	-33.5514	2.888	-28.0418
2.892	-45.4174	3.02	-31.7023	3.08	-31.2321	3.084	-28.289
3.048	-39.3721	3.204	-31.7501	3.272	-25.3405	3.184	-22.8973
3.38	-41.8704	3.38	-29.2372	3.492	-24.5578	3.432	-23.7456
3.64	-9.9048	3.668	-23.8523	3.696	-19.2931	3.796	-16.3204
3.744	-31.8223	3.952	-15.1561	4.104	-13.6186	4.204	-12.4474

4.4 Spectral Signature Coding Technique

In spectral signature technique, data bit is usually encoded with the presence or absence of a resonant peak/dip at a predetermined frequency in the spectrum. The presence or absence of resonance in the predetermined spectrum is used to encode logic 1 or logic 0 respectively. In order to avoid a particular resonance from predetermined spectrum the corresponding resonator is disconnected from transmission line as shown in Figure 4.13. Consequently, the effect will be same as absence of resonance in the frequency spectrum. This technique can be extended to encode different spectral signatures of the tag as shown in Figure 4.15.

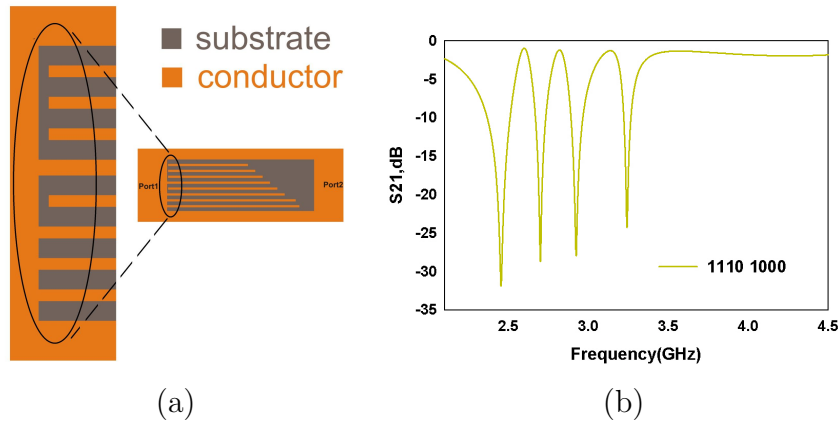


Figure 4.13: (a) Data encoding technique (b) corresponding S_{21}

4.4.1 Generation of different Bit Combinations

In spectral signature based tags, the accuracy of bit encoding depends on the mutual interactions between the resonators. The mutual coupling of the resonator should be avoided to obtain better results. Here investigating the performance of different multiresonators by varying the number resonators. The 8-bit multiresonator is taken as a reference and the generated bit patterns are shown in Figure 4.14. in order to encode the pattern 10000000 only one resonator $L_1 = 18mm$ is accommodated inside the slot to resonate the Meast significant bit (MSB) . The transmission response is shown in Figure 4.14(a). The resonant frequency is shown at 2.476GHz with insertion loss

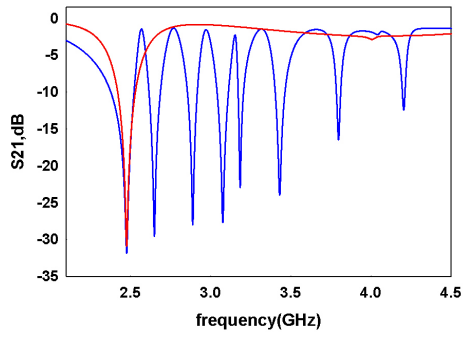
-33dB. The spectral ID is coded as 1000 0000. In order to encode ID: 1100 0000, two resonators of corresponding frequency are accommodated in the slot. The length of resonators are 18mm and 17mm for 2.476GHz and 2.6482GHz respectively. The transmission characteristics is shown in Figure 4.14(b). The transmission characteristics of ID: 1110 0000, 1111 00000, 1110 1000 and 1111 1100 are also depicted in Figure 4.14. The presence or absence of resonator determines the logic 1 and logic 0.

In order to encode a data, the resonators are connected or disconnected. ID: 1111 1111, 1111 1100, 1110 1000, 1110 0000, 1100 0000 and 1000 0000 are plotted in Figure 4.15.

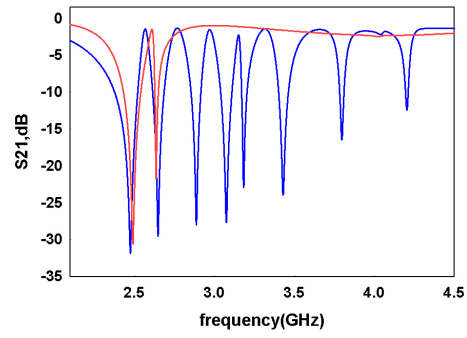
4.5 Chipless RFID Tag Development

High bandwidth disc loaded monopole antennas are used for chipless RFID tag applications. The geometry of disc loaded microstrip fed monopole antenna is shown in Figure 3.15. The radius of circular patch R is 15mm and width of transmission line (W) is 3mm, the gap between circular disc and ground edge (g) is 0.6mm, dielectric constant of substrate ϵ_r is 4.3, rectangular ground width W_g and length L_g are 20mm and 40mm respectively. The electrical characters such as returnloss, surface current distributions and radiation pattern are plotted in Figure 3.16, 3.17 and 3.18 respectively. Circular disc structure supports multiple resonant modes. The wide bandwidth is achieved by overlapping of these resonant multiple resonant modes. The overall gain of disc loaded monopole antenna is about 3dBi and it offers efficiency of about 85%.

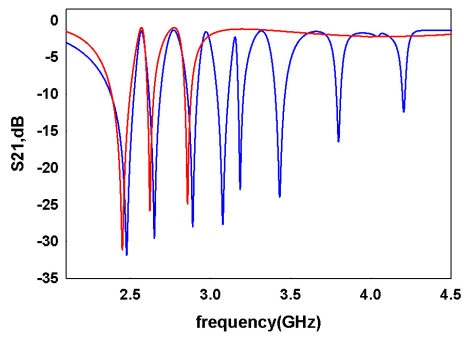
Two orthogonally polarized wideband antennas are connected with multiresonator to form a chipless tag. Two antennas are required for receiving and re-transmitting an interrogating signal from reader. These antennas are connected orthogonally to achieve better isolation between receiving and re-transmitting signals from reader. The photographs of the multiresonator prototype and tag is shown in Figure 4.16 and Figure 4.17 respectively. The transmission characteristics, group delay and phase of multiresonator are shown in Figure 4.18. The resonant frequencies are 2.47GHz, 2.77GHz, 2.98GHz, 3.19GHz, 3.39GHz, 3.76GHz, 4.03GHz and 4.39GHz corresponding to bit-pattern 1111 1111. In Figure 4.19, the 3.19GHz resonator is absent, corresponding spectral signature 1110 1111 and in Figure 4.20 the fourth resonance



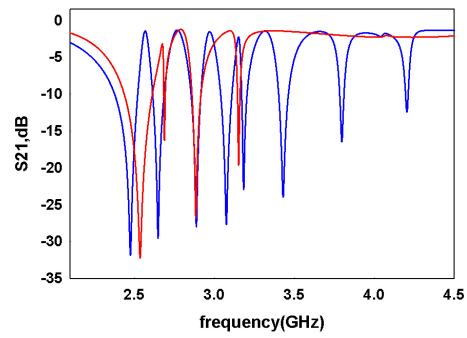
(a)1000 0000



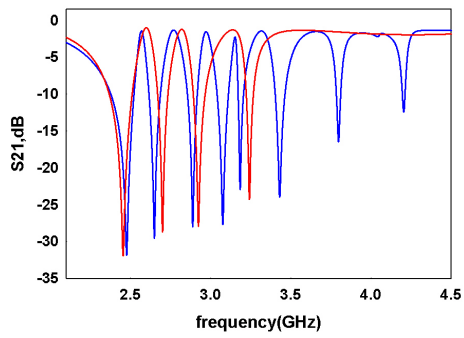
(b)1100 0000



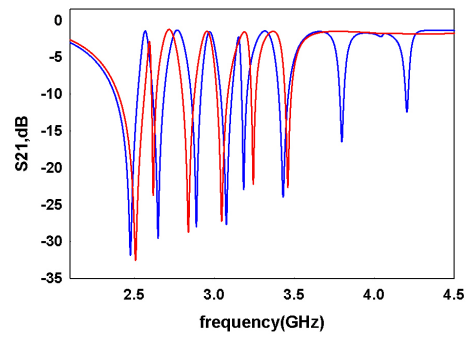
(c)1110 0000



(d)1111 0000



(e)1110 1000



(f)1111 1100

Figure 4.14: Different bit combinations compared with 8 bit resonator

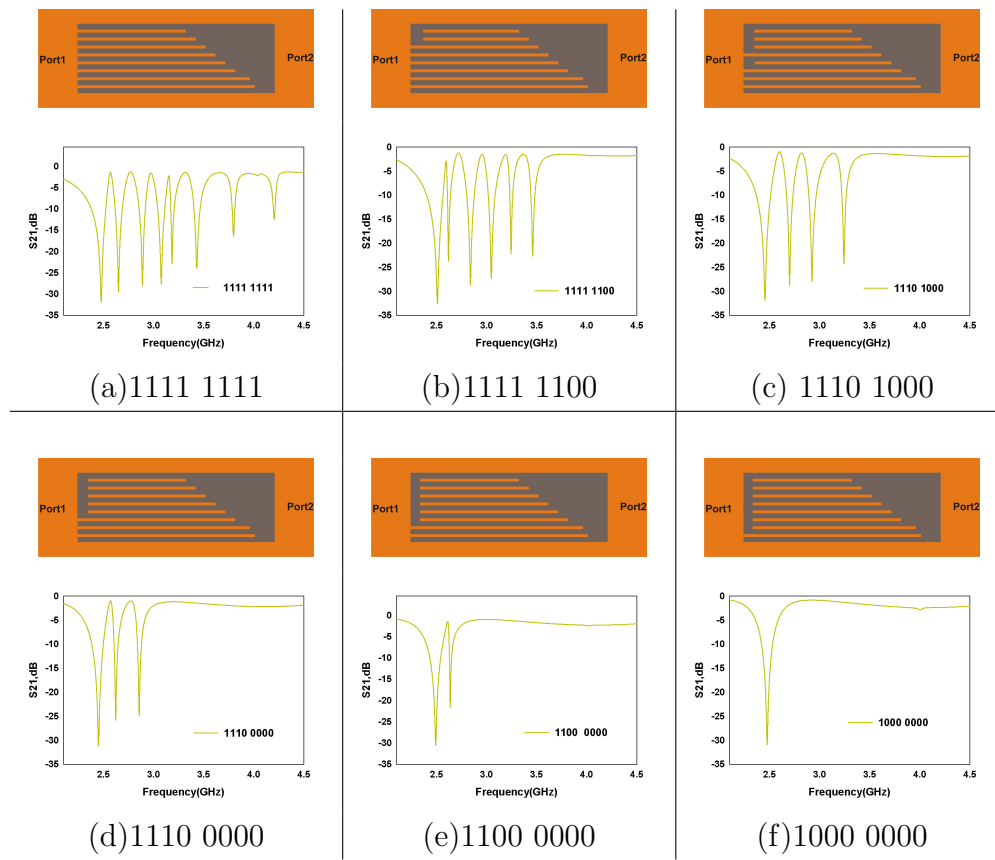


Figure 4.15: Generation of different bit combinations

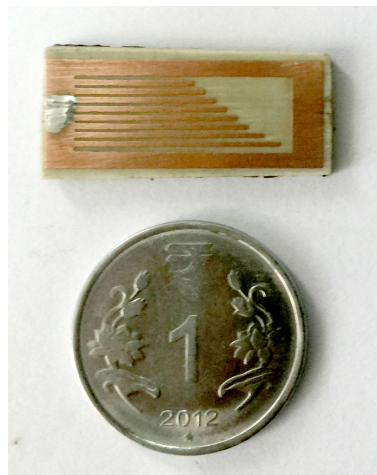


Figure 4.16: Photograph of proposed multiresonator compared with INR 1 coin

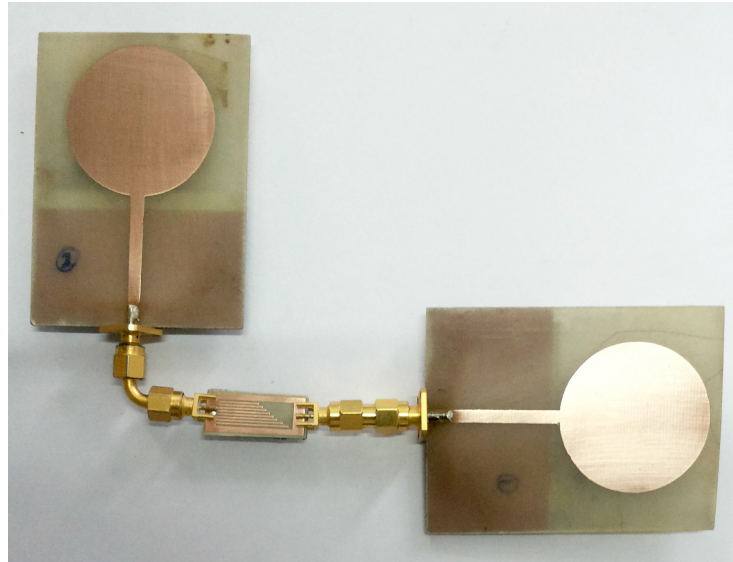


Figure 4.17: Photograph of proposed chipless tag

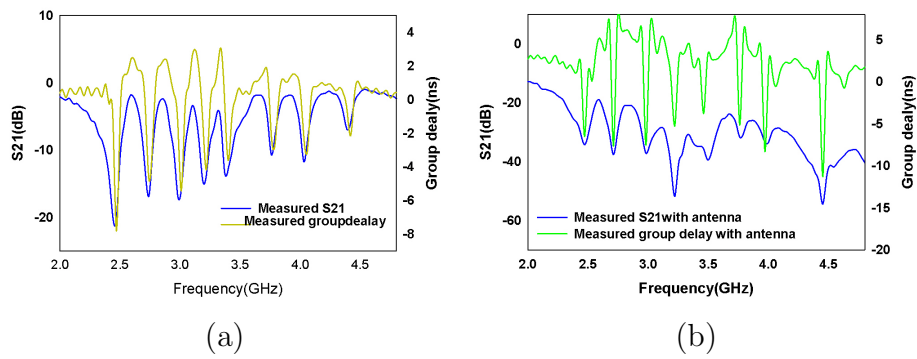


Figure 4.18: Measured response of byte: 1111 1111 (a) Multiresonator (b) chipless tag

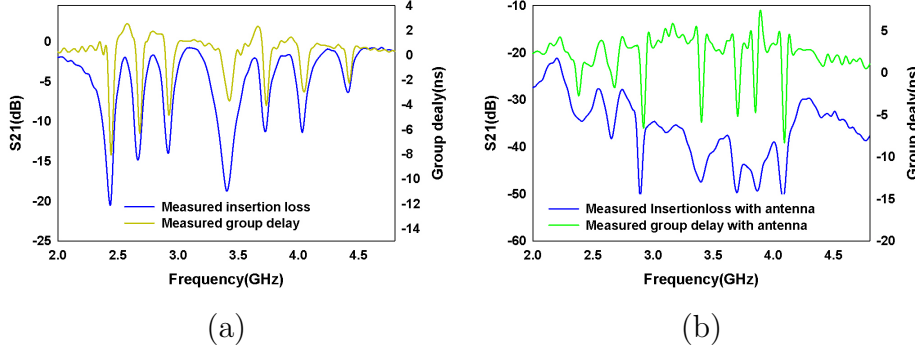


Figure 4.19: Measured response of byte: 1110 1111 (a) Multiresonator (b) chipless tag

at 3.19GHz and eighth resonance at 4.39 are absent and corresponding byte is 1110 1110. The tag enables data encoding of 8-bits in a narrow band of 1.92GHz extending from 2.47 to 4.39 GHz. The far-field response is shown in Figure 4.18, 4.19 and 4.20.

The tag is mounted on a stand, 35cm away from the reader antenna. The system is calibrated with 50 Ω transmission line is connected with two cross polarized wide band antennas. The 50 Ω transmission line is replaced with multiresonator to identify the tag. The amplitude attenuation and group delay are depicted in Figure 4.18, 4.19 and 4.20.

The multiresonator is a modified version of open stub resonator, all the resonators are accommodated in the MMTL. The length of open stub resonator determines the resonant frequency and it can be easily controlled by trimming and tuning. Each stub in the multiresonator operates at its own resonant frequency. Consequently, multiple number of bits can be encoded in the multiresonator. The proposed resonator is a good candidate for spectral signature tag applications. The comparison between fractional bandwidth of coupled bunch hair pin resonator and open stub resonator are shown in Table.4.6. Fractional bandwidth of open stub resonator is lower than coupled bunch resonator. The tag response as a function of distance from the reader is depicted in Figure 4.21.

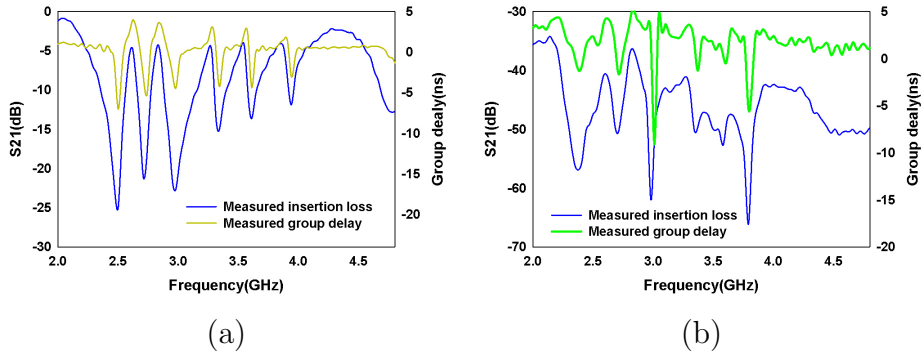


Figure 4.20: Measured response of byte: 1110 1110 (a) Multiresonator (b) chipless tag

Table 4.5: Measured response of eight bit multiresonator

Resonant frequency(GHz)	Insertion loss(dB)	Group delay(ns)
2.47	-20	7.8
2.74	-16	4.73
2.98	-16	5.44
3.19	-14.7	4.16
3.37	-13.2	3.6
3.76	-10.7	2.6
4.03	-11.74	3.05
4.39	-6.94	2.6

Table 4.6: Fractional bandwidth of Bunch coupled multiresonator and Open stub multiresonator in modified transmission line

Bunch coupled resonator		open stub multiresonator	
Resonant frequency	FBW	Resonant frequency	FBW
2.476	0.011750149	2.6784	0.068263
2.6482	0.011390671	2.744	0.05672
2.888	0.010330205	2.8552	0.05048
3.076	0.009819583	2.957	0.04762
3.184	0.008745654	3.129	0.05731
3.432	0.008346373	3.231	0.05317
3.796	0.007438756	3.3832	0.02753
4.204	0.00703305	3.4856	0.02217

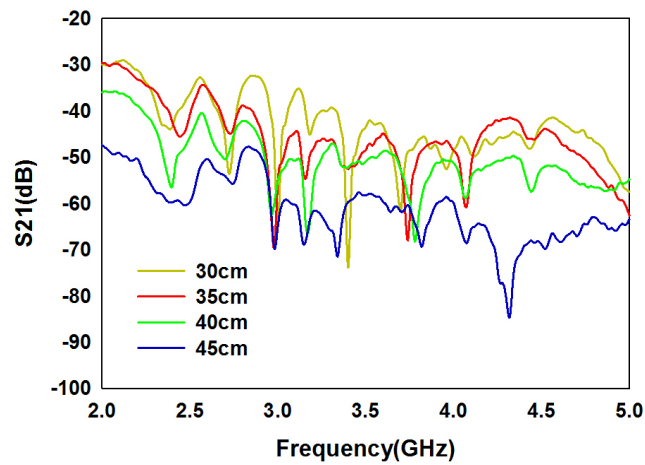


Figure 4.21: Tag response as a function of distance from the reader

4.6 Conclusion

The open stub multiresonator is a suitable option for spectral signature based chipless tag. Multiple bit encoding is done by varying the length of the resonator. A detailed investigation of transmission characteristics is carried out. The spectral signature based encoding using magnitude attenuation or groupdelay or phase jumping or combination of these parameters has been discussed. Two orthogonally polarized UWB antennas are connected with multiresonator to make a tag. The concept is validated from the measurements using bistatic approach for an 8-bit prototype.

REFERENCES

- [1] J.A.G Malherbe, “Microwave transmission line filters,” *Artech House*, 1979.
- [2] C. M. Nijas, R. Dinesh, U. Deepak, A. Rasheed, S. Mridula, K. Vasudevan, and P. Mohanan, “Chipless RFID Tag Using Multiple Microstrip Open Stub Resonators,” *IEEE Transactions on Antennas and Propagation*, vol. 60, no. 9, pp. 4429–4432, Sep. 2012.
- [3] G. Matthaei, L. Young, and E. Jones, “Microwave filters, impedance matching networks, and coupling structures,” *Artech House*, 1985.

Chapter 5

Loop Multiresonator Based Chipless RFID Tag

1. Different Loop Resonators
 2. Loop Resonator Placed Near Transmission Line
 3. Loop Resonator Placed on Slotted Ground
 4. Loop resonator on Bifurcated transmission line shorted with ground through via.
 5. Loop Multiresonator
 6. Results and Discussions
 7. Conclusion
-

This chapter presents investigations of different types of loop resonators and their characteristics. Shorted loop resonators are operated in its half wavelength ($\frac{\lambda_g}{2}$). The following sections present the investigations of loop resonators placed near the transmission line, loop resonators placed on the slotted ground and loop resonators on bifurcated transmission line connected with the ground.

5.1 Different Loop Resonators

Loop is a closed path such as circular ring, square ring, hexagonal ring, etc., even it may be an irregular shape closed path. Closed path resonators operate in its full wavelength (λ_g) i.e. perimeter of loop is equal to the guided wavelength (λ_g). The evolution of shorted loop multiresonators is discussed in following sections.

5.1.1 Loop Resonator Placed Near Transmission Line

The structure consists of circular ring of uniform width with full wavelength (λ_g) circumference. A rectangular ground plane is printed on the opposite side of substrate as shown in Figure 5.1(a). The radius of ring resonator $r = 7.9\text{mm}$, width $w = 0.3\text{mm}$, relative permittivity of substrate $\epsilon_r = 3.7$ and height $h = 1.6\text{mm}$. The ring structure is placed very near to transmission line feed structure is about 0.2mm . The transmission characteristics is shown in Figure 5.1(b) it is seen that the structure resonate at 3.742GHz with fractional bandwidth of 0.0384 .

Microstrip ring resonator is a full wavelength resonator. When it is placed near the transmission line, energy is coupled electromagnetically and produce a band notch at the resonant frequency. At resonance, it absorbs majority of electromagnetic energy propagating through the line. This is due to the shunt resonance effect of coupled loop resonator. The equivalent circuit of conventional transmission line consists of series resistance, series inductance, shunt conductance and shunt capacitance. The coupled resonator consists of an inductance and the coupled energy is grounded through capacitors.

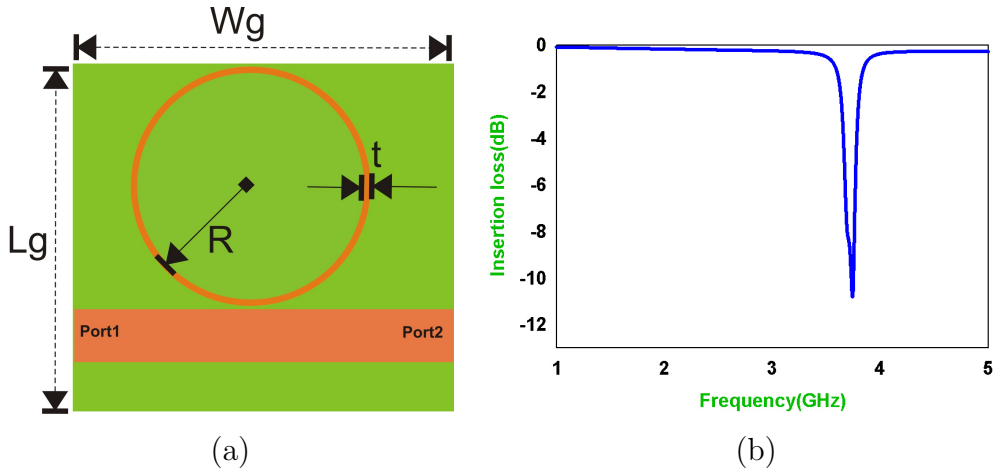


Figure 5.1: (a) Loop resonator coupled with transmission line ($W = 3.4\text{mm}$, $W_g = 25\text{mm}$, $L_g = 30\text{mm}$, $t = 0.3\text{mm}$, $R = 7.9\text{mm}$, $\epsilon_r = 3.7$ and $h = 1.6\text{mm}$) and (b) insertion loss

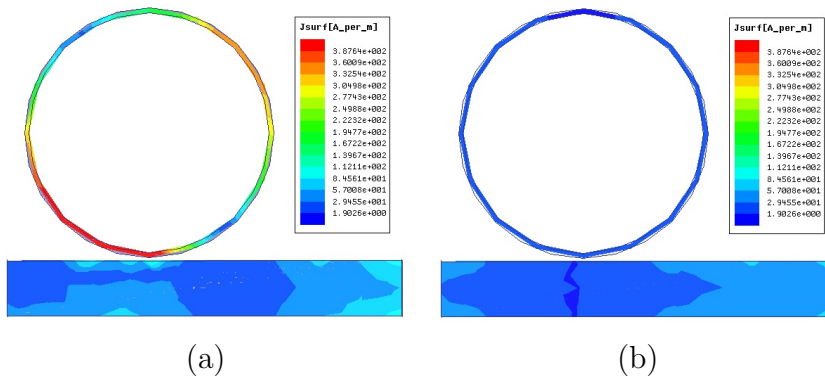


Figure 5.2: Surface current distribution of ring resonator at (a) resonant frequency 3.742 GHz and (b) non-resonant frequency 3GHz

The surface current distribution at resonance and non-resonance are shown in Figure 5.2. A full wavelength current variation occurs at its resonance. For non-resonant frequency, the ring is not excited and only a feeble current density is observed on the ring. i.e, the electromagnetic propagation in the transmission line is unperturbed at the non-resonant frequencies.

Design

Based on the observations, a design procedure for the ring resonator can be framed as explained in this subsection.

1. Design a 50 microstrip line on a substrate with permittivity ϵ_r and thickness h . Calculate ϵ_{eff} using the strip width, w and height, h of microstrip line. Effective dielectric constant can be calculated by using Ross and Howes empirical formula

$$\epsilon_{reff} = \frac{\epsilon_r + 1}{2} + \frac{\epsilon_r - 1}{2} \left(1 + \frac{10h}{w}\right)^{-\frac{1}{2}} + 0.468 \left(\frac{\epsilon_r + 0.5}{1.5}\right) \sqrt{\frac{t}{w}} \quad (5.1)$$

for $\frac{w}{h} \leq 2$

$$\epsilon_{reff} = \frac{\epsilon_r + 1}{2} + \frac{\epsilon_r - 1}{2} \left(1 + \frac{10h}{w}\right)^{-\frac{1}{2}} \quad (5.2)$$

for $\frac{w}{h} \geq 2$

2. Design a circular ring resonator of perimeter is equal to full wavelength λ_g
radius of circular ring

$$r = \frac{1}{2\pi} \left(\frac{c}{f_r \sqrt{\epsilon_{eff}}}\right) \quad (5.3)$$

where c is velocity of light in vacuum.

Loop multiresonators are not compact in nature. More over, this is not suitable to chipless RFID applications. In order to miniaturize the multiresonator, ring resonators can be arranged in concentric manner but coupling of transmission line and inner resonators are very small. So it cannot be used as multiresonator.

5.1.2 Loop Resonator Placed on Slotted Ground

A circular slot printed on the ground of microstrip transmission line produces an insertion loss in transmission characteristics. It infers that truncation of ground causes losses in transmission. A loop resonator placed inside the circular slot as shown in Figure 5.3 which inhibits the propagation of corresponding

resonant frequency depicted in Figure 5.4. The ring resonates at 3.988 GHz and a slight variation in resonance is observed as compared to the previous case due to the change in effective permittivity.

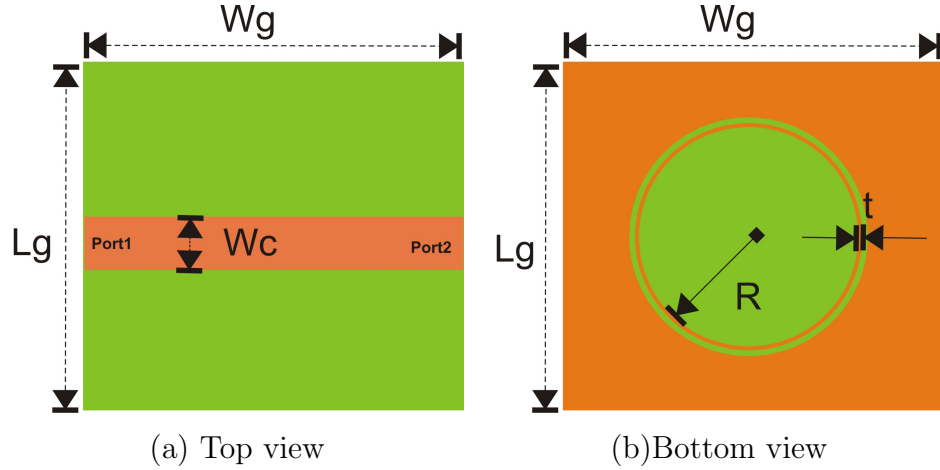


Figure 5.3: Geometry of single loop resonator on slotted ground of transmission line ($W_c = 3.4\text{mm}$, $W_g = 25\text{mm}$, $L_g = 30\text{mm}$, $t = 0.3\text{mm}$, $s = 0.5\text{mm}$, $R = 7.9\text{mm}$, $\epsilon_r = 3.7$ and $h = 1.6\text{mm}$)

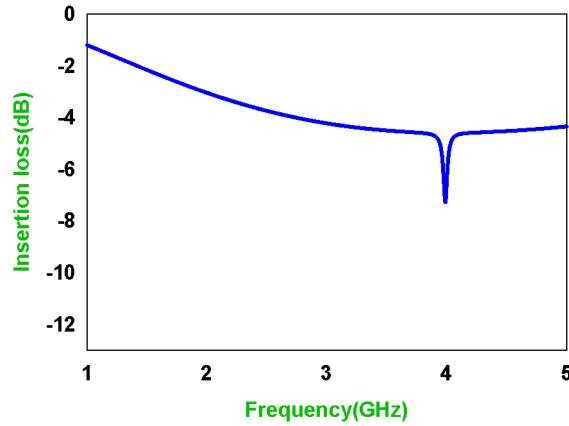


Figure 5.4: Insertion loss of loop resonator on truncated ground plane of transmission line ($W_c = 3.4\text{mm}$, $W_g = 25\text{mm}$, $L_g = 30\text{mm}$, $t = 0.3\text{mm}$, $s = 0.5\text{mm}$, $R = 7.9\text{mm}$, $\epsilon_r = 3.7$ and $h = 1.6\text{mm}$)

The surface current distribution at resonance and non-resonance are shown

in Figure 5.5. A full wavelength current variation occurs at its resonance. Size miniaturization of the resonator is difficult to achieve in this case due to ring operates at its full wavelength resonance.

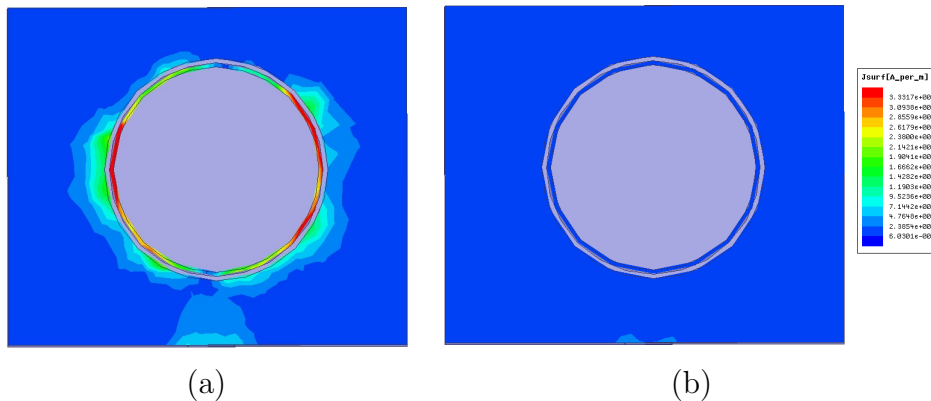


Figure 5.5: Surface current distribution of slotted ground ring resonator at (a) resonant frequency and (b) non-resonant frequency

5.1.3 Loop resonators Placed on Bifurcated Transmission Line shorted with Ground through via

The low resonant frequency can be achieved by connecting the loop resonator and ground through via. The conventional loop resonators are resonate at its full wavelength, whereas the shorted loop resonators operate at half wavelength. The geometry of single ring resonator with shorted via is shown in Figure 5.6(a). The transmission characteristics of this structure is shown in Figure 5.6(b). The circular ring of radius 7.9mm resonates at 1.92GHz. The surface current distribution of shorted ring resonator is shown in Figure 5.7. From the figure, it is clear that it is a half wavelength resonator with the proposed via.

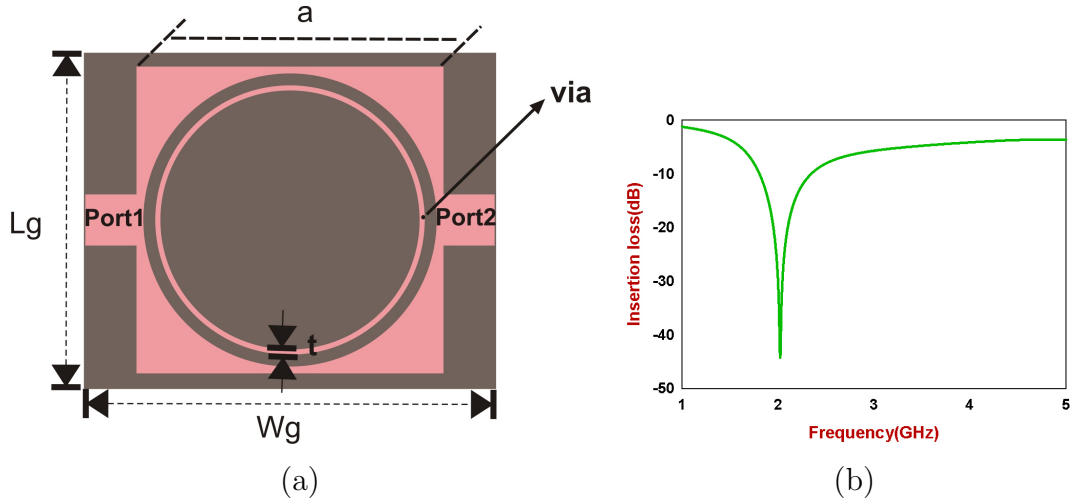


Figure 5.6: (a) Geometry of loop resonator on bifurcated transmission line shorted with ground ($a = 20\text{mm}$, $W_c = 3.4\text{mm}$, $W_g = 25\text{mm}$, $L_g = 30\text{mm}$, $t = 0.3\text{mm}$, via diameter = 0.2mm $s = 0.5\text{mm}$, $R = 7.9\text{mm}$, $\epsilon_r = 3.7$ and $h = 1.6\text{mm}$) (b) Transmission characteristics of loop resonator on bifurcated transmission line shorted with ground

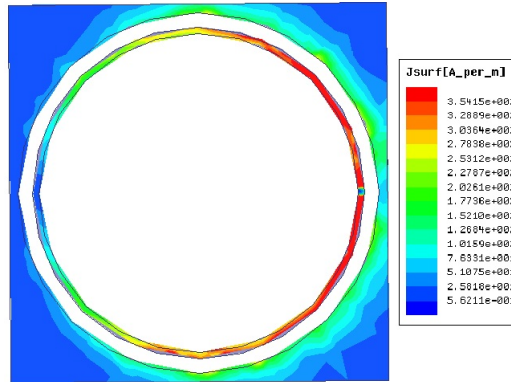


Figure 5.7: Surface current distribution of loop resonator on bifurcated transmission line shorted with ground

Design

Based on the above mentioned observations, a design procedure for loop resonator with shorted via is framed as following.

Design a loop resonator on bifurcated transmission line which fabricated on a substrate of dielectric constant ϵ_r and height, h . First determine the resonant frequency, f_r . Then calculate corresponding free space wavelength λ_0 and find out guided wavelength, λ_g . Guided wavelength and free space wavelength are related to the equation

$$\lambda_g = \frac{\lambda_0}{\sqrt{\epsilon_{reff}}} \quad (5.4)$$

The physical dimensions of resonator and guided wavelength are related to the following equations

$$\lambda_g = 2(2\pi r + h) = 4\pi r + 2h \quad (5.5)$$

where $2\pi r$ is outer perimeter of ring resonator and h is length of via that equal to thickness of substrate. The resonator operates in their half wavelength.

$$r = \frac{1}{4\pi} \left(\frac{c}{f_r \sqrt{\epsilon_{reff}}} - 2h \right) \quad (5.6)$$

This technique is utilized for making compact multiresonator circuit. These multiresonators are explained in below.

Loop resonator on bifurcated transmission line shorted with ground

Here a seven bit shorted ring multiresonator is proposed for chipless tag application. The proposed structure consists of seven concentric rings on bifurcated line and these are connected to ground through via as shown in Figure 5.8. The physical dimensions of multiresonator are shown in Table.5.1. These resonators inhibit the propagation of resonant frequency from port1 to port2. Consequently, it shows seven notches in their transmission characteristics as shown in Figure 5.9. The resonant frequencies of multiresonator are 1.9277 GHz, 2.1237 GHz, 2.354 GHz, 2.6431 GHz, 3.0645 GHz, 3.6035 GHz and 4.412 GHz. The frequency difference between higher band notch frequency and lower band notch frequency is 2.784GHz. i.e, seven resonant frequencies within this range.

Table 5.1: Geometric parameters of the shorted ring multiresonator

Parameter	Physical dimension (mm)
Hieght of substrate, h	1.6
Width of square,a	20
Radius of the resonator, R1	7.9
Radius of the resonator, R2	7.1
Radius of the resonator, R3	6.3
Radius of the resonator, R4	5.5
Radius of the resonator, R5	4.7
Radius of the resonator, R6	3.9
Radius of the resonator, R7	3.1
width,t1	0.3
spacing,s	0.5

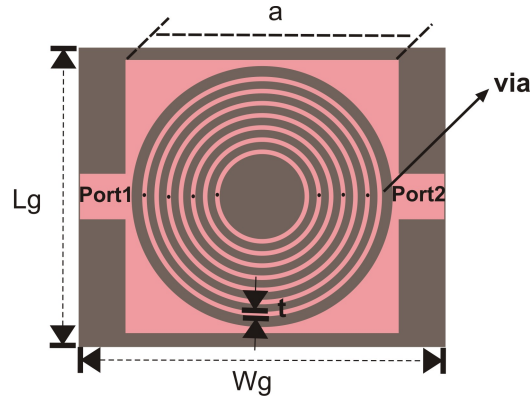


Figure 5.8: Geometry of loop resonator on bifurcated transmission line shorted with ground ($W_c = 3.4mm$, $W_g = 25mm$, $L_g = 30mm$, $a = 20mm$, $R_1 = 7.9mm$, $R_2 = 7.1mm$, $R_3 = 6.3mm$, $R_4 = 5.5mm$, $R_5 = 4.7mm$, $R_6 = 3.9mm$, $R_7 = 3.1mm$, viadiameter = $0.2mm$ and $s = 0.5mm$)

The length of resonator, resonant frequencies, insertion loss at resonance, bandwidth and FBW are shown in Table.5.2. Surface current distribution at each resonance is depicted in Figure 5.10 that exhibits apparent half wave-length current variation at its resonance.

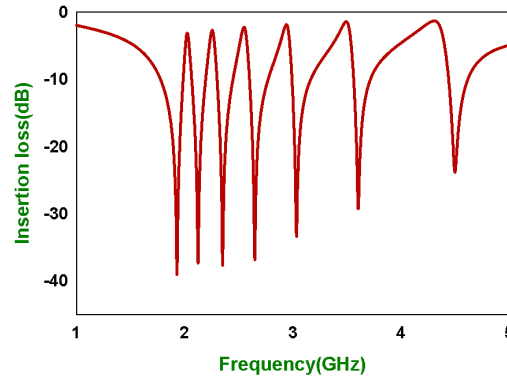


Figure 5.9: Transmission coefficient of loop resonator on bifurcated transmission line shorted with ground ($W_c = 3.4\text{mm}$, $W_g = 25\text{mm}$, $L_g = 30\text{mm}$, $a = 20\text{mm}$, $R_1 = 7.9\text{mm}$, $R_2 = 7.1\text{mm}$, $R_3 = 6.3\text{mm}$, $R_4 = 5.5\text{mm}$, $R_5 = 4.7\text{mm}$, $R_6 = 3.9\text{mm}$, $R_7 = 3.1\text{mm}$, viadiameter = 0.2mm and $s = 0.5\text{mm}$)

Table 5.2: Shorted loop multiresonator's insertion loss and bandwidth at their resonant frequencies

Radius of Resonator(mm)	Resonant frequency(GHz)	Insertion loss(dB)	3-dB Bandwidth(GHz)	Fractional bandwidth
7.9	1.9277	-38.833	0.747	0.38750843
7.1	2.1237	-37.969	0.2216	0.104346188
6.3	2.354	-36.1205	0.2585	0.109813084
5.5	2.6431	-35.5442	0.3532	0.133630964
4.7	3.0645	-34.1138	0.4698	0.153303965
3.9	3.6035	-27.8288	0.5718	0.158679062
3.1	4.412	-22.3831	0.2294	0.05199456

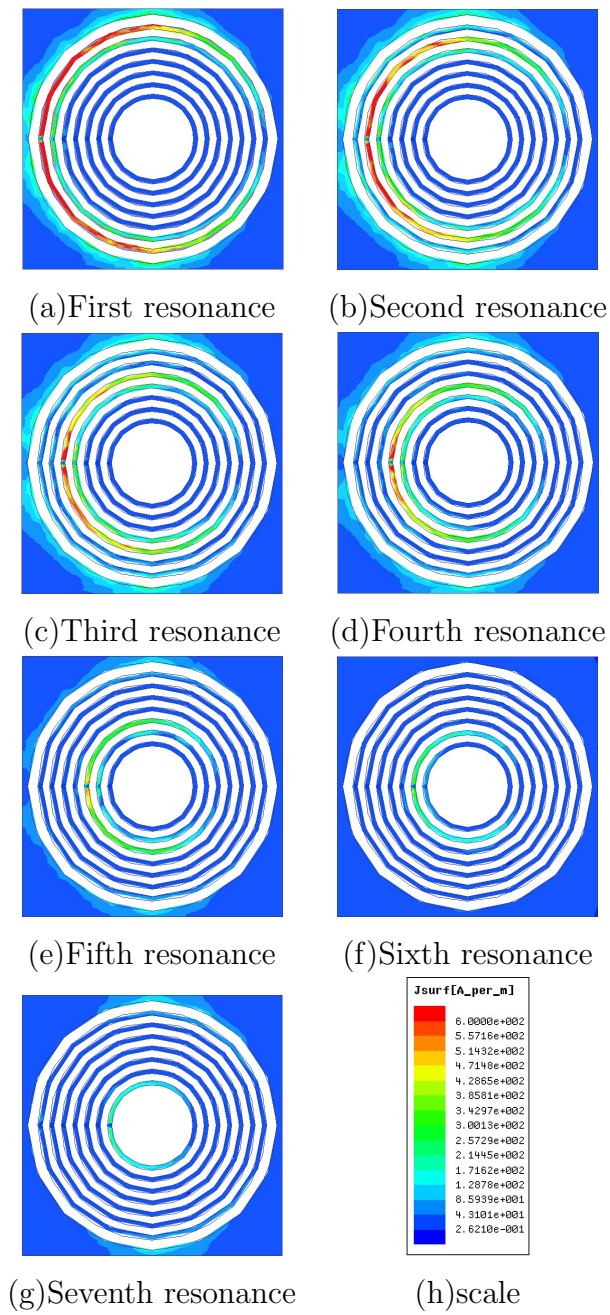


Figure 5.10: Surface current distribution

5.2 Results and Discussions

There are seven shorted loop resonators placed on the bifurcated transmission line as shown in Figure 5.11. The prototype is fabricated on substrate with dielectric constant, $\epsilon_r = 3.7$, loss tangent, $\tan \delta = 0.003$ and thickness, h 1.6mm. Experimental measurements are carried out inside anechoic chamber by using PNA E8362B analyzer. The prototype of the tag consists of a multiresonating circuit and two orthogonally polarized antennas. The photograph of the tag is shown in Figure 5.12. The measured response of loop resonator on bifurcated transmission line shorted with ground is shown in Figure 5.13. The insertion loss and group delay are plotted in it. The resonant frequencies are found to be 2.25GHz, 2.33GHz, 2.45GHz, 2.58GHz, 2.7GHz, 2.91GHz and 3.17GHz. The spectral signature encoding technique is described in the previous chapters is used for making unique spectral ID. The lower 2.25GHz resonance is taken as Most significant bit (MSB) and the higher 3.17GHz resonance is known as Least Significant Bit (LSB). The loop resonator on bifurcated transmission line shorted with ground exhibits comparatively low Q-factor. In fact, loop resonator on bifurcated transmission line shorted with ground has high insertion loss over the entire band . consequently, the -3dB bandwidth is large compared to the open stub resonators. But the sharpness of each resonance is high. Table.5.3 shows a comparison of fractional bandwidth of previous work. Shorted loop multiresonator as a good candidate for spectral signature RFID tag applications.

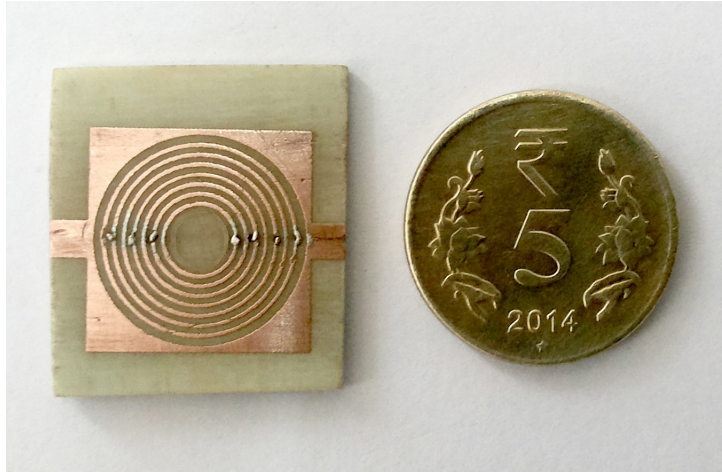


Figure 5.11: Photograph of the shorted loop multiresonator compared with INR 5 coin

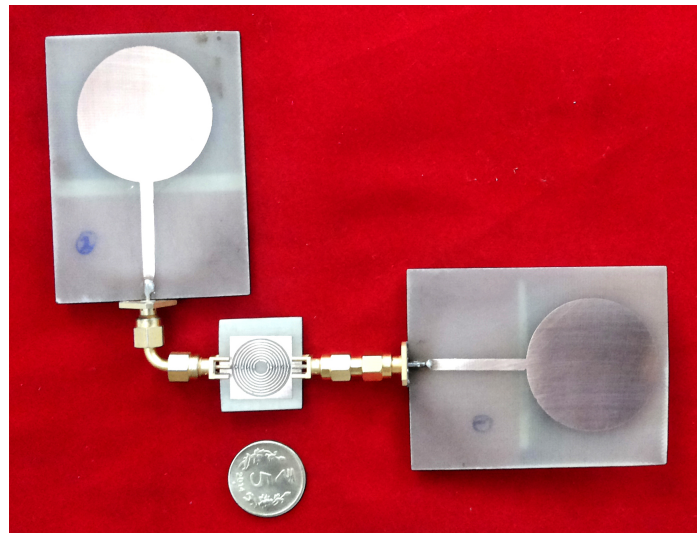


Figure 5.12: Photograph of shorted loop multiresonator based tag

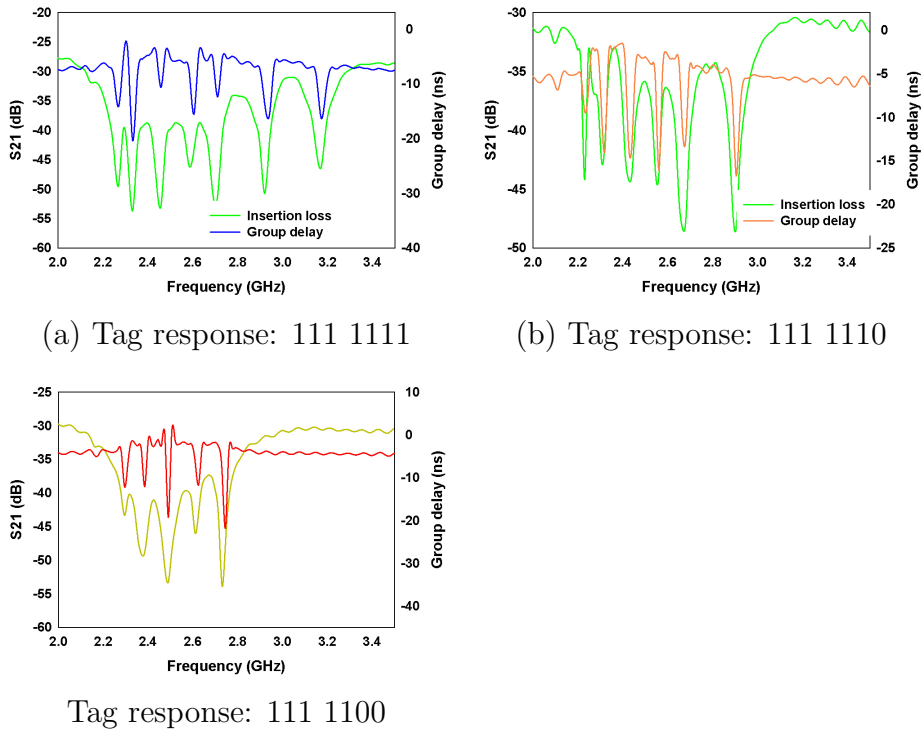


Figure 5.13: Different measured tag responses

Table 5.3: Comparison of fractional bandwidth

Coupled bunch multiresonator	Fractional bandwidth of	
	Open stub resonators in MMTL	shorted loop multiresonator
0.011750149	0.068263	0.3875
0.011390671	0.05672	0.1043
0.010330205	0.05048	0.1098
0.009819583	0.04762	0.1336
0.008745654	0.05731	0.1533
0.008346373	0.05317	0.1586
0.007438756	0.02753	0.0519
0.00703305	0.02217	

5.3 Conclusion

A loop resonator based multiresonator circuit for chipless tag application is presented. In order to achieve compactness, the full wavelength resonator is shorted either to the ground or to the feed line of the transmission line. The shorted loop resonator acts as half wavelength resonator. This principle is utilized for implementing loop resonators on bifurcated transmission line shorted with ground. The effective half wavelength of this type of resonator is the sum of perimeter of loop and length of shorting via in the case of loop resonator connected with ground of transmission line.

Chapter 6

Conclusion

This chapter summarizes and highlights the conclusions drawn from the present study. The research work accomplished in this thesis has focused on the design and development of different multiresonator circuits for spectral signature based chipless tag. Spectral signature based RFID tags are designed using standard planar resonator structures, antennas, filters, space filling curves, and fractals. In this thesis, a comprehensive study on the design, simulation, and testing of different multiresonating circuit for spectral signature based chipless tag are presented. The three novel multi resonator designs are presented in this thesis. They are Coupled bunch hair pin resonator, Open stub multi resonator placed inside transmission line and Shorted slot ground loop multiresonators. The advantage of the tag is its compact size and higher Q of resonators compared to other existing chipless RFID tag designs.

Coupled hair pin resonators have higher coupling compared to conventional line resonator and also it exhibits higher Q. In order to reduce the size of multiresonating circuit all resonators are combined together to form a bunch hairpin resonator. One arm of all hair pin resonators are common which provides same coupling strength. But each resonator works independently that helps data encoding.

Open stub resonators are quarter wave resonator which are placed inside the bifurcated transmission line that rejoins its far end to form a multiresonator with moderate Q. For the first time the idea of bifurcated line used for multiresonating applications. Open stub resonators are suitable option for spectral signature tags.

The subsequent work is concentric circular rings printed on the bifurcated transmission line which connected to ground through via. The loop resonators on bifurcated transmission line operate at half wavelength. To reduce overall size of tag, antenna size should be reduced and incorporated into the tag.

The main objectives of research work is to design and develop compact, narrow bandwidth multiresonators for chipless tag. Even though Preradovic et al presented a lot of published papers in spectral signature chipless tag, they all used only spiral resonators for band notch applications. Spiral resonator based multiresonators can be replaced easily by using the proposed multiresonators such as bunch hair pin resonator, shorted loop multiresonator on slotted ground, open stub multiresonator inside the modified line.

Based on the conclusions and limitations of the present work, prospects for future works are identified as below. The overall size of tag depends mainly on the size of antennas connected with it. So new reading technique to be proposed in future.

So far, the RFID tag has been designed to operate in predefined alignment situations and applications since the polarization of the antennas is crucial for successful reading. Further studies could focus on developing planar circularly polarized tag antennas which would remove the present stringent alignment requirements.

DINESH R.

*Senior Research scholar,
Centre for Research in Electromagnetics and Antennas,
Department of Electronics,
Cochin University of Science and Technology,
682022, INDIA.*

*Kuzhikandathil
Poopara, Idukki
+91-9961866746
dineshr@cusat.ac.in
dinsh84@gmail.com*

Education

Cochin University of Science and Technology, Cochin
Pursuing Ph.D., Microwave Engineering

Cochin University of Science and Technology, Cochin
M.Sc. Electronic science, April 2008

Mahatma Gandhi University, Kottayam
B.Sc. Electronics, January 2005

Research Experience

Research Scholar
Centre for Research in Electromagnetics and Antennas,
Department of Electronics,
Cochin University of Science and Technology, Cochin
October 2009- till the date

- 6 –year Research experience in Microwave field
- Broad theoretical knowledge, strong analytical skills and measurement experience in Electromagnetics and Antennas.
- Research experience in planar antennas, Ultra wide band antennas and Composite Right Left Handed Transmission line based Metamaterial antennas.
- Design experience in S-band Dielectric Diplexer for Vikram Sarabhai Space Centre (VSSC), Trivandrum
- Research experience in chipless RFID tags
- Experience in Microwave material characterization measurements
- Experience in Microwave design tools such as Ansoft HFSS and CST Microwave Studio
- Experienced in using HP 8510C Vector Network Analyzer, PNA E8362B Network Analyzer, R&S ZVB 20, Anritsu Spectrum Analyzer, Anechoic chamber measurements etc.

Research Interests

- Antennas, Filters, Radar, Millimeter Wave Technology, Electromagnetics, Developing new techniques for material characterization measurements, Metamaterials and MEMS.

List of Publications

1. M. Sumi, C.M. Nijas, **R. Dinesh**, S. Mridula & P. Mohanan, “Spectral signature-encoded chipless RFID tag with planar multiresonators”, Journal of Electromagnetic Waves and Applications (Taylor & Francis),pp. 1-10, Oct. 2014. (Volume 28, Issue 18 pp. 2266-2275 | DOI: 10.1080/09205071.2014.964371)
2. M Sumi, **R Dinesh** , C.M. Nijas, S. Mridula & P. Mohanan “High Bit Encoding Chipless RFID Tag Using Multiple E-Shaped Microstrip Resonators”, Progress In Electromagnetics Research B, Vol. 61, 185–196, Nov. 2014.
3. Sumi M, **Dinesh R**, Nijas C M,S Mridula and P Mohanan “Frequency coded chipless RFID tag using spurline resonators” Radio engineering, vol. 23, 203-207, April 2014

4. **Dinesh R**, Vinod VKT, Jithin P, Deepak C M, Anila P V and P Mohanan “A compact Zeroth order directional antenna” *Microwave and optical Technology Letters*/56,No.4,929-932, April 2014.
5. Sarin V P, Rohit K Raj, Vinesh P V, **Dinesh R**, P Mohanan and K Vasudevan “A metaresonator inspired dual band antenna for wireless applications” *IEEE Transactions on Antennas and Propagation*,vol.62,No.4, 2287-2291, April 2014
6. **Dinesh R**, Vinod VKT, Deepak U, Vinesh P V and P Mohanan “CPW-Fed Zeroth Order Resonator Antenna using Shorted CRLH Transmission line” *Microwave And Optical Technology Letters / Vol. 55, No. 12, 2844-2847,929-932,December 2013.*
7. **Dinesh R**, Vinod VKT, Sarin V P, Shameena VA, and P Mohanan “Asymmetrical grounded CPW fed antenna for WLAN applications” *Microwave And Optical Technology Letters / Vol. 55, No. 11, 2739-2741, November 2013.*
8. S Sreenath, P Ashkar ali, P Thomas, **R Dinesh**, and CK Anandan “CPW-FED compact bent monopole antenna for UWB applications” *Microwave and Optical Technology Letters* 55 (1), 56-58, January 2013.
9. Nijas C M, **Dinesh R**, Deepak U, Abdul Rasheed, Mridula S, K. Vasudevan and P. Mohanan, “Chipless RFID Tag using Multiple microstrip Open Stub Resonators” *IEEE Transactions on Antennas and Propagation*, Vol. 60, No. 9, 4429-4432, September 2012.
10. P Ashkarali, S Sreenath, R Sujith, **R Dinesh**, DD Krishna, and CK Anandan “A compact asymmetric coplanar strip fed dual-band antenna for DCS/WLAN applications” *Microwave and Optical Technology Letters* 54 (4), 1087-1089, April 2012.
11. S M Nair, VA Shameena, **R Dinesh**, and P Mohanan “Compact semicircular directive dipole antenna for UWB applications” *Electronics letters* 47 (23), 1260-1262, November 2011.
12. R Sujith, S Mridula, P Binu, D Laila, **R Dinesh**, and P Mohanan “Compact CPW-fed ground defected H-shaped slot antenna with harmonic suppression and stable radiation characteristics” *Electronics letters* 46 (12), 812-814, June 2010.

Conferences

1. **Dinesh R** and P. Mohanan, “Semielliptical ring Asymmetrical Coplanar Waveguide fed UWB antenna”, 2011 IEEE – Applied Electromagnetic Conference And 2011-IEEE –Indian Antenna Week ,Hyatt Regency, Kolkatta December 18th-22nd 2011.
2. **Dinesh R**, Laila D, V P Sarin, Nijas C M, Shameena V A, P Mohanan “Asymmetric coplanar strip semielliptical dual band antenna”, PIERS 2012 Kualalumpur.
3. D Laila, R Sujith, CM Nijas, VA Shameena, **R Dinesh**, and P Mohanan “A Metamaterial Antenna with Reduced Radiation Hazards towards Human Head” PIERS March 27,30, 2012
4. Paulbert Thomas .S Sreenath, **R. Dinesh** “Compact CPW fed band-notched antenna for portable UWB applications”. ICACC 2012.
5. Sarin V P, Nishamol M S **Dinesh R**, Vinesh P V, Abdul Rasheed and Vasudevan Kesavath A, “Novel Compact Truncated-Ground Monopole Quasi Yagi Antenna” 2012 IEEE Asia-Pacific Conference on Antennas and Propagation (APCAP2012).
6. **Dinesh R** , Vinod V K T, Deepak U, Anila P V and P Mohanan “ Chip Inductor Loaded Microstrip fed antenna for WLAN applications” Indian Antenna week ,Aurangabad, Maharashtra 2013.
7. **Dinesh R** , Vinod V K T, Ashkar ali, Sarin VP and P.Mohanan “A dual band asymmetrical grounded CPW fed antenna for WLAN applications” APSYM 2012, 17-19, Cochin, Kerala.
8. Deepak U ,Roshna T K , Nijas C M , **Dinesh R** and P Mohanan “Compact CPW Fed ZOR Antenna for WLAN Application” IEEE International Symposium on Antennas and Propagation and USNC-URSI National Radio Science Meeting July7-13, 2013 , Orlando, Florida, USA
9. Sarin V P, Rohit K Raj, Vinesh P V, **Dinesh R**, P Mohanan and K Vasudevan “A meta resonator inspired dual band antenna for wireless applications” 2013IEEE applied electromagnetic conference, Dec 18-20, Bhubaneswar, INDIA.
10. **Dinesh R**, and P Mohanan “CRLH Transmission line based Zeroth Order Resonator Antenna” 2013IEEE applied electromagnetic conference, Dec 18-20, Bhubaneswar, INDIA.

11. **Dinesh R**, Anila P V, M P Jayakrishnan and P Mohanan “CRLH based ACS Fed zeroth order directional antenna for WLAN applications” National conference on Recent Trends in Electronics communication and signal processing CECASP-2013,DEC 20-21
12. Sumi, Nijas, **Dinesh R**, Mridula and P.Mohan “Compact chipless RFID tag using coplanar multiresonators” NATCON 2014 (National Technological Congress, Kerala).
13. **Dinesh R**, Anila P V,Sumi, Nijas and P.Mohan “Modified Open Stub Multi-Resonator Based Chipless RFID Tag” 2014 URSI General Assembly and Scientific Symposium, Beijing, China on August 16-23, 2014.
14. **Dinesh R**, Anila P V,Sumi, Nijas and P.Mohan “Open Loop Multi-Resonator Based Chipless RFID Tag” 2014 URSI General Assembly and Scientific Symposium, Beijing, China on August 16-23, 2014.
15. Sumi M, Nijas C M, **Dinesh R**, S.Mridula “Chipless RFID tag based on Spurline resonators”, Proc. of the National Symposium on Microwave Antennas and Propagation, (APSYM-12).pp 165-168,Cochin 2012.

References

Dr. P.Mohanan

Professor
Department of Electronics,
Cochin University of Science and Technology,
Cochin-682022,
drmohan@gmail.com
+91-9447325765
Fax: +91-484-2575800

Dr.K.Vasudevan

Professor
Department of Electronics,
Cochin University of Science and Technology,
Cochin-682022,
vasudevankdr@gmail.com
+91-9447357328
Fax:+91-484-2575800

Dr. Praveen.N

Associate Professor
Department of Electronics,
NSS College, Rajakumary,
Idukki-685619
praveen_nanniyatt@gmail.com
+91-9447608163

Index

A		Matrix Pencil Method29
Active RFID tag5		Modified Transmission Line 96
Anti-collision20		O
B		Open Stub Multiresonator 98
Bidirectional IDT 19		Open Stub Resonator 96
C		Orthogonal Frequency coding ... 20
Capacitively tuned dipoles 24		P
Chip RFID and chipless RFID tag 7		Passive RFID tag 4
Chipless RFID Tag 113		Piano curve25
Coupled Bunch Hairpin Resonator 73		Piezo-electric material18
D		R
Data Encoding technique78		Reflective delay lines 18
Delay line 21, 135		RFID tag 1
Different Loop Resonators 120		S
Disc-Loaded Monopole Antennas .80		Semi-lumped resonators52
Dual polarization 31		Semi-passive RFID tag6
F		Singularity Expansion Method ... 29
Field trials 88		Spectral signature 24, 25, 27, 30, 36,
Frequency domain 28, 38, 39		37, 39
H		spectral signature135
hairpin resonator66		Spectral Signature Coding Technique
I		110
Inter digital transducer18		Spiral multiresonators25
M		Stepped Impedance Resonator ... 47
Magneto Inductive Delay line 22		Substrate integrated tag35
		Surface acoustic wave16, 20
		Surface current distribution 71

T

Time Domain Reflectometry 16

Time domain reflectometry16

U

Unidirectional IDT19